Synthetic Membranes in Microfluidic Interfaces

Hang Zhao

A thesis submitted to

The School of Engineering

College of Science and Engineering

The University of Glasgow

In fulfilment of the requirements for

The Degree of Doctor of Philosophy

Abstract

This thesis explores the development of microfluidic technology for generating and manipulating micro-sized vesicles with the incorporation of specific membrane proteins as artificial cellular systems to mimic natural existing cells.

Synthetic biology (SynBio) is an emerging area of research concerned with the application of engineering methods to the creation of new biological processes and constructs. Understanding the working principle of living cellular system is one of significant issue for scientists working in this field. Cells are known as the basic unit of life: creating model synthetic analogues offers opportunities for us to deepen our insights of complex interaction and to understand features and functions of the living cells.

Microfluidic technologies have provided the capabilities of compartmentalisation, monodispersity and high-throughput generation for engineering architectures resembling cell-like structures. *In vitro* transcription and translation (IVTT) enables the expression of specific proteins of interest within synthetic cells via encapsulation of cell-free protein expression solution has demonstrated artificial cells with the capability of containing the process of central dogma of molecular biology.

The thesis investigates the building of synthetic cell-like constructs by microfluidics. The first area of investigation focusses on the fabrication of lipid/polymer vesicles transformed from ultra-thin shell double emulsions, which were prepared using microfluidics. To bring the biological function into both vesicle-based synthetic chassis, a fluorescent protein and a pore-forming membrane protein were *in vitro* expressed in the artificial cell chassis.

The second area of study centres on the viscosity analysis of artificial cell membranes using a combination of molecular rotors and the fluorescence lifetime imaging microscopy. The membrane viscosity plays a crucial role in membrane proteins insertion that influences the cell function regulation through functional

biomembranes. The alteration of lifetime of the molecular rotors trapped in the artificial membranes reports the viscosity changes in the membrane environment induced by the dewetting process. Comparisons of viscosity values over time between lipid vesicle templated by thin-shell double emulsions with GUVs produced by an oil-free method (electroformation) offers the ability of measuring the amount of oil phase (organic solvent mixture) in artificial cell membranes.

In the final chapter, the research detailed the construction of lipid bilayers with asymmetric arrangement used as more complex artificial cell models compared with most of synthetic cells with symmetric composition in their bilayers. A vesicle with hybrid asymmetric bilayer is also fabricated in same microfluidic fashion where phospholipid deposits on the inner-leaflet and block copolymer coats the outer monolayer.

Taken together, the work presented in this thesis shows the potential to exploit the microfluidic construction of a functioning synthetic cell from individual molecular components, which could advance new application areas in biotechnology and health. Further developments in this research will aim to develop microfluidic technologies for: (i) physically investigating cell division process using lipid vesicles as cell models; and (ii) producing complex multicompartmental systems for the use of mimicking natural cells. The asymmetric bilayers will be studied for their influences on the integration of transmembrane proteins.

Table of Contents

List of Tables

List of Figures

List of Publications and Conferences

Publications

Gaolian Xu,† Hang Zhao,† Jonathan M. Cooper and Julien Reboud, A capillary-based multiplexed isothermal nucleic acid-based test for sexually transmitted diseases in patients, *Chemical Commutations*, 52, 12187-12190, 2016. (co-first author)

Conferences

Hang Zhao, David Paterson, Julien Reboud and Jonathan Cooper, High-throughput synthesis of cell-like asymmetric bilayer vesicle within a single microfluidic device, *EMBL Microfluidics 2016*, 24-26 July 2016, Heidelberg, Germany.

Julien Reboud,* Hang Zhao, et al, Artificial protocells for water remediation, *XVth World Water Congress*, 25-29 May 2015, Edinburgh, United Kingdom.

Acknowledgement

My PhD has been an incredible, and extraordinary adventure in my life, full of highs and lows. This journey would not have been possible without the support of many people and herein, I would like to express my gratitude to each of them. Their guidance and encouragement will always fondly be remembered.

First of all, I would like to express my sincere gratitude to my supervisor Prof. Jonathan Cooper for giving me the opportunity to pursue my PhD in such a dynamic and friendly research group and for providing funding and facilities toward the success and completion of my projects as well as the chance to present my work in overseas. I am grateful for his guidance, wisdom, optimism, enthusiasm, ideas, time, and support, which have given me every opportunity to expand my research interests and skills and shaped me into a better researcher and a better communicator in science.

I am especially grateful to Dr. Julien Reboud, my second supervisor, who has always been there for me from day one throughout my PhD candidature. He has been an excellent mentor, spending enormous amount of time and efforts to guide, support, and assist me during my growth as a PhD student while allowing me to work in my own way. He is always available for stimulating discussions whenever I need them and I am thankful for his many ideas, knowledge, patience, and support. All of these training and mentoring will never be forgotten.

I am also thankful to Dr. Andrew Glidle and Dr. Rab Wilson for their knowledge and advices they have shared through helpful and detailed discussions. These were of great assistance for my projects and for that I am grateful. Additionally, I would like to thank Dr. Manlio Tassieri and Dr. Xize Niu for serving as the internal and external examiner respectively for my PhD viva.

I wish to thank Dr. David Paterson and Dr. Niall Geoghegan for their assistance in all things related to lipids and advanced imaging techniques. Special thanks to Mr.

Ross Eaglesfield who has spent enormous time and efforts for the preparation synthetic plasmids, which allowed me to explore protein synthesis in artificial cell chassis.

I would like to thank all past and present members within the Prof. Jonathan Cooper's group – Dr. Xiaofei Yuan, Dr. Yanqing Song, Dr. Ying Zhou, Dr. Gaolian Xu, Dr. Malgorzata Baranowska, Dr. Faroha Liaqat, Dr. Zhugen Yang, Xi King, Dr. Han Cui, Fan Gao, Eloise Larson and Alice Garrett, Pracha Yambangyang and Muhammad Khalid who have gone through the rollercoaster experiences as a scientific research together, sharing the excitement, the thrill, and the frustration. They have been wonderful company and have helped me out in a number of ways throughout the years. Working in the lab would definitely not be as enjoyable without all of them!

An essential contribution was given by The University of Glasgow that funded this research through the James Watt Scholarship.

I would also like to thank my wonderful Chinese friends for their constant support and caring through the tough times, and for reminding me the life outside the lab. A special thanks to Dr. Lei Zhang who was my flatmate at undergraduate and has always been there for me, encouraged me in many ways.

I would like to thank my parents, who have always been behind me and supporting me from thousands of miles away. You are the best parents I could ever asked for. Herein, I would like to dedicate this thesis to them.

Lastly, I would like to thank Ying Zheng, not only for her love, patience, and constant encouragement, but also for the valuable advices and stimulating scientific chats. She has made valuable support in a number of ways and importantly, kept my sanity in check.

Author's Declaration

"I declare that, except where explicit reference is made to the contribution of others, this dissertation is the result of my own work and has not been submitted for any other degree at the University of Glasgow or any other institution".

Hang Zhao

Abbreviations

μTAS	Micro Total Analysis System
BCP	Block Copolymer
BODIPY	Boron-dipyrrin
CLSM	Confocal Laser Scanning Microscopy
CV	Coefficient of Variation
DI Water	Deionised Water
DIB	Droplet Interface Bilayer
DOPC	1,2-Dioleoyl-sn-glycero-3-phosphocholine
DOPE	1,2-Dioleoyl-sn-glycero-3-phosphoethanolamine
EGFP	Enhanced Green Fluorescent Protein
ESR	Electron Spin Resonance
FCS	Fluorescence Correlation Spectroscopy
FITC	Fluorescein Isothiocyanate
FLIM	Fluorescence Lifetime Imaging Microscopy
FRAP	Fluorescence Recovery After Photobleaching
GUV	Giant Unilamellar Vesicle
IRF	Instrument Response Function
ITO	Indium Tin Oxide
IVTT	*In Vitro* Transcription Translation
NBD-PC	1-palmitoyl-2-{6-[(7-nitro-2-1,3-benzoxadiazol-4-yl)amino]hexanoyl}-sn-glycero-3-phosphocholine
NBD-PE	1,2-dipalmitoyl-sn-glycero-3-phosphoethanolamine-N-(7-nitro-2-1,3-benzoxadiazol-4-yl) (ammonium salt)
NMR	Nuclear Magnetic Resonance
PBS	Phosphate Buffered Saline
PCR	Polymerase Chain Reaction
PDMS	Poly(dimethylsiloxane)
PEG	Poly(ethylene glycol)

PEG-*b*-PLA	Poly(ethylene glycol)-block-Poly(D,L-lactic acid)
PMOXA-*b*-PDMS-*b*-PMOXA	Poly(2-methyloxazoline)-block-Poly(dimethylsiloxane)-block-Poly(2-methyloxazoline)
PMT	Photo Multiplier Tube
PURE	Protein Synthesis Using Recombinant Elements
PVA	Poly(vinyl alcohol)
ROI	Region of Interest
SLB	Supported Lipid Bilayer
SPAD	Single Photon Avalanche Diode
SynBio	Synthetic Biology
TCSPC	Time Correlated Single Photon Counting
TICT	Twisted Intramolecular Charge Transfer
TR-PE	n-(Texas Red sulfonyl)-1,2-dihexadecanoyl-sn-glycero-3-phosphoethanolamine
Vpp	Peak to Peak Voltage
αHL	α-Hemolysin

Chapter 1 Introduction

1.1 Synthetic Biology

This thesis starts by introducing Synthetic Biology (SynBio), an exciting new discipline that combines science and technology and has arguably resulted in some of the most astonishing scientific breakthroughs, and led to the greatest increase of knowledge, in life sciences in the last few decades. Defined by a group of European experts, a consensus definition of SynBio is described as: 'Synthetic Biology is essentially the engineering of biology that involves synthesis of complex systems which are either biologically based or inspired, to display functions that do not appear in nature. It is believed that this approach will enable the rational and systematical design of systems that might be applied into all scales of biological structure – from individual molecules to whole cells. (1)

Despite being a relatively new research field, SynBio has undergone dramatic growth and has already led to unprecedented insights into the production of organisms for drugs (2) and biofuels (3), as well as the creation of a synthetic tissue using only genetic data. (4) In addition, a large number of reviews and books have been published discussing its worldwide economic impact. (5-8) In Figure 1.1, a timeline charts the technological and cultural lifetime of SynBio. All current, or intended, investigations focus on the design of artificial living systems, such as the construction of synthetic cells featured with natural cell functions that could be exploited to explore how a living system works and interacts.

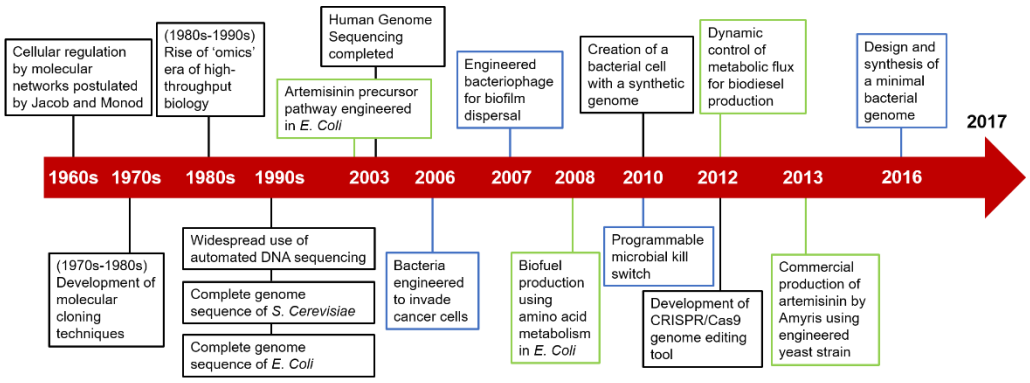

Figure 1.1 A timeline shows the brief history of SynBio. Key to coloured boxes: scientific milestones (black), SynBio in metabolic engineering (green), therapeutic applications (blue). Image is modified from indicated reference. (9)

1.1.1 Engineering Principles

How is SynBio different from other subfields of biology? The crux lies in the application of engineering principles employed for the design of biological systems. (10) Standardisation of biological components is a foundation of SynBio and is also a significant research area that aims to develop standards for biological parts in order to enable them to be interchangeable. Modularisation places emphasises on separately designed component that can be either added together to yield complex functioning organisms or rationally removed to reduce the complexity to a simpler problem that can be independently understood and addressed by researchers.

The aforementioned principles have already widely been applied to an important subfield of DNA design, namely the creation of BioBricks by Drew Endy, a pioneer in SynBio (11). BioBricks demonstrates the concept of designing genetic components that perform specific functions. In this thesis, these themes are translated to the engineering of both symmetric and asymmetric bilayer functional vesicles, built with naturally occurring molecules and synthetic compounds.

1.1.2 Top-Down and Bottom-up Approaches in SynBio

The SynBio field is diverse, but it can be broadly divided into two separate and competing themes, Figure 1.2: the top-down approach, to design systems based on a natural organism that is used as a host for the engineering of new functions within it; the bottom-up methodology, seeking to assemble artificial biomimetic systems that are built on basic biological or synthetic compounds, creating synthetic cell mimicry. The molecular systems constructed using the bottom-up approach resemble biological cells and are referred to as artificial/synthetic cells or protocells.

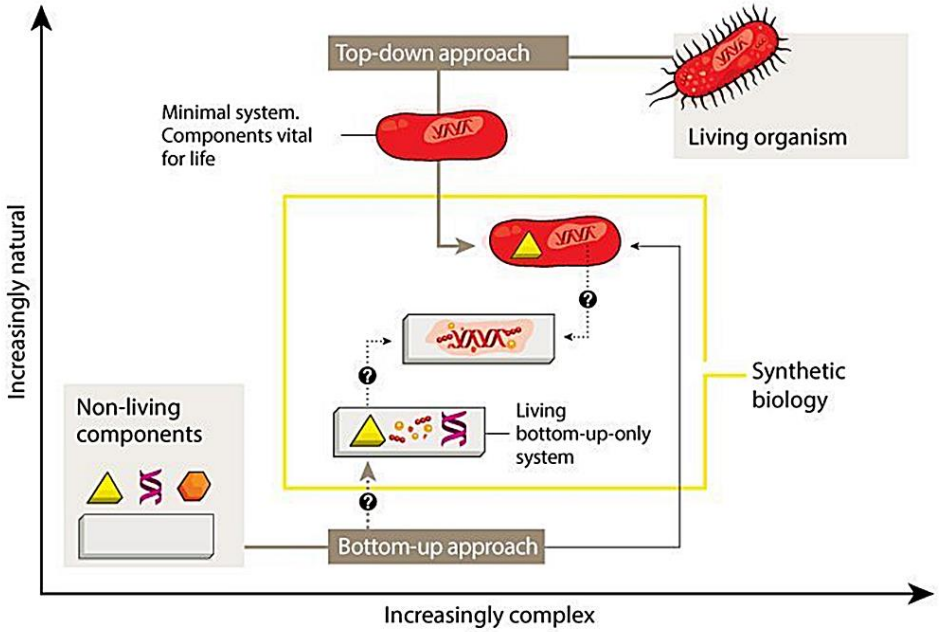

Figure 1.2 Two main approaches of synthetic biology, particularly in attempting to develop minimal living system. Top-down approach – minimal units derived from an existing organism. Bottom-up approach – refine the minimal units with synthetic or biological components. Image taken from the reference. (12)

Well-established genetic engineering technologies give rise to broad applications of the top-down approach in the SynBio research. In terms of creating synthetic life, where many synthetic biologists attempt to move to, the top-down methodology can

be exploited to generate a minimal cell through rationally reducing a natural cell's genomes until only essential genes remain. In this manner, exploring the specific functions of a living unit is achieved by decreasing the complexity of a modern living cell host. (13)

Recent progress by Venter et al. demonstrated that synthesised genomes comprised hundreds of genes and can constitute a brand new synthetic species. (14, 15) However, this top-down strategy does not reveal how the gene products act together to create this brand new artificial life since the function of a third of its genes are unknown, leaving many open questions to scientists on how these viable cells essentially work. As our understanding of both the fundamental basic biological molecules and the application of advanced engineering technologies in SynBio rapidly grow, we are able to make further inroads into building cell-like structures by reconstructing a set of individual biological compounds.

It is noteworthy that significant progress has been made in the bottom-up reconstitution of synthetic cellular machinery. (16-18) Beginning with simple molecules, scientists are not restricted to the natural principles of biological cells and brand new cell-mimetic systems can be designed, shedding light on specific biological process within cells and individual cell functions. Taking these approaches together, researchers are progressively better equipped to integrate basic individual biological systems into synthetic complex cell-like entities, bringing synthetic cells from the imagination to the reality.

1.1.3 Ultimate Goal of SynBio

Cells are the smallest representation of a natural living organism. It is therefore one goal of SynBio to build a living cell out of non-living molecules. SynBio is emerging as a powerful technology, capable of engineering novel biological counterparts, and attempting to fulfil the audacious concept of the construction of a fully synthetic, activated cell. Design of synthetic cells is not only trying to understand better the

molecular underpinnings of cell behaviour to answer the question of how a cell works, but also developing diverse solutions to real-world problems. (19)

1.2 Artificial Cell Models

Artificial cell models can be defined as those cell-like counterparts bounded by bilayers constructed of either lipid molecules or block copolymers, which are referred to as the chassis. Compared with complex biological membranes integrated with membrane proteins, these model membranes are simply designed and produced only with building blocks, which retain key features of biomembranes, and allow investigations performed in relatively simple environments. As such, artificial cell models have proved to be a significant tool in the study of the mechanical properties of the membranes, as well as for studying transmembrane proteins. (20) In addition, efforts have been spent on the applications of these cell-mimetic systems, such as bio-sensing, (21) and DNA sequencing. (22)

Generally, the model systems include bilayers in the form of solid substrate supported bilayers, Figure 1.3(A), droplet interface bilayers (DIBs), Figure 1.3(B), and vesicles, Figure 1.3(C). These three forms of model systems will be outlined as follows.

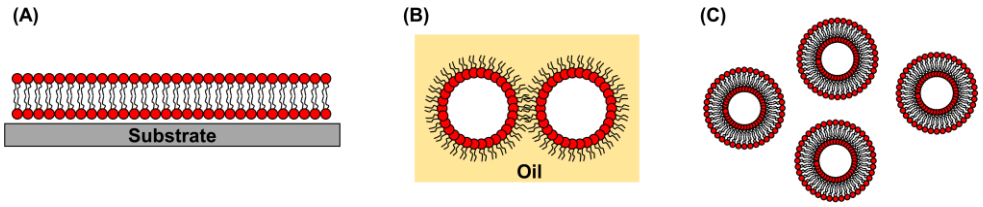

Figure 1.3 Artificial cell model systems: (A) Schematic of lipid bilayers supported by a solid substrate; (B) Schematic of droplet interface bilayer (DIB) formed when droplets are brought into contact; (C) Schematic of lipid vesicular structures.

1.2.1 Supported Lipid Bilayers (SLBs)

A supported bilayer is a biomimetic model membrane constituted of a planar structure of phospholipid molecules depositing on a solid support, which is typically formed by adsorption and fusion of vesicles, as shown in Figure 1.4. In such artificial membrane systems, the hydrophilic head groups of the bottom lipid monolayer are facing towards the substrate while hydrophobic tails of this lipid monolayer are in contact with the lipid tails of the upper monolayer. Because of the architecture of the SLB, the upper lipid monolayer is exposed to the aqueous medium, allowing SLBs to not only be used to characterise the chemical interactions between two free monolayers, but also to provide various tools for surface specific analyses. (20)

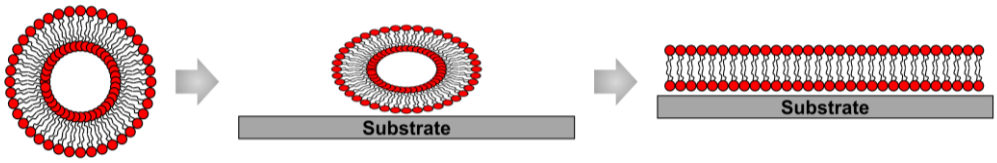

Figure 1.4 Schematic illustration of common techniques for the formation of supported lipid bilayers. Vesicles in solution adsorb and spontaneously fuse to the solid surface to form a supported lipid bilayer.

As an artificial cell membrane model, SLB has been popularly utilised to investigate the reconstitution of membrane proteins into artificial membranes. (23-25) However, one side of the polar head group freely floats in solution whereas the other side is tightly attached to the non-biological support, which may affect the mobility of membrane components that is the vital property of biomembranes in terms of the incorporation of transmembrane proteins. Additionally, within SLB model systems, random insertion orientations of integral membrane proteins have been frequently observed resulting in difficulty characterising the functions of targeted membrane proteins.

1.2.2 Droplet Interface Bilayers (DIBs)

Droplet interface bilayers (DIBs) are artificial membrane models formed between two self-assembled lipid-monolayer stabilised water droplets brought into contact inside a droplet incubator of oil, Figure 1.3(B). The concept was first proposed by Tsofina et al. in 1966, (26) but it was not further studied until 2006 when Bayley and his team, as well as Takeuchi and his group, from Oxford and Tokyo respectively, started to investigate DIBs in great details pushing the research of artificial cell membranes a step forward. (27, 28)

DIBs have provided facile and robust platforms as a consequence of the various advantages they confer, such as their high kinetic stability resulting in extended lifetime ranging from days to weeks, readily controlled electrical measurement by attaching hydrophilic electrodes and the ability to form asymmetric bilayer. (27, 29)

There are two distinct methods of forming DIBs pioneered by Hagan et al. and Takeuchi et al., depending on how phospholipid molecules are assembled into the monolayers at the water-oil interfaces. The lipid-out technique uses lipids dissolved in the oil phase, Figure 1.5(A), whereas in the lipid-in approach, the lipid vesicles are encased in the inner aqueous phase, and burst at the water-oil interface forming a lipid monolayer, stabilising the droplets, Figure 1.5(B). In both approaches, the formation of symmetric DIBs, in terms of lipid composition where the two monolayers are identical, are readily controlled. However, the asymmetric bilayer, which is a more accurate membrane model of biomembranes, can be manufactured using the lipid-in method by using two specific lipid composition vesicles in separated water droplets, as shown in Figure 1.5(B). (30)

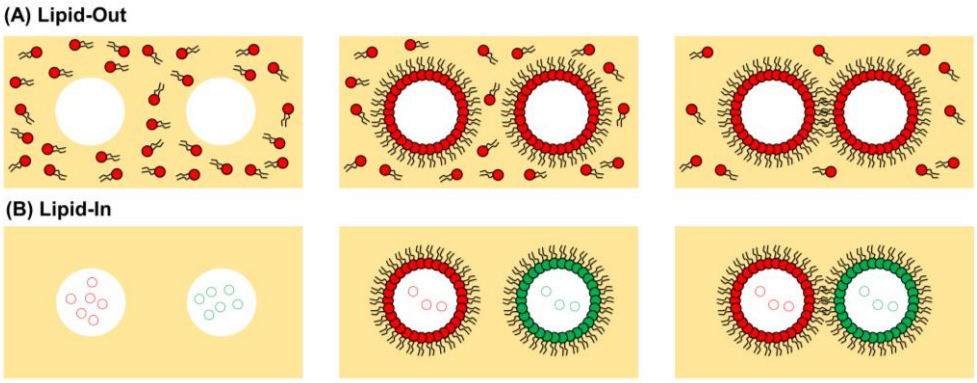

Figure 1.5 Schematic of formation of DIB: (A) Lipid-out DIB formation. Lipids are dissolved in the organic phase and self-assemble as a monolayer around each droplet. Two droplets are positioned in-pair forming a bilayer; (B) Lipid-in DIB formation. Two types of lipid vesicles with different compositions are present inside the water droplets. Vesicles fuse with the water-oil interface of the droplets and form monolayers. The droplets are then brought in contact to form an asymmetric bilayer.

DIBs have been exploited for the incorporation of membrane proteins as well as electrophysical characterisation, including α-hemolysin (nano-size pore-forming protein), outer membrane protein G (OmpG), bacteriorhodopsin (BR, light-sensitive proton pump) and potassium channels of Kcv and KcsA. (27) Besides the functionalisation of DIBs with integral membrane proteins, by using the lipid-in approach, Bayley and his group have demonstrated that the effect of asymmetric DIBs on OmpG gating behaviour is based on the orientation of protein in asymmetric DIBs. (31) DIBs have also been conjugated with *in vitro* transcription and translation (IVTT) to cell-free express membrane protein inside droplets as an alternative method for electrical measurements of membrane proteins. Two reviews from Bayley et al. in University of Oxford have illuminated DIBs from concept to recent applications. (27, 29)

1.2.3 Vesicles

Vesicles are fluid-filled spherical architectures formed spontaneously by self-assembly of phospholipids or of other molecules (e.g. fatty acids, block copolymers) as shown in Figure 1.6. In this thesis, efforts focus on the vesicles constructed with either phospholipids or block copolymers, which are liposomes and polymersomes, respectively.

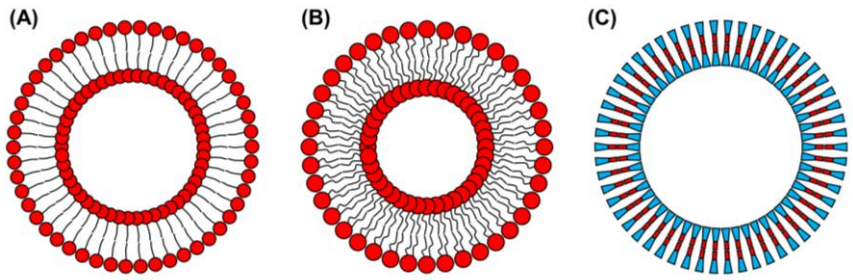

Figure 1.6 Schematic of vesicles: (A) A fatty acid vesicle. Fatty acid molecule is composed of a polar headgroup and a single-chained tail; (B) A lipid vesicle. Phospholipid molecule has a hydrophilic headgroup and hydrophobic double-chained tail group; (C) A polymeric vesicle (polymersome). Block copolymer is made of hydrophilic block and hydrophobic moiety.

Vesicles have served as versatile biomimetic model membranes for studying membrane phase behaviour and membrane processes, including membrane fusion and molecular recognition. In early 1990s, Pier Luigi Luisi experimentally pioneered the construction of liposome-based cell models in the laboratory at the Swiss Federal Institute of Technology (Zurich). (32) Since then, vesicle-based models have been typically used as materials for cell-mimetic compartments that are also termed as artificial or synthetic cells, offering a promising tool for the insight into the understanding of the working of the living cell. (13, 16, 33)

Traditionally, vesicles have been produced by a method called the gentle hydration, discovered by Bangham in 1964. (34) In this method, phospholipids are first

dissolved in an organic solvent, and then evaporated under vacuum until lipid films are formed on the container surface. After drying lipids, the films are hydrated at temperatures above the phase transition by adding an aqueous solution, forming liposomes finally. However, in this approach, vesicles cannot be produced with high encapsulation efficiency and it is difficult to control over the lamellarity property.

A key step forward was the introduction of electro-formation approach pioneered by Angelova and Dimitrov in 1986. (35) The appearance of electroformation technique has dramatically increased the yield ratio and reduced time for preparation at the temperatures friendly with the biological components. (36) In electro-formation production of vesicles, an alternating current (AC) is applied to the lipid films to enhance the hydration of the lipid films, resulting in tightly controlled sizes of vesicles.

Progress in the application of vesicle-based artificial cell models has been achieved since vesicles can be manufactured in a more controlled manner. (37, 38) It is worth noting that restrictions exist to electro-formed vesicles prepared under physiological conditions or during the inclusion of charged phospholipid (such that lipid asymmetry found in native biomembrane cannot be mimicked using electroformation method). Recent developments in tool technologies have enabled monodisperse and asymmetric lipid vesicles to be engineered by using double emulsions as templates produced by microfluidics. (39, 40) In addition, the encapsulation efficiency of biomolecules into vesicles can be greatly enhanced using microfluidic technologies. The formation mechanism relies on the generation of water-in-oil-in-water double emulsions, where bilayer building blocks are dissolved in the oil phase. The residual volatile solvent in the oil phase is removed subsequently leading to the formation of the vesicle bilayers. Vesicles constructed using such double-emulsion templated approaches have been shown to be capable of performing as cell-like compartments. (38)

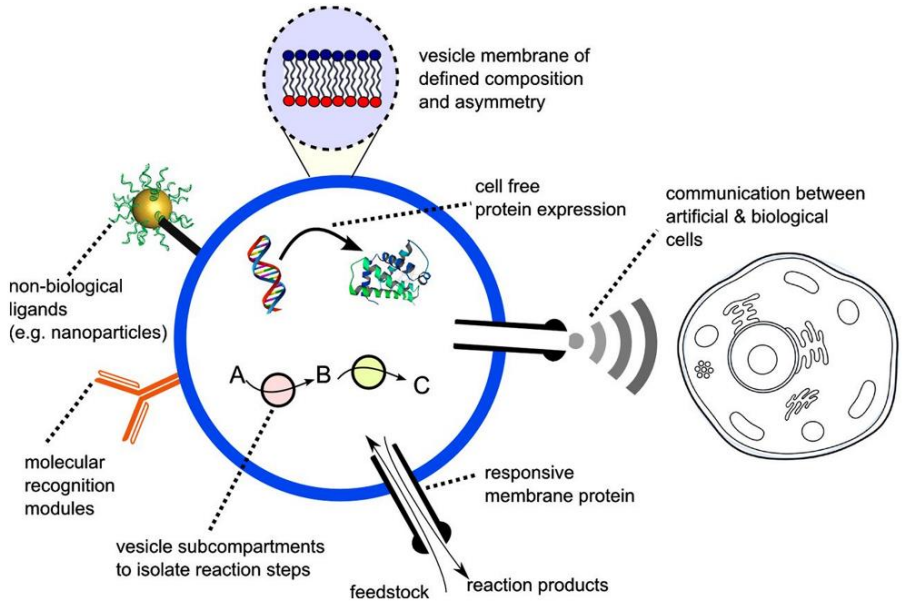

Figure 1.7 Schematic illustration of applications of vesicle-based artificial cells. Image taken from (18).

Cell-like systems templated by vesicular architectures have been variously incorporated into either synthetic or biological modules, endowing the structures' functionality, Figure 1.7. For example, high loading efficiency method enables vesicles containing cell-free protein synthesis machinery to investigate the proteins of interests; by reconstituting biological components into bilayers, essential cellular processes can be recreated, including the uptake of nutrients and the expulsion of waste, intracellular singling processes, commutations with natural cells and cell replication and division into daughter cells. (18, 41)

1.3 Microfluidics

Microfluidics is a science and technology of systems that deals with the control and manipulation of fluids of small volumes down to less than picolitres, that are geometrically constrained in chips at a microscale. (42, 43) The chips are often comprised of micro-sized channels and an individual micro-fabricated chip is integral to multiple laboratory functions enabling better analytical performance in high speed,

precise data collection, low sample consumption and minimal exposure to hazardous materials. (44) Such features have paved the way for the large numbers of applications of this technology span across science, for instance in biology, (45, 46) chemical, (47) and biomedical context. (48) Thus, this fascinating technology has shed light on multidisciplinary research from physics to synthetic biology.

1.3.1 Droplet-based Microfluidics

One subcategory of microfluidics is droplet-based microfluidics, which involves the generation and manipulation of discrete droplets with the use of immiscible phases inside microfluidic devices. (49, 50) Although the technology is still in its relative infancy, microfluidics was initially concerned with continuous flowing streams of miscible fluids. Droplet-based microfluidics has emerged from this, motivated by the construction of uniform-sized droplets with nanolitre volume as reactors for micrometre-scale total analysis systems (μTAS) research and fabrication of particles templated by droplets for materials research. (51) In the past decade, several groups have made an impressive success of droplet-based microfluidics in generating emulsion systems as novel micro-environments. (52, 53) Further, scientists from interdisciplinary background are taking the opportunity to engineer the cell-like architectures (synthetic cells) using a bottom-up approach by means of droplet-based microfluidics to study living cells. (41, 54)

The fabrication of microfluidic devices is the first principle step in droplet microfluidics. To produce and control droplets and further achieve specific functions, the devices should be designed with a defined geometries and physicochemical properties, especially the surface properties. (55, 56) This requires demand-driven selection of materials determined by fabrication methods. At present, there are several types of manufacturing techniques for microfluidic chip fabrication; in droplet-based microfluidics, soft lithography and assembly of glass capillaries. (52, 57)

Soft lithography was first proposed by Whitesides and his team members (Harvard University) and refers to a set of techniques for fabricating structures using an elastomeric material. Typically, the elastomer is poly(dimethylsiloxane), PDMS, which widely used for fabricating microfluidic chips in cellular applications because its nontoxicity and permeability to gas as well as being optically transparent for visualisation. The PDMS microfluidic chips are usually manufactured using following procedure. The liquid PDMS pre-polymer is cast into a silicon or photoresist mould fabricated by a photolithography process and treated by exposing to a vapour of fluorinated silane - which is used to prevent irreversible bonding to the PDMS. The pre-polymer is then degassed and then cured into solid PDMS before being peeled off the master. PDMS can be bonded irreversibly to substrate surfaces, such as glass after exposure to an oxygen plasma, Figure 1.8. Even with these advantages, PDMS is limited by the ease of surface property modification and the poor chemical compatibility with organic solvents. In addition, PDMS absorbs small molecules on its surface and is intolerant to high pressure, which results in damage of the microchannel geometry.

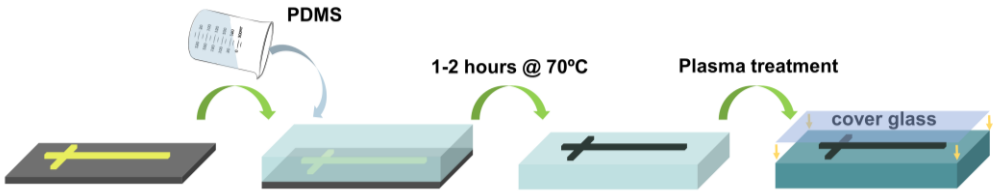

Figure 1.8 Schematic illustration of soft lithography for fabricating PDMS microchannel. Image is modified from (58).

Glass capillary microfluidic devices have superior optical and chemical properties and offer 3D symmetrical microchannels of which the surfaces can be straightforward functionalised. Weitz et al. from Harvard University have established an explicit droplet microfluidic system that aligns tapered round glass capillaries within a square capillary, which are then assembled on a glass slide as a whole, as

depicted in Figure 1.9. (52, 59, 60) The coaxial geometry is ensured by the size match between the outer diameter of the circular capillary and the inner diameter of the square capillary. In these capillary-based devices, the 3D configuration provided by the coaxial system allows the generation of droplets in either hydrophobic or hydrophilic systems, Figure 1.9(A). Moreover, by means of a complex design, capillary channels can align into sequential insertion or multichannel injection regimes for complex structure construction, Figure 1.9(B, C).

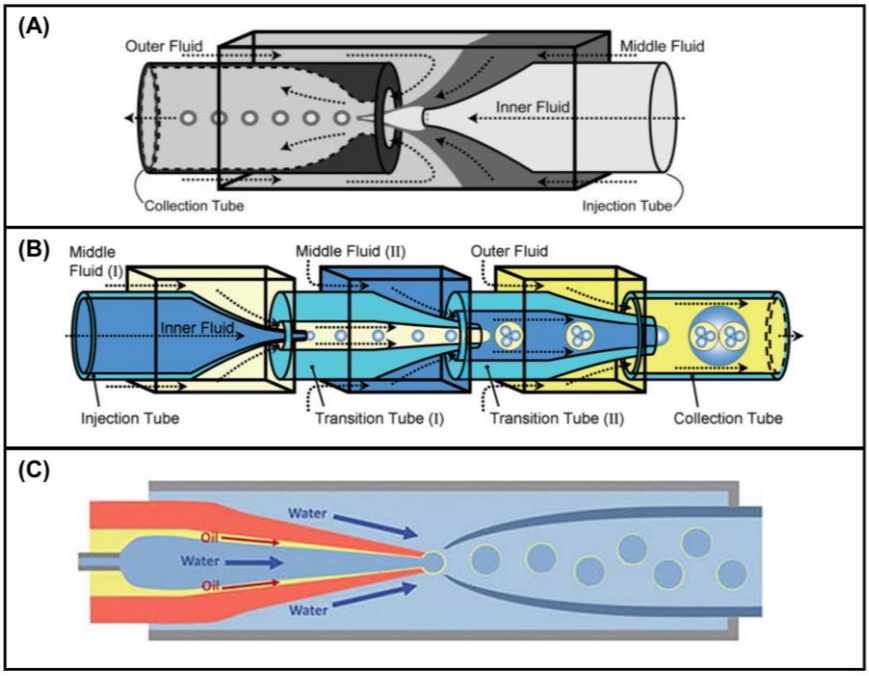

Figure 1.9 Schematic demonstration of three types of microfluidic chips fabricated by coaxial assembly of size-matching cylindrical and square capillaries. Image taken from indicated references. (52, 59, 60)

In terms of formation of droplets within microfluidic devices, depending on the specific design of the microfluidic channels and fluid configurations, droplet generation can be categorised into cross-flow, flow-focusing and co-flow techniques, Figure 1.10. In cross-flow, T-junction is the most common geometry used to generate droplets, in which the dispersed and continuous phases meet at an angle,

Figure 1.10(A). (61) In the flow-focusing geometry, the two immiscible phases are hydrodynamically focused and generate an elongation filament when passing through a contraction, then eventually forms into droplets, as illustrated in Figure 1.10(B). (62) Co-flow streams, Figure 1.10(C) are produced by using a set of coaxial microchannels where the dispersed and continuous fluids meet in parallel in the same direction. (63) This format of droplet microfluidics is typically achieved by a set of capillary-based devices, in which the size of droplets can readily control by altering the flow rate of continuous fluid with the viscous shear stress applied to the dispersed phase.

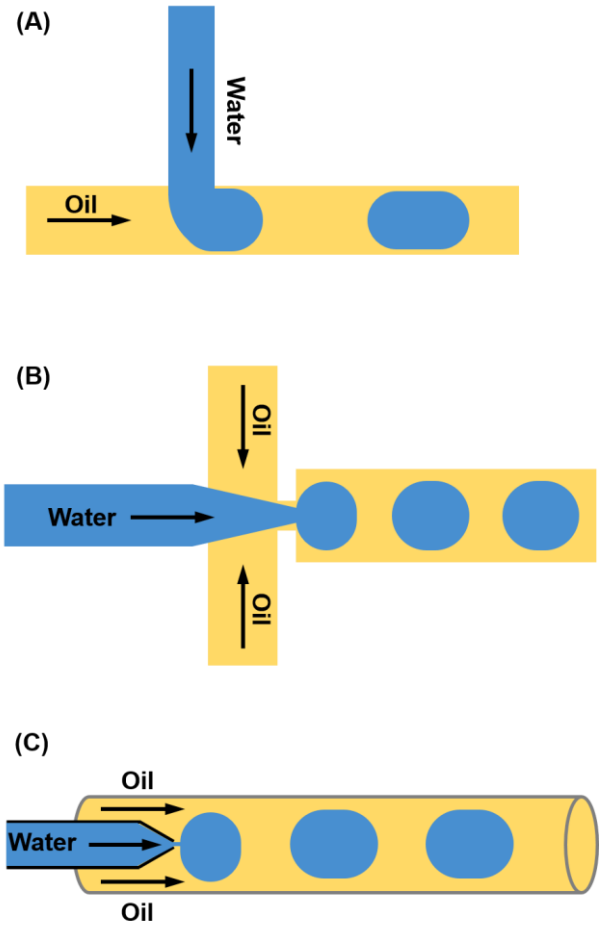

Figure 1.10 Three geometries of microfluidic drop generators: (A) Schematic of T-junction droplet microfluidics; (B) Schematic of flow-focusing droplet microfluidics; (C) Scheme of coflow droplet microfluidics.

1.3.2 Droplet-based Microfluidics in Artificial Cells

The droplet-based microfluidic technique enables the construction of microscale materials, such as water-in-oil-in-water double emulsion droplets, that mimic cell functions and features, or in other words artificial cells. The study of artificial cells is promoted by the abilities of compartmentalisation, high-throughput generation and monodispersity of droplet microfluidic technology, which have expanded the scope of engineering highly controlled cell-like systems as synthetic cells that are assembled by simple building blocks from the bottom-up. By taking the advantages of droplet microfluidics, not only can the size, shape and lamellar nature of artificial cells be readily customised according to experimental conditions, but the membrane composition with asymmetric lipid arrangement and functional complexity of cell-mimics can be engineered. Although a large number of microfluidic approaches for the assembly of artificial cells have emerged, sophisticated artificial cells have not yet been assembled using the indispensable tool of droplet-based microfluidics.

1.4 Thesis Aims

The core objectives of this thesis are to construct and study synthetic cells by using microfluidic technologies in synthetic biology in order to synthesise membranes that at their interface mimic living cells. The first key research area investigated is the development of microfluidic techniques to design novel geometries and in so doing generate new cell-like systems. The second area of research concerns the characterisation of artificial membrane fluidity based on molecular rotors. The aims of the thesis are as follows.

1. To design new microfluidic devices to prepare double emulsion droplets with ultra-thin membranes.

2. To use thin-shelled double emulsion droplets as templates to form either lipid vesicles or polymeric vesicles.

3. To use these lipid vesicles and polymersomes as artificial cellular systems to perform *in vitro* transcription and translation.

4. To develop a Fluorescence Lifetime Imaging Microscopy system to determine ability of molecular rotors to reveal on artificial cell membrane viscosity.

5. To design and fabricate of a new microfluidic device to build artificial cell chassis with asymmetric arrangement in composition within the bilayers.

1.5 Thesis Outline

This thesis is organised in six Chapters, which are structured as follows.

Chapter 2 gives the theory background of the fluorescence as well as the advanced fluorescence imaging techniques: Confocal Laser Scanning Microscopy and FLIM. The fundamental theory of the fluid mechanics at microscale for microdroplet formation.

Chapter 3 details work relating to the construction of lipid vesicles and polymeric vesicles based on thin-shelled double emulsion droplets that are generated by microfluidic technique and introduction biological functionalities (*in vitro* transcription and translation) into these cell-like compartments, transforming them into artificial cells.

Chapter 4 describes the utilisation of a FLIM system to perform measurements on the BODIPY based molecular rotor in artificial cell membrane synthesised in the microfluidic device.

Chapter 5 outlines the development of the microfluidic strategy to generate vesicle-based cell-mimic systems with asymmetric bilayers at high-throughput.

Chapter 6 summarises the presented work and indicates some of the avenues that future works could focus on.

Chapter 2 Instrumentation and Theory of Techniques

2.1 Fluorescence Microscopy of Biomembranes

Biological research has benefited from the advance of key methodologies. In fact, it was the development of microscopy by Robert Hooke in 1665 that shaped and deepened our understanding of cells as the basic units of living systems. (64) Biological membranes play a significant role in cell structure, shape, and functions. At its most basic level, the biomembrane encloses the cell and isolates its interior from the outer environment. Nowadays, it is well recognised that biological membranes are highly heterogeneous systems in which embedded molecules show complex diffusion behaviours and change of spatiotemporal organisation in response to signals, rather than the simplistic picture of "fluid mosaic model". Fluorescence spectroscopy and microscopic techniques are central to the elucidation of biological membranes' properties, which are attributable to the sensitivity to access the single molecule level, and the large spatial resolution. This powerful widely used method has propelled modern biomembrane studies to fully new levels. (65-68)

2.1.1 Fluorescence

Since Sir John Herschel made the first observation of fluorescence from his quinine sulfate in tonic water as it was illuminated by sunlight in 1845, (69) the phenomenon known as fluorescence has been a long-standing interest in the use of studying the structure and functioning of biomembranes. (65, 70, 71) Fluorescence is a process in which light is emitted from molecules after photons of light are absorbed. The molecules that exhibit fluorescence are called fluorophores or fluorochromes. Upon the absorption of a photon of light, a range of photo-physical processes take place within fluorophores, which are demonstrated in the Jablonski energy diagram in Figure 2.1.

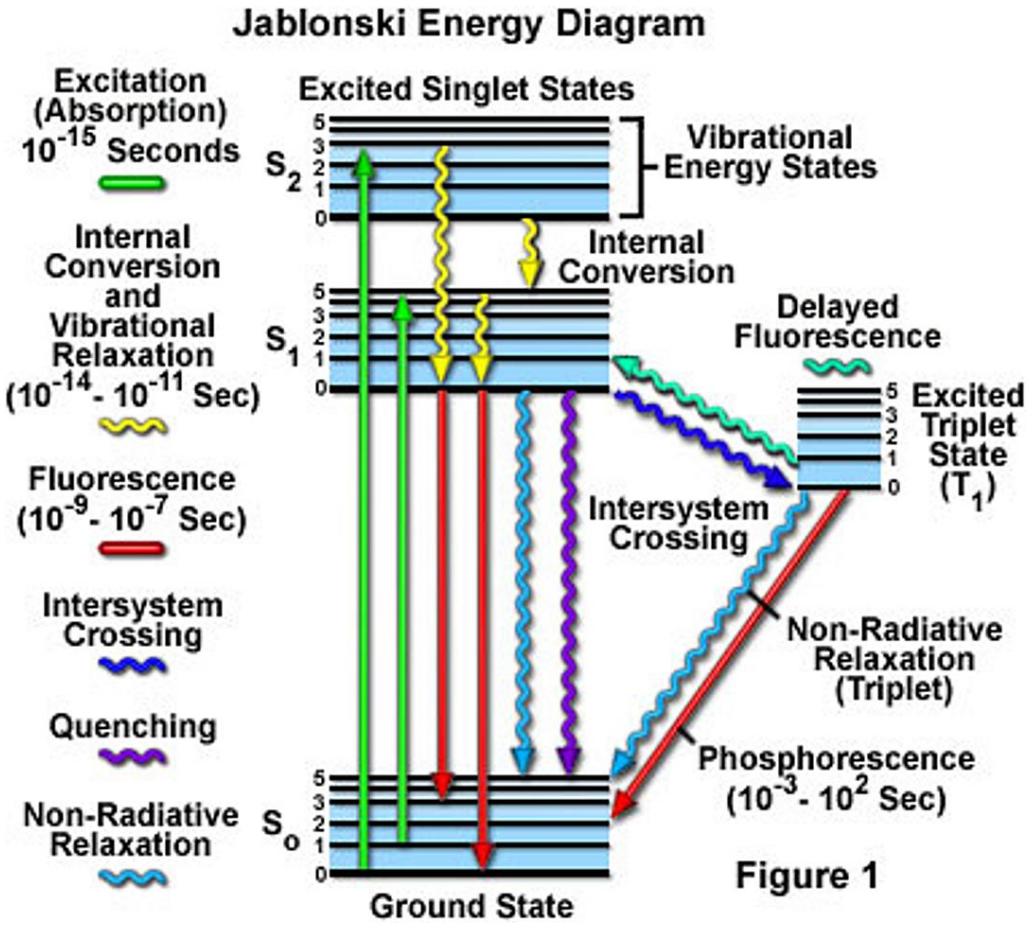

Figure 2.1 Jablonski energy diagram. Graphic demonstration of the paths that electrons, after excitation at the light of the corresponding wavelength, go back to their previous ground state (S_0). Absorption of light occurs in 10^{-15} seconds. In the case of fluorescent light emission, the process is rapid and it takes 10^{-9} seconds whereas the phosphorescent emission is slower taking 10^{-3} - 10^{-2} seconds. Image taken from (72).

When a photon is absorbed, orbital electrons in fluorophores are elevated to higher energy levels. In Figure 2.1, the thick black lines illustrate the electronic states and thinner lines represent the vibrational states. If the transition is associated with absorption or emission of a photon, the transitions between the states are illustrated as straight arrows. Transitions that results from a molecular internal conversion or non-radiative relaxation process are shown as wavy arrows. (72) Excitation of a fluorescent molecule by an incoming photon occurs on the order of 10^{-15} seconds,

whereas vibrational relaxation of excited state electrons to the lowest energy level, S_1, is much slower and can be assessed in 10^{-12} seconds. The final process, emission of a longer wavelength light and return of the molecule to the ground state, S_0, happens in the relatively long time frame of 10^{-9} seconds.

One pathway for molecules to react as a result of the energy received from photons is to emit a photon, termed as fluorescence. Electrons decaying directly from S_1 to S_0 emit energy, however in some molecules the spins of the excited electrons can be switched to a triplet state through a process called intersystem crossing, which is an another path a molecule may take in the dissipation of energy. Following this path, the electron changes spin multiplicity from an excited singlet to an excited triplet state. When occupying an excited singlet state, an electron's spin is paired with the ground state electrons. However, when occupying an excited triplet state, an electron's spin is not paired to the ground state. Electrons in an excited triplet state can therefore persist for longer than if they were in an excited singlet state. Inevitable decay to the ground state emits a photon, termed phosphorescence, on a time frame several orders of magnitude slower than fluorescence. Phosphorescent emission usually occurs over a time frame of 10^{-3} – 10^{2} seconds compared to the 10^{-9} second time frame for fluorescent emission, known as the fluorescence time. Excitation to an excited triplet state is far less probable than to an exited singlet state as it involves a forbidden electron spin transition. (72, 73)

The resultant energy associated with fluorescence emission transition as shown in Figure 2.1 is typically lower than that of incident excitation, the resulting emitted photons have less energy and are shifted to longer wavelength. This shift in wavelength is generally known as the Stokes Shift that was first observed and reported by Sir G. G. Stokes in 1852, (74) and is represented in Figure 2.2.

This shift in emitted wavelength is the basis for any technique deriving information as a result of fluorescence. The ability to selectively detect light based on its wavelength enables systems to separate the emitted fluorescence photons from the incident excitation photons.

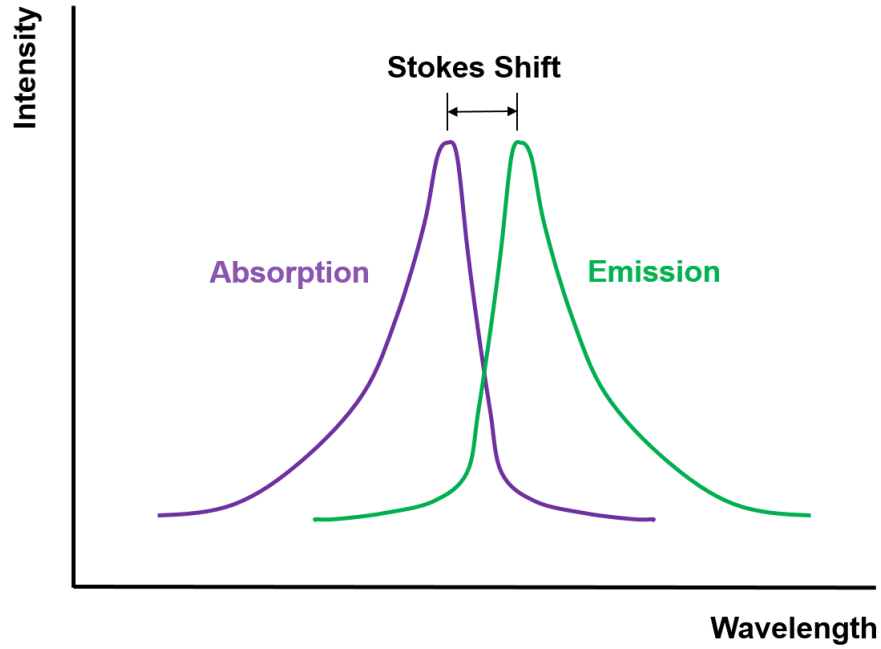

Figure 2.2 Schematic illustration of stokes shift spectra. Shift in excitation and emission spectra due to loss of excitation energy by electron relaxation and intramolecular vibration taking place between the different excited states.

Many factors affect the fluorophore performance as related to fluorescence. Amongst the most important are: the fluorescence quantum yield, φ , the fluorescence lifetime, τ_L and the extinction coefficient, ε. (70)

The fluorescence quantum yield of a fluorophore is the ratio of fluorescence photons emitted to photons absorbed. Quantum yield values below 1 occurs and results in the loss of energy through non-radiative pathways, such as heat or a photochemical reaction, rather than the radiative pathway of fluorescence. The quantum yield, φ, is dependent on the constants of radiative rate, k_r, and non-radiative rate, k_{nr}, shown in Equation (2.1).

$$\varphi = \frac{k_r}{k_r + k_{nr}} \tag{2.1}$$

The fluorescence lifetime (τ_L) is theoretically defined as the average time the molecule spends in the excited state prior to return to the ground state. Generally, fluorescence lifetimes are of the order of a few nanoseconds and are reciprocally proportional to the sum of the radiative (k_r) and non-radiative (k_{nr}) rate constants:

$$\tau_L = \frac{1}{k_r + k_{nr}} \tag{2.2}$$

The radiative decay rate is an intrinsic property of the fluorescent molecule; however, the non-radiative decay rate can be affected by the environment in which the fluorophore resides. Various processes are known to alter this pathway such as: internal quenching, dynamic quenching, and energy transfer. (75)

The third key parameter relating to a molecule's fluorescence is the extinction coefficient. This is a measure of the efficiency of a fluorophore to absorb a photon of light at a certain wavelength and is denoted as ε, in units of $M^{-1}cm^{-1}$. The value of ε is specified for the absorption maximum wavelength and typical values are found between 25,000 to 200,000 $M^{-1}cm^{-1}$. Larger extinction coefficients indicate that the absorption of a photon in a given wavelength region is more likely.

2.1.2 Fluorescence Microscopy

The technique of fluorescence microscopy has become an essential tool in biology and biomedical science due to its unique attributes that are not readily available in other contrast modes within conventional optical microscopy. Using fluorescence instead of, or in addition to, reflection and absorption facilitates the study of labelled biological molecules in samples with spatial and temporal resolution at the single cell level. The microscopy techniques exist in numerous forms and configurations with advantages depending on the desired applications.

Most fluorescence microscopes commonly used in biology are based upon the epifluorescence configuration, where "epi" is from the Greek to mean "same". In

this arrangement, both the illuminated and emitted light travels through the same objective lens. Key to the function is a dichroic mirror (No. 3 below). The fluorescence passes emitted by the specimen is focused on the detector or a camera by an objective lens that is also used for the excitation light being guided into. (66) The basic configuration can be seen in Figure 2.3.

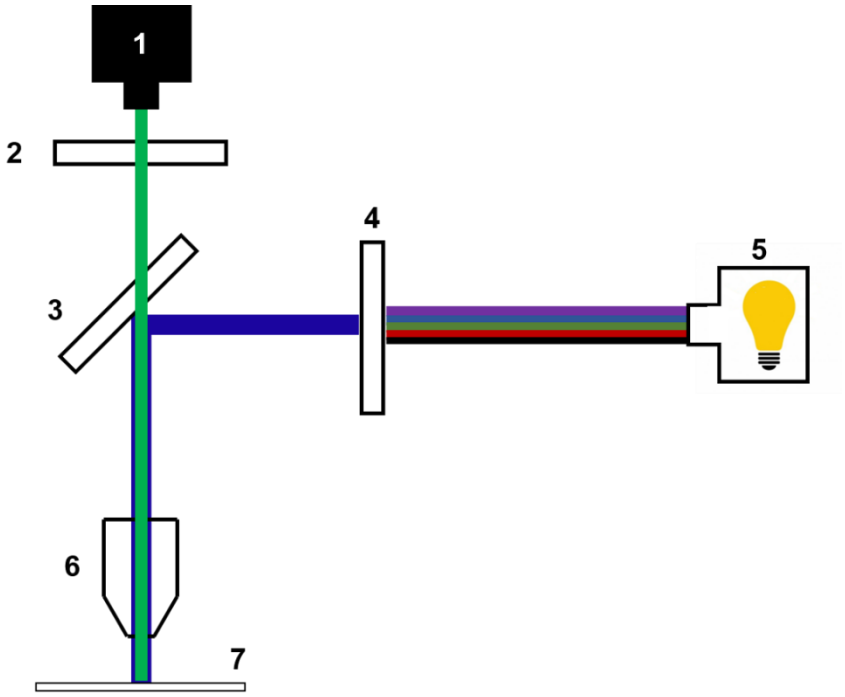

Figure 2.3 Epifluorescence microscope. 1 – Detector which is typically a CCD. 2 – Emission filter passing fluorescence light only. 3 – Dichroic mirror separating excitation light from fluorescent signal. 4 – Excitation filter. 5 – Light source typically a mercury arc light source. 6 – Objective lens. 7 – Sample.

Typically, the light from the source, which is placed vertically to the optical path, passes through an excitation filter and hits a special mirror called a chromatic beam splitter, also known as a dichroic mirror. The dichroic mirror is positioned above the objective lens and oriented at 45° to the light beam. The dichroic mirror has a special interference coating, which reflects light with wavelength shorter than a certain wavelength and transmits light of longer wavelength. Thus the higher energy

excitation light is reflected and directed through the objective lens towards the specimen. The emission light passes back through the objective lens to the dichroic mirror. The emitted light has a longer wavelength than the excitation light and is instead transmitted. Incident emission light with shorter wavelength that is reflected by the sample is not able to pass through the dichroic mirror and will be blocked. If the excitation light is able to pass through the dichroic mirror it will be further filtered by a barrier or emission filter before reaching the eyepiece or camera. (71, 76) Although epifluorescence microscopy has several advantages, such as low cost of set up with fast temporal resolution, providing good XY dimension resolution, all of the emitted fluorescence light is integrated through the specimen in the Z dimension collected by the detectors. Therefore, it is difficult to tell where the fluorescence from a point in the sample originated in the Z dimension. (77)

2.1.3 Confocal Laser Scanning Microscopy (CLSM)

Confocal microscopy is a technique first developed in 1957 by Marvin Minsky. It is capable of imaging optical sections of biological samples and overcomes the limitation of conventional fluorescence microscopy. (78) This is achieved by means of using a point illumination source and a pinhole in an optically conjugate plane in front of the detector to filter out-of-focus signals. As a result, only light emitted by fluorescence close to the focal plane can pass the pinhole, thus resolving an image of the specimen at a particular depth as depicted in Figure 2.4.

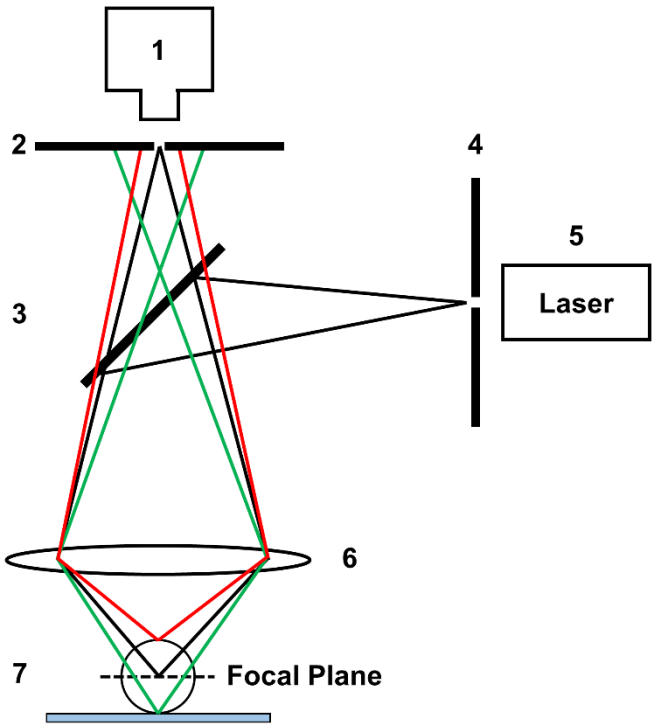

Figure 2.4 Confocal laser scanning microscopy. 1 – Detector. 2 – Confocal aperture. 3 – Dichroic mirror. 4 – Illuminating aperture. 5 – Point source. 6 – Objective lens. 7 – Sample; Principle of confocal detection optics. Fluorescence light is collected by the objective lens and directed to the detector via a small pinhole. The pinhole blocks light that does not originate from the focal plane creating a thin optical section. The red and green lines represent fluorescence originating from out of focus regions, whereas black line represents fluorescence light originating from focal plane in the sample.

A laser is used to provide coherent light that interacts with two mirrors that directs the light to the sample and scan the laser across the sample. A microscope objective lens is adopted to focus the laser beam onto the specimen, where it excites fluorescence. As the laser is reflected by the dichroic mirror and scanned across the specimen in a defined focal plane, secondary fluorescence emitted from points on the specimen (in the same focal plane) pass back through the dichroic mirror and are focused as a confocal point at the detector pinhole aperture. (79) However, as a

significant amount of the fluorescence light from the specimen is blocked at the pinhole in front of the detector, this increased resolution is at the cost of decreased signal intensity, thus long exposure time are often required while operating a confocal microscope. To aid sensitivity, the fluorescence light is typically detected by a sensitive detector, usually a photomultiplier tube (PMT) that transforms the light signal into an electrical one that is recorded by a computer. (77) Due to the advantages of the confocal microscopy imaging technique, biomembrane research has been boosted in recent decades, such as in the study of the phase separation of lipid mixtures in artificial membranes, (80) asymmetry feature of biomembranes, (81, 82).

2.1.4 Fluorescence Lifetime Imaging Microscopy (FLIM)

Fluorescence lifetime imaging microscopy (FLIM) has emerged as a reliable imaging technique driven by measurement of the fluorescence lifetime of molecules. The first instrument integrating time resolved fluorescence spectroscopy with microscopy dates back to 1959, (83) but only single point measurements could be done. In 1989 an instrument enabling spatially resolved lifetime measurements was introduced. (84) Since then, a variety of fluorescence lifetime microscopy tools, mainly utilised for biomedical applications, have been developed independently by several groups. As detailed above, optical imaging techniques especially fluorescence imaging tools are widespread techniques in the biological and biomedical application. These standard fluorescence microscopies rely on generation of contrast in images through manipulation of the fluorescence intensity, which can be acquired from absorption, polarisation and fluorescence parameters in a fluorescence microscope. (70) However, fluorescence intensity is intrinsically dependent upon various environmental factors, such as the concentration of the fluorophore, quenching by other molecules, aggregation and energy transfer, and can therefore provide incorrect quantitative results and be open to misinterpretation.

FLIM provides contrast according to the fluorescence lifetime of a fluorescent molecule. The fluorescence lifetime depends upon the intrinsic characteristics of the

fluorophore itself and is mostly independent of its concentration. The lifetime of a fluorescent molecule is sensitive to its local environment in general, the local viscosity, pH, temperature as well as interactions with other molecules. (75) What makes FLIM such an attractive technique for imaging intricate systems where control over probe distribution is difficult is the fact that the property of the lifetime is unaffected by the probe concentration and photobleaching. Theoretically, the fluorescence lifetime is defined as the average time a fluorophore spends in the excited state before emitting a photon and returning to the ground state and this is characterised by the decay of fluorescence intensity upon excitation. This decay of the excited state of a fluorescent molecule to the ground state is defined as:

$$I(t) = I_0 e^{\left(\frac{-t}{\tau}\right)} \tag{2.3}$$

where I_0 represents the intensity at time zero, just after excitation and τ indicates the fluorescence lifetime.

FLIM techniques can be classified according to the two major methods of data acquisition: time-domain FLIM and frequency-domain FLIM. In this chapter, the fundamental theory of time-domain FLIM will be discussed as time-domain FLIM as this is the technique used in this thesis. In the time-domain method, the fluorescent probe is excited by a short laser pulse that is usually applied repetitively in the MHz ranges. The time-dependent emission intensity is measured against time, and the decay time is determined from the slope of the decay curve, Figure 2.5. There are two fluorescence detection methods are available for time-domain lifetime measurements, of which, time-correlated single photon counting (TCSPC) enables simple data collection and enhanced quantitative photon counting. (85)

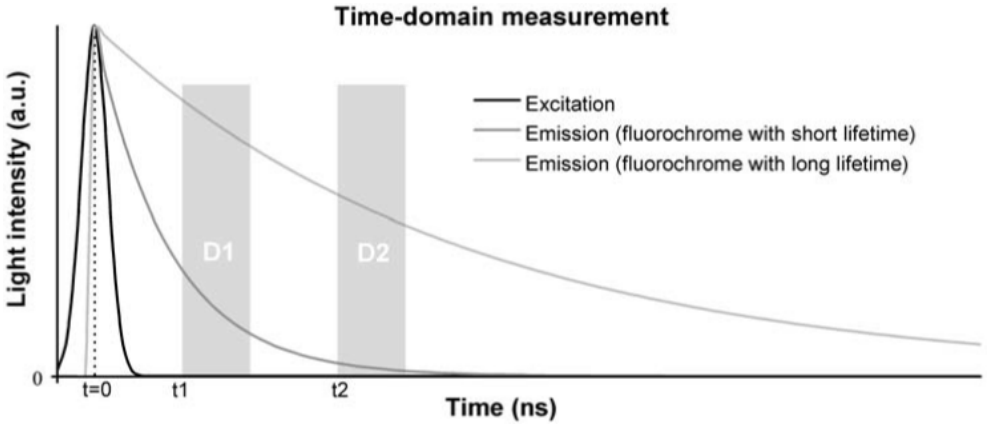

Figure 2.5 Principle of time-domain lifetime measurement. Fluorophores are excited using a short pulse of laser, after which the emitted fluorescence is measured time-resolved. Image taken from indicated reference. (86)

2.1.4.1 The Principle of TCSPC

TCSPC based FLIM systems are sensitive techniques that provide high precision fluorescence decay data from even just a few hundred photons. (87) TCSPC is based on the detection of single photons of a periodic light signal, the measurement of the detection time of an individual emitted photon, and the reconstruction of the waveform from the individual time measurements. (88) Excitation is enabled by using a short flash of light through commercially available, affordable laser diode sources presently offering repetition rates up to 100 MHz with extremely short pulse widths. The resultant fluorescence is most frequently detected by a highly sensitive photomultiplier tube (PMT) that is designed for low level detection of light. Single photons can also be detected by semiconductor diodes which can operate in the triggered avalanche mode, single-photon avalanche diode (SPAD). In Figure 2.6, the detection of photon events relative to the high repetition rate optical signal is demonstrated.

Figure 2.6 (A) shows the stream of excitation originated from a high repetition laser diode at 40 MHz in this case. The photon detection rate shown in trace, Figure 2.6(C), is about 10^7 s^{-1}, which is on the order of the maximum possible detection rate

of most photon counting detectors. It can be seen in Figure 2.6 that, as detection is rather unlikely, the recorded photon stream is a random sequence of uncorrelated events, in contrast to the expected continuous signal of individual decays from each excitation pulse. Thus, the fluorescence decay waveform has to be constructed from the photon density as a function of the time after the excitation pulse.

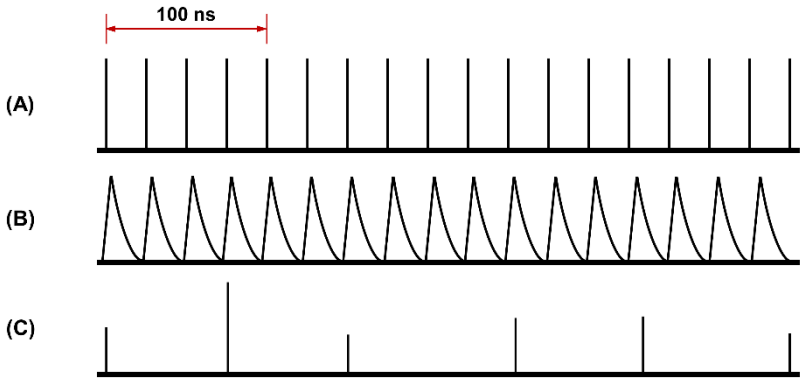

Figure 2.6 Schematic illustration of detection of individual photon events: (A) Fluorescence of a sample is excited by a laser of high repetition rate (40 MHz); (B) The expected fluorescence decay waveform; (C) The detection of single photon events representative of a realistic system consists of a few pulses randomly spread over the time axis.

This concept shown in Figure 2.7 is the classic principle of TCSPC. (89, 90) The trace, Figure 2.7(A), illustrates the expected decay waveform within the signal period defined by the high repetition rate of laser. Trace (B) demonstrates a representative distribution of detected photon events within each sample period, continuing for the duration of the acquisition. Histogram (C) reveals the typical result of TCSPC that is the histogram with an exponential drop of counts at increasing times reflecting the fluorescence decay.

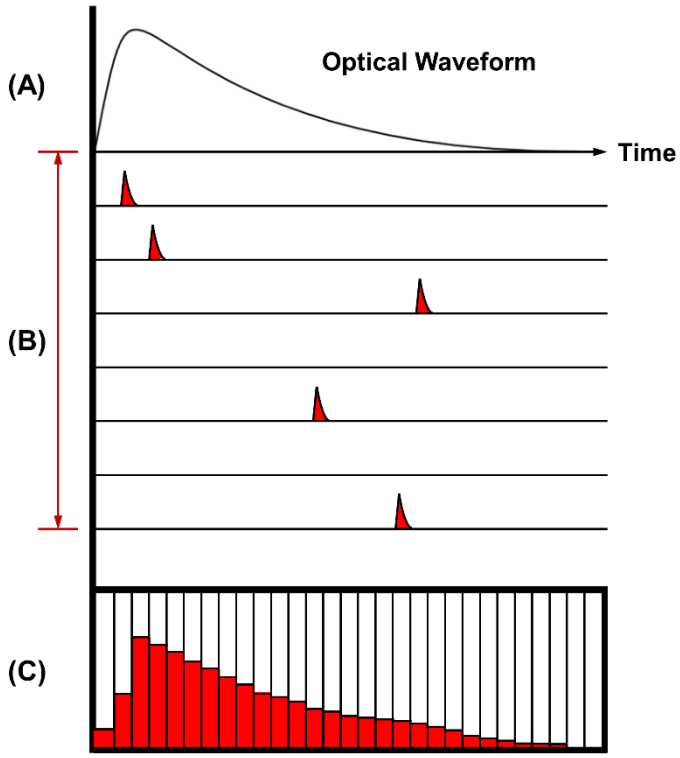

Figure 2.7 Principle of TCSPC: (A) Original decay curve representative of the distribution of photon probability; (B) Individual periods defined by the pulse of a repeating laser signal; (C) The build-up of all detected photon events for a number of time bins after numerous repetitions of the laser pulsed detection period.

2.1.4.2 Exponential Curve Fitting

In all time-domain based FLIM measurements, once the data has been acquired the information is interpreted and analysed by fitting to exponential decay functions. A single exponential of fluorescence decay is observed from a single molecule, or a homogeneous sample in which all fluorescent molecules within are observed under the same environment. Decay functions of complex samples of different molecules or of molecules within spatially resolved location are sums of exponential functions with different decay times. The model functions used in fluorescence lifetime analysis for a single, double and triple exponential systems are shown below.

Single exponential model:

$$f(t) = e^{-t/\tau} \quad (2.4)$$

Double exponential model:

$$f(t) = a_1 e^{-t/\tau_1} + a_2 e^{-t/\tau_2} \quad (2.5)$$

Triple exponential model:

$$f(t) = a_1 e^{-t/\tau_1} + a_2 e^{-t/\tau_2} + a_3 e^{-t/\tau_3} \quad (2.6)$$

The models are characterised by the measured lifetimes of the exponential components, τ_i, and the amplitudes of the exponential components, a_i. In principle, models with any number of exponential components can be defined, thus most of modern FLIM image analysis software packages are able to fit up to 3 or 4 exponential decay components. However, higher-order models with more than 4 components require significant signal resolution in order to accurately fit each component curve uniquely. In practice, the accuracy of the interpretation of such complex data can be difficult to obtain. Therefore, FLIM analysis does not use model functions with more than three components. (87)

2.1.4.3 The Instrument Response Function (IRF)

In a real FLIM system the fluorescent molecules are excited by laser pulses of non-zero width, and detected by a detector that has a temporal response of non-zero width. These factors must be considered when operating FLIM systems and analysing fluorescence decay functions. To compensate for these elements in practical measurements, the instrument response function (IRF) which describes the spread of photon arrival times due to purely instrumental effects, including the detector, laser profiles and any optical reflections within the system, must be known. Thus, the IRF is central to the correct analysis of FLIM measurements as it takes into account anything that will alter the shape of the measured fluorescence decay

function. The convolution of the IRF with the decay function results in the recorded decay function. Mathematically, this can be expressed as:

$$f_m(t) = \int_{\tau=0}^{t} f(\tau) IRF(t-\tau) d\tau \quad (2.7)$$

where $f_m(t)$ is the measured fluorescence function and $f(\tau)$ represents the true fluorescence decay function. In the above convolution integral, $f_m(t)$ is not accurately known as a result of systematic noise in photon detection. The standard approach to obtain final fitted function is to convolute both the IRF and the defined model exponential fluorescence decay function as shown in Equations (2.4 – 2.6). (89) By using DCS – 120 Confocal Scanning FLIM System the IRF can be measured at a width of only a few tens of picoseconds with detection of a pulse directly from the illuminating source. The FLIM image analysis software packages have the ability to use a measured IRF that can be deconvoluted from the recorded fluorescence decay function delivering correct lifetime data.

2.2 Theoretical Background

2.2.1 Physical Background of Microfluidics

The term microfluidics refer to the science and technology that deals with the flow of liquids inside micrometre-size channels, and is utilised as systems to manipulate fluids of small amounts, generally on the nanolitre scale and below. (43) The dimensions of microfluidic systems exploit the counter intuitive characteristics of fluids at these scales. The fluid motion in a micrometre-size channel can be represented by laminar flow. (91)

By controlling and understanding fluid dynamics and chemical composition, it has been demonstrated that microfluidic devices are able to fabricate emulsions, which are structures of two immiscible fluids mixed together, where one fluid is dispersed in the form of small droplets inside the other fluid. To understand the behaviours of

fluids at the micro scale, and the formation of microdroplets within devices, it is necessary to be familiar with the underlying physics of fluid mechanics.

The first fundamental equation of fluid mechanics for the most general case of motion of a material is expressed by the continuity equation, which expresses the conservation of mass, as shown:

$$\frac{\partial \rho}{\partial t} + \nabla \cdot (\rho \mathbf{u}) = 0 \tag{2.8}$$

In many cases, especially in microfluidics, where the flow velocities are much smaller than the sound velocity in the liquid. Thus, the fluid can be treated as being incompressible. Considering a constant density in space and time, and the continuity equation (2.8) becomes

$$\nabla \cdot \mathbf{u} = 0 \tag{2.9}$$

For a Newtonian fluid, the velocity field obeys the Navier-Stokes equation, Equation (2.10), which essentially represent the continuum version of Newton's 2nd Law $(\mathbf{F} = m\mathbf{a})$, on a per unit volume basis:

$$\rho \left(\frac{\partial \mathbf{u}}{\partial t} + \mathbf{u} \cdot \nabla \mathbf{u} \right) = -\nabla p + \eta \nabla^2 \mathbf{u} + \mathbf{f} \tag{2.10}$$

where ρ is the fluid density (Kg m^{-3}), $\mathbf{u}$ is the flow velocity (m s^{-1}), p is the pressure (N m^{-2}), η is the fluid viscosity (Pa s) and $\mathbf{f}$ represents the sum of the body forces (N). As previously stated, for an incompressible fluid, where the density is considered uniform in every part of the fluid so that in microfluidic devices inertial forces are small compared to viscous forces and thus the nonlinear term can be neglected, the equation can be simplified to the Stokes equation, Equation (2.11):

$$\frac{\partial \rho}{\partial t} + \nabla \cdot (\rho \mathbf{u}) = 0 \tag{2.11}$$

In fluid dynamics, the ratio of inertial and viscous forces is represented with the dimensionless Reynolds number (Re), Equation (2.12), which is the one most often mentioned in connection with microfluidics defined as:

$$\mathrm{Re} \equiv \frac{\rho U_0 L_0}{\eta} \tag{2.12}$$

where ρ is the density, U_0 is a the fluid velocity and L_0 is a characteristic length. For common microfluidic devices, the Reynolds number can be estimated. Considering water as the working fluid, typical velocities in the range between 1 μm s^{-1} – 1 cm s^{-1}, and channel radii of 1 – 100 μm, the Reynolds numbers range between 10^{-6} and 10. With these low values of Re, microfluidic systems are able to exploit linear regular deterministic flows.

In the form of laminar flow two streams flowing side by side will flow parallel to one another, and mixing between them will occur via diffusion. Figure 2.8 depicts this regime.

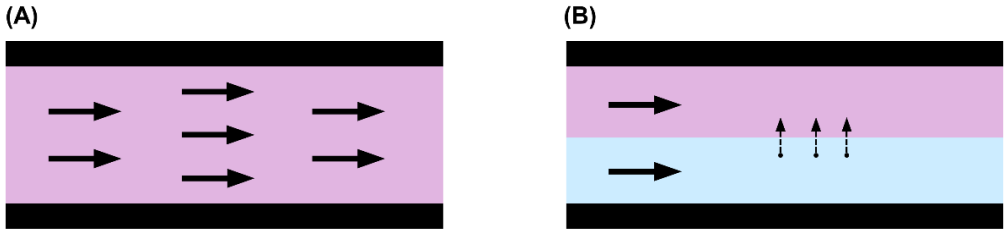

Figure 2.8 Schematic of laminar flow: (A) Schematic depiction of laminar flow; (B) In laminar flow, two streams flowing parallel to each other with only mix through diffusion (black dotted arrows).

Typically, when Re $<$ 2300 viscous forces dominate, leading to laminar flow, which occurs in most situations of microfluidic experiment. The presence of laminar flow

in microfluidic devices has been used for applications such as reagent separation, rapid mixing, and for the creation of concentration gradients. (92)

In the laminar fluid flows that naturally arise in the low Reynolds number world of microfluidics, however, mixing occurs only by diffusion and can therefore result in long mixing times. The dimensionless Peclet number (Pe) expresses the relative importance of convection to diffusion, Equation (2.13).

$$\mathrm{Pe} \equiv \frac{U_0 w}{D} \tag{2.13}$$

where D is the diffusivity of a substance ($m^2\ s^{-1}$), and w is the width of the channel. The interplay of these two effects can be demonstrated in a microfluidic device, called a T-sensor, which is a very useful tool for applications. (93) Furthermore, the relationship between diffusion and convection can also be exploited for sorting and filtering. (94, 95) Thus, low Reynolds and Peclet numbers characterise a laminar flow regime where mixing of two joining fluids is dominated by diffusion.

2.2.2 Physical Background of Microdroplet Formation in Microfluidic Devices

Emulsions, the products fabricated by microfluidics concerned in this thesis, are one form of micro-sized droplets. (96-98) An emulsion is a mixture of two immiscible liquids, where one liquid is dispersed as droplets in another, and has been extensively studied ever since Lord Rayleigh started research on the breakup of fluid jets projected on another fluid in 1879. (99) Early investigations on emulsions all used bulk mixtures of immiscible phases to produce quantities of droplets having a wide range of sizes by shear or impact stresses generated by manual or mechanical agitation. (100, 101)

As previously described in Chapter 1, with the advent of microfluidic techniques, it is possible to produce highly monodispersed microdroplets in high-throughput with size ranging from a few micrometres to hundreds of micrometres, manipulate

individual droplets and precisely control their properties. (101) Generally, the monodispersity of the prepared emulsion is characterised by the coefficient of variation index (CV), shown in Equation (2.14), defined as the standard deviation of the droplet diameters in the emulsion, expressed as a percentage. (102)

$$CV = \frac{1}{\overline{d}}\left[\sum_{i=1}^{n}\left(d_i - \overline{d}\right)^2 \Big/ (n-1)\right]^{\frac{1}{2}} \times 100\% \qquad (2.14)$$

where d_i is the diameter of the emulsion, $\overline{d}$ is the arithmetic average diameter, and n is the number of emulsions measured.

Various methods for droplet formation have been exploited in recent years. All of them have in common a carrier phase, known as a continuous phase, and a dispersed phase which represents the actual fluid of the droplet. The most common strategy of droplet production, which is flow rate-driven flow accomplished using syringe pump, involves the use of immiscible fluids actuated by constant volumetric flow rate (l s^{-1}) of dispersed and continuous phase liquid (Q_D and Q_C).

Between immiscible fluids, a surface tension γ affects the dynamics of the free surface. Todd Thorsen first demonstrated that controlled droplet emulsions in immiscible phases could be created by a microfluidic device, in which viscous shear forces tend to extend and drag the interface, whereas surface tension tends to reduce the interfacial area, shown in Figure 2.9. (103) These stresses destabilise the interface between two immiscible fluids and lead to formation of droplets. (104)

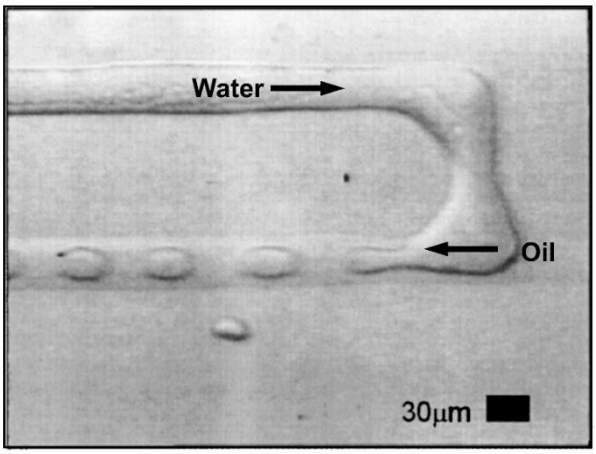

Figure 2.9 Uniform microdroplet generation in a simple microfluidic device. Image taken from (103).

In the understanding of droplet (emulsion) generation within a microfluidic device that comprises two immiscible fluids, the Capillary number (Ca), Equation (2.15), is a dimensionless parameter found whenever interfacial stresses compete with viscous forces. Moreover, the Capillary number is the most important of several key dimensionless parameters that can be used to analyse the relative importance of each of the key forces for droplet breakup. (105)

$$\mathrm{Ca} \equiv \frac{U_0 \eta}{\gamma} \tag{2.15}$$

in which U_0 is the main velocity of the continuous phase in the microfluidic channel, η the viscosity of the outer phase and γ the surface tension between the two fluids. In microfluidic droplet formation, Capillary numbers typically range from 10^{-3} to 10^{1} for flow rates accessible using syringe pumps. Commonly, inertia also plays a role in the droplet production, even if it is the least significant of the three key entities in microfluidics (viscous stress, capillary pressure and inertia). (50, 53)

Different regimes of droplet breakup can be achieved by adjusting the value of the Capillary number, resulting in differing droplet sizes, degrees of monodispersity as well as mechanism of droplet formation, as displayed in Figure 2.10.

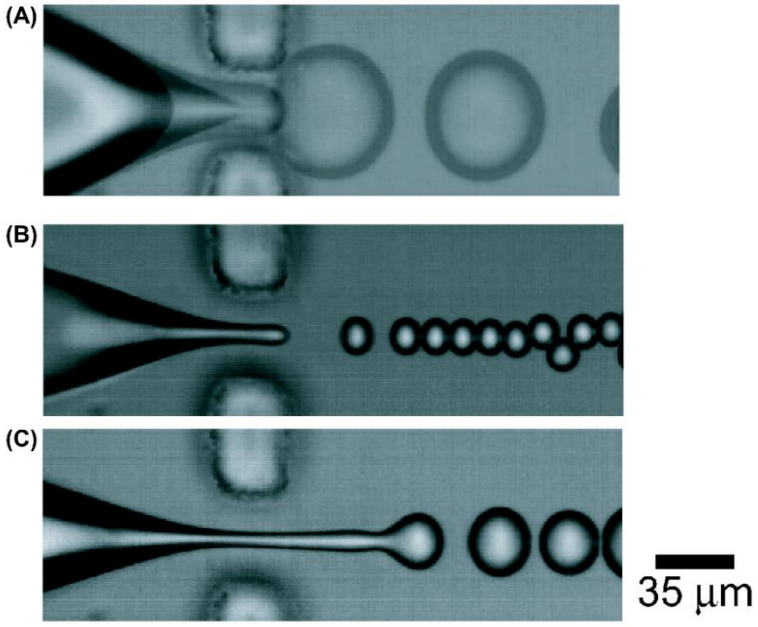

Figure 2.10 Regimes of droplet formation in a microfluidic device, in order of appearance as capillary number increases. Image taken from (106).

When a microfluidic device is operated at low Capillary numbers, droplet generation occurs in the geometry controlled regime, (107) where the minimum droplet size is restricted to the same order of magnitude as the orifice. During droplet formation, the dispersed fluid interface is drawn into the orifice, which forces the continuous phase liquid to flow in a narrow region around the fluid-fluid interface. To maintain the flow rate employed by syringe pumps, the shear force from the continuous fluid is higher in this narrow region, resulting in a pinching of the interface that forms discrete droplets of the dispersed phase. The finger of dispersed phase fluid then retracts back to the position of the orifice and this process repeats itself, exemplified in Figure 2.10(A). With further increasing of the Capillary number, the formation of

droplet occurs into dripping mode, Figure 2.10(B), where the droplets turn out to be smaller than the size of orifice. In addition, the finger of the dispersed phase becomes longer and narrower than the one in the geometry controlled regime. Continuing to increase the Capillary number gives way to the jetting regime shown in Figure 2.10(C), in which dispersed fluid liquid finger extends beyond the orifice and mimics a jet. (52) Typically, the jetting regime is not appropriate in microfluidic experiments as the fluid jet breaks into discrete droplets that are less monodisperse.

2.2.3 Wetting and Dewetting

Wetting is the ability of a liquid to maintain contact with a surface, whereas dewetting indicates the rupture of a thin liquid film on a substrate forming a droplet. In the fabrication of microfluidic devices, it is important to select materials with the right wetting property since wettability of microchannel surfaces has a strong influence on the formation of droplets and determines which liquid phase is dispersed. (105) For instance, in the generation of an oil droplet in a continuous aqueous phase, in order to produce droplets consistently, it is significant that the continuous water fluid preferentially wets the channel surface within the microfluidic device. Additionally, in Figure 2.11, a convex meniscus of dispersed oil phase forms in the microchannel that is helpful for the droplet formation.

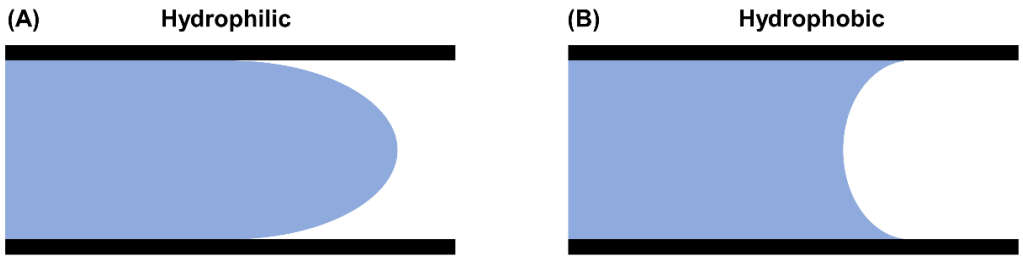

Figure 2.11 Schematic illustration of oil behaviour in hydrophilic and hydrophobic channels: (A) the cohesion forces of molecules of the fluid are higher than adhesion forces to the surface; (B) is the inverse.

Direct measurement of wettability within microchannels is difficult, however it can be indirectly obtained through an assessment of the contact angle θ formed at the liquid-substrate interface, Figure 2.12, where the substrate surface is modified by means of the same method as used for the microchannel. A contact angle of less than 90° (low contact angle) usually indicates a favourable high degree of wetting with fluid spreading over a large area of the surface, displayed in Figure 2.12(A). Contact angles greater than 90° (high contact angle) generally express unfavourably low wetting, so the fluid on the surface minimises contact with the substrate surface and forms a compact liquid droplet. Water solution on the substrate surface, for example, which is with a low contact angle is termed hydrophilic, whereas that with high contact angle is referred to as hydrophobic surface.

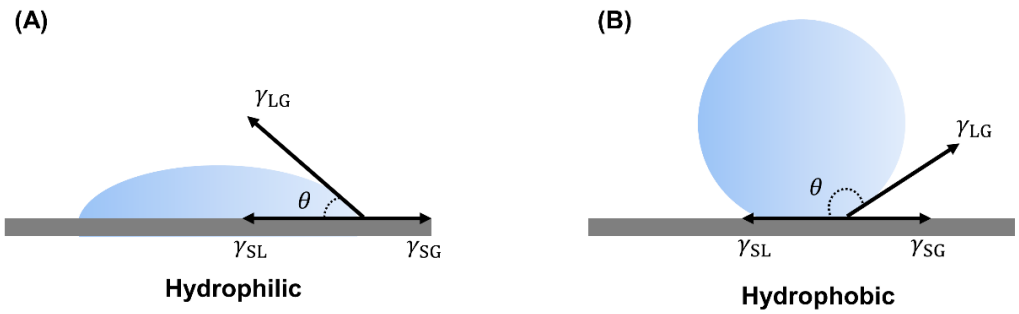

Figure 2.12 Contact angle θ of a water droplet on hydrophilic and hydrophobic surfaces and vectorial representation of surface tension between solid and liquid γ_{SL}, solid and gas γ_{SG} and liquid and gas γ_{LG}.

The contact angle of a liquid droplet on a solid surface can be described by Young's equation, Equation (2.16) first proposed by Thomas Young in 1805. (108) The contact angle is defined by the mechanical equilibrium of droplet under the action of three surface tensions: solid-liquid, liquid-gas and solid-gas.

$$\gamma_{SG} = \gamma_{SL} + \gamma_{LG} \cos\theta \tag{2.16}$$

where γ_{SG} is the surface tension between solid and gas, γ_{SL} is the surface tension between solid, liquid and γ_{LG} is the surface tension between liquid and gas and θ is the contact angle.

The opposite process compared with the wetting of water droplet on the solid surface is dewetting, which is the process that occurs at a solid-liquid or liquid-liquid interface. Dewetting describes the rupture of a thin liquid film on the substrate, which could be either a liquid or a solid, and the formation of a droplet. In this thesis, we focus on the liquid-liquid dewetting process, for example, the dewetting of a drop of oil placed on a water liquid phase, which can be determined by the parameter called the spreading coefficient (*S*). The oil-water system is displayed in Figure 2.13 and the spreading coefficient can be calculated based on Equation (2.17).

$$S = \gamma_{WA} - (\gamma_{WO} + \gamma_{OA}) \tag{2.17}$$

in which γ_{WA} is the surface tension between water and the ambient gas phase, γ_{WO} is the surface tension between water and oil liquid phase and γ_{OA} is the surface tension between oil and gas phase. When *S* is a positive value, the spontaneous spreading of oil on the water surface occurs, whereas if *S* is negative a dewetting process between oil and water liquid phase occurs.

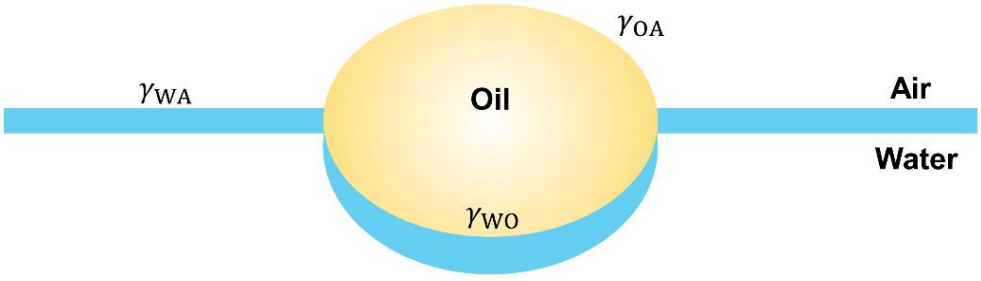

Figure 2.13 Schematic demonstration of the displacement of an oil droplet on a water surface is represented by the spreading coefficient (*S*). When $S > 0$, droplet spontaneously spreads on the surface forming a layer, whereas $S < 0$, dewetting occurs with forming an oil lens on the water surface.

In microfluidic device, in order to form the double emulsion droplets, either water-in-oil-in-water or oil-in-water-in-oil, with desirable lifetime requires that the middle phase wets the inner core completely. When this is not the case, a dewetting of the shell occurs with consequent disruption of the double emulsion droplets. Interestingly the dewetting between the inner core and the outer shell of a double emulsion droplet has been exploited as a transition process for the preparation of polymersomes. (109-112) Figure 2.14 illustrates the mechanism of dewetting transition between the inner and the middle phase and the formation of a thin bilayer of copolymer dispersed in the middle phase. In the system the coefficient *S* is described as in Equation (2.18).

$$S = \gamma_{IO} - \gamma_{IM} - \gamma_{MO} \tag{2.18}$$

where γ_{IO}, γ_{IM} and γ_{MO} are respectively the surface tensions between the inner-outer interface, the inner-middle interface and the middle-outer interface.

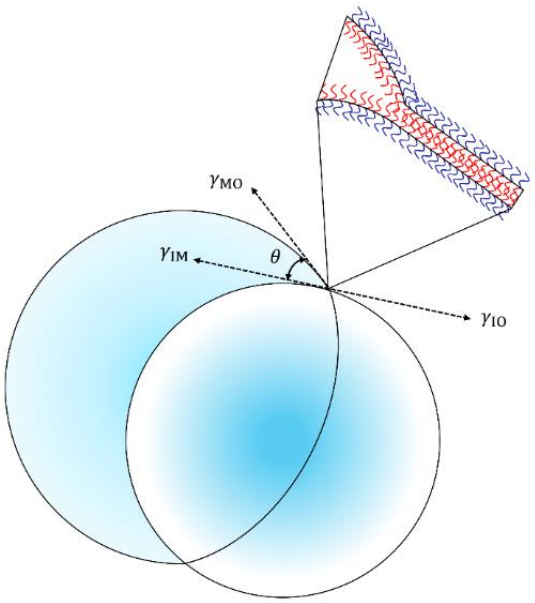

Figure 2.14 Dewetting of the middle volatile organic phase, from the aqueous core, of a double emulsion droplet dispersed in a water based solution (water-in-oil-in-water). Copolymer molecules are dissolved in the middle phase. Dewetting event allows the formation of a bilayer of copolymer. θ is the contact angle at the three-phase contact point.

Chapter 3 Microfluidic Assembly of Lipid/Block Copolymer Vesicles as Artificial Cells Models

In Chapter 3, a microfluidic method of fabrication of lipid vesicles (liposomes) and polymeric vesicles (polymersomes) with thin-shells, in order to resemble natural cell structures is presented. Using the biphasic microfluidic device, highly uniform double-emulsion droplets with ultra-thin membrane were generated to recreate artificial cell chassis for the study of *in vitro* transcription-translation (IVTT) reaction and integration of transmembrane protein into artificial biomembranes. To mimic the architecture of natural cell compartment, the IVTT reaction of enhanced green fluorescent protein (EGFP) was performed with a novel cell-free translation system called PURE (Protein Synthesis Using Recombinant Elements) inside the vesicle systems. Moreover, the unilamellar vesicles assembled by microfluidics supports functional insertion both of purified and of *in situ* expressed transmembrane proteins.

3.1 Introduction

3.1.1 Lipid Vesicles (Liposomes)

Lipid vesicles, also known as liposomes (113) are vesicular structures composed of self-assembled phospholipids encapsulating a volume of aqueous medium, which are considered as models for investigating the physical nature of membranes. (114-117) Phospholipids are amphipathic molecules that contain two components with different water solubilities. One moiety is the hydrophilic group, referred to as the polar head, while the hydrophobic segment, the non-polar tail region. A typical lipid molecule can be seen in Figure 3.1.

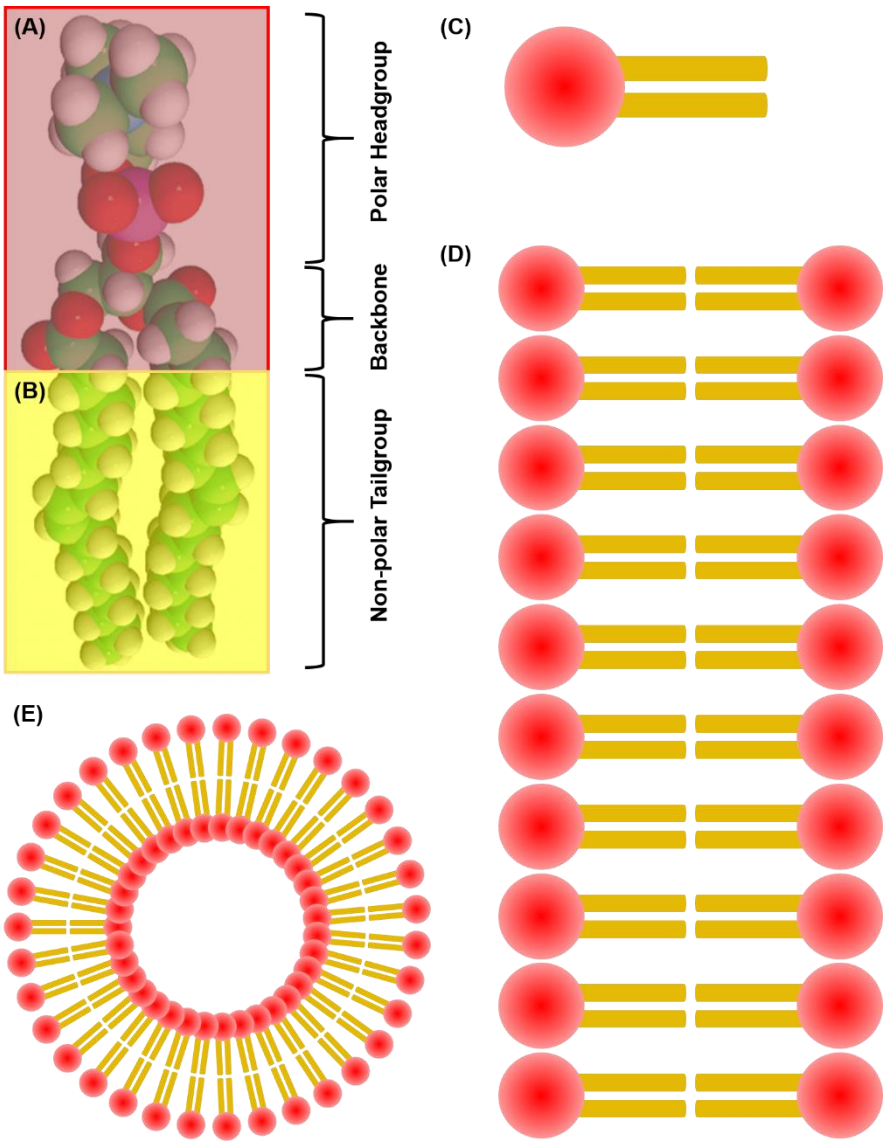

Figure 3.1 Space filling diagram of DOPC, a polar (hydrophilic) headgroup region consists of a glycerol backbone (A) and the hydrophobic non-polar tailgroup region (B); (C) depicts a single DOPC molecule composed of two major sections: a hydrophilic head (red) and hydrophobic tails (yellow); (D) displays a resultant lipid bilayer self-assembled with phospholipid molecules with a hydrophobic core; (E) demonstrates a simplified resultant lipid vesicles with an aqueous core and hydrophobic bilayer membrane. A single bilayer is typically ~ 5 nm thick and composed of neatly arranged individual lipid molecules with their "water-hating" tailgroups facing each other and their polar headgroups facing toward the interior and exterior aqueous medium.

Lipid vesicles can fall into several categories, most frequently classified by their size and lamellarity: (118, 119) (i) multilamellar vesicles (MLVs), (ii) small unilamellar vesicles (SUVs), (iii) large unilamellar vesicles (LUVs) and (iv) giant unilamellar vesicles (GUVs). These vesicles are schematically depicted in Figure 3.2.

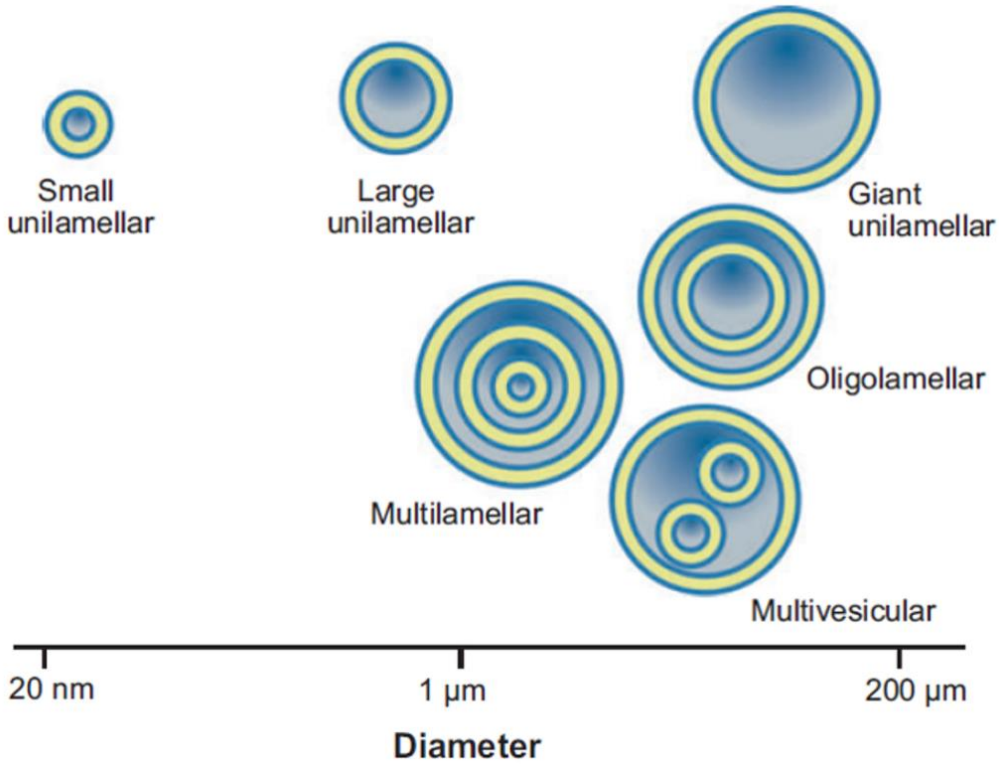

Figure 3.2 Schematic representation of the difference in the number of layers (lamellarities) and relative size of various types of lipid vesicles. The image is taken from (118).

Lipid vesicles are excellent structures to entrap small compounds due to their ability to isolate the ingredients in interior of the vesicles from the external aqueous medium, providing a small volume of environment for reaction of those compounds. Nature takes advantage of the self-assembly mechanism and encapsulation property to enable formation of biological cells, where important biological processes take place within the phospholipid vesicles. (119, 120) As a result of resemblance of the vesicular structure to biological membranes, giant unilamellar vesicles (GUVs) have

served as attractive models of minimal cells because they exhibit a set of features: namely size, lamellarity, and the ability to control the lumen content (which closely mimics the structural organisation of living systems). This makes GUVs the platform of choice for a number of simplified, model cellular processes such as compartmentation (121, 122) phase behaviour of lipid bilayer, (80, 123) and membrane protein insertion into lipid bilayers. (124-127)

3.1.2 Polymeric Vesicles (Polymersomes)

Phospholipids are compounds nature uses to form barriers within living cells. They are also used in artificial lipid chassis. In biotechnology, there is another class of synthetically artificial vesicles, polymeric vesicles, or polymersomes. (128-131) Polymersomes are hollow spherical compartments, delimitated by a membrane of amphiphilic block copolymers (BCP). Block copolymers are macromolecules comprising of two or more types of polymers and similar to naturally occurring lipids. They are amphiphiles in which there is at least one fraction (block) of each molecule is hydrophilic, whereas the other block is hydrophobic. In an analogous fashion to the phospholipids, block copolymers can also aggregate in aqueous media, producing vesicular structures, as depicted in Figure 3.3. (128, 132)

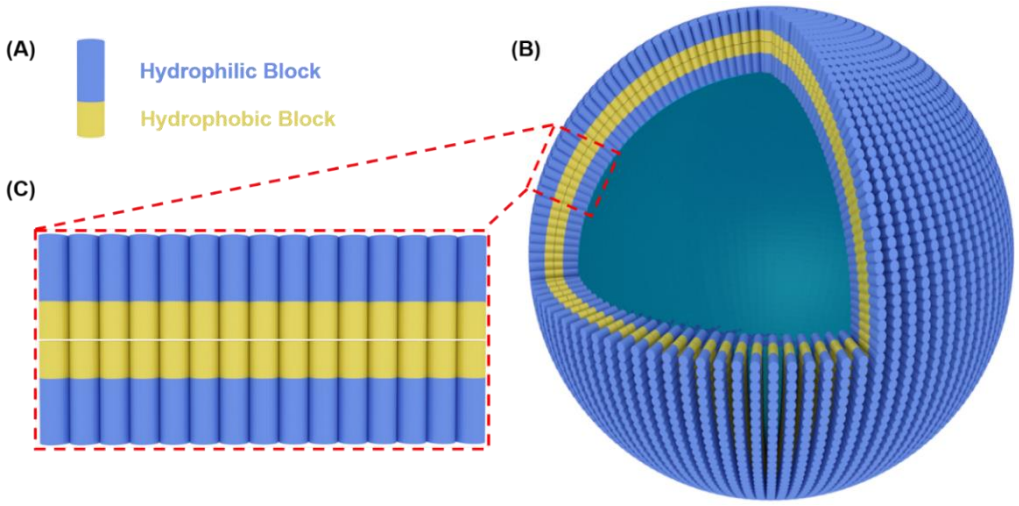

Figure 3.3 Schematic representation of self-assembly of amphiphilic diblock copolymer into polymeric vesicles, or polymersomes: (A) A diblock copolymer molecule with "water loving" section, or hydrophilic block and "water hating" section, or hydrophobic block; (B) Polymersomes formed by amphiphilic diblock copolymer; (C) Bilayer with hydrophobic blocks facing each other, forming the hydrophobic core derives from the polymersome membrane

The use of block copolymers instead of phospholipids can be used to synthesise artificial vesicles and has attracted much attention due to the advantages of their chemical properties and mechanical stabilities of polymersomes over liposomes. In particular, polymersomes can be constructed by a huge variety of hydrophobic and hydrophilic blocks, (128) allowing the control of mechanical properties and permeability. (133)

The diversity of chemical properties of polymersomes can be adjusted by modifying the building block chemistry to make polymersomes responsive, either to external or internal stimuli, in a controlled manner. (134) Thus, polymersomes are the biomimetic analogues of phospholipid vesicles revealing their ability to act as an alternative artificial cell model. (135) Owing to the higher molecular weight of building blocks, the membrane thickness can be at least ten-fold than that of liposomes, which makes polymeric vesicles "stronger" and more stable. In the liquid state, polymersomes are much stronger in their mechanical properties than lipid

vesicles, and are able to support much more membrane stretching. (136) Phospholipids can also be subject to oxidation, whereas polymeric vesicles could be synthesised by more stable blocks and can have significantly longer lifetimes. (137, 138) All aforementioned advantages of polymersomes indicate that vesicles based on block copolymers could be more suitable as artificial cell chassis.

3.1.3 Droplet-Based Microfluidic Fabrication of Vesicular Structures

As previously descried in Chapter one, the advances in microfluidic technologies with the capabilities of generating and manipulating small volume droplets in controlled manners have led to new routes for preparation of vesicles. (139, 140) With the variety of available techniques for production of microfluidic devices, the geometry of the devices can be easily customised, making it possible to explore diverse device design for forming vesicular structures.

3.1.3.1 Phase Transfer

One of the most well-established methods to transform droplets into vesicles uses a process referred to phase transfer. Matosevic et al. described an emulsion transfer method, which was fully integrated into a microfluidic device as shown in Figure 3.4(A). (141) In this formation process, lipid stabilised water-in-oil droplets were formed which were then guided through a Y shape junction into a co-flow laminar aqueous stream. The key point in this paper was the use of a triangular post, positioned in the microchannel to mediate phase transfer, helping droplets to pick up a second single lipid layer at the laminar oil-water interface. This "push" process was disruptive, with only 1 – 5 % of droplets surviving as they crossed the interface. In Figure 3.4(B), Malsmstadt et al. exploited a PDMS microfluidic device to produce monodispersed water-in-oil droplets, which were then transferred through an oil-water interface forming another lipid monolayer to reduce polydispersity of droplet size distribution. (142)

Recently, Chu et al. introduced a wetting-induced approach for droplet transfer to generate vesicular structures, Figure 3.4(C). (143) The dispersed aqueous phase was injected into a microchannel containing PEG-*b*-PLA diblock copolymer solution as continuous phase to generate uniform water-in-oil droplets. A second water phase was injected into device to form a laminar flow with diblock copolymer stabilised the interface. Due to the evaporation and diffusion of the volatile solvent – chloroform, leaving oil phase a hexane-rich solvent, which induced an attraction between monolayers on the droplets and the one at the interface. At this time, the combination of interfacial tensions became negative and the droplets entirely travelled across into interface producing vesicles with bilayers.

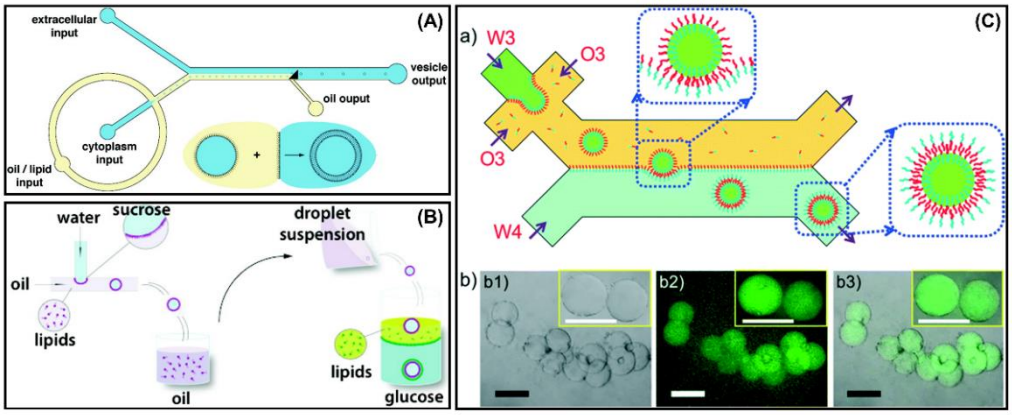

Figure 3.4 (A) Schematic illustration of a device where droplet generation and subsequent droplet transfer occurs on chip with the aid of a triangular post; (B) Droplets are formed in a single microfluidic device, and then expelled above oil-water column to yield vesicles; (C) Schematic of the transfer of water droplets stabilised by PEG-*b*-PLA across an oil-water interface to produce polymersomes, and CLSM images of resultant diblock copolymeric vesicles dyed by FITC-dextran. Images taken from (141-143).

3.1.3.2 Emulsion-Templating with Single Emulsions

To form monodispersed single emulsions using two immiscible liquid phases can be readily realised in microfluidic device. This approach of droplet production can be applied for preparation of single emulsion-templated vesicles, as depicted in Figure

3.5. Lee et al. developed a method using microfluidic device and oleic acid to generate lipid stabilised water-in-oil single emulsions. These single emulsions were subsequently injected into an aqueous mixture consisting of ethanol and water. (144) The rapid dissolution of oleic acid in ethanol forces the phospholipids to rearrange around the emulsions to assemble into a vesicle with bilayer, Figure 3.5(A). Matosevic et al. also detailed another single emulsion-templated method offered the ability of controlling membrane composition as well as lamellarity of membrane of vesicles. (82) Single emulsions with a lipid monolayer were formed and entrapped subsequently in a single microfluidic device, and then one to three more lipid monolayers were individually deposited on the droplet templates as illustrated in Figure 3.5(B).

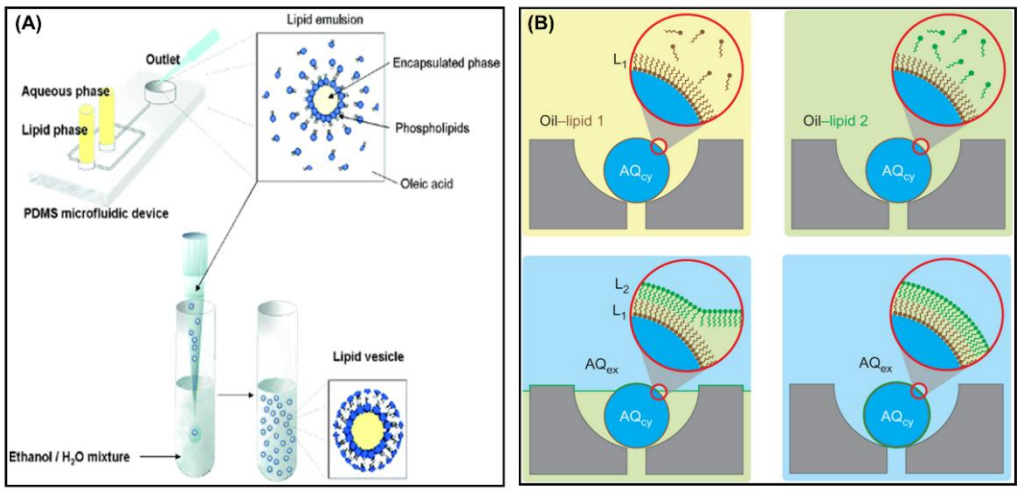

Figure 3.5 (A) Preparation of single emulsion-templated vesicular models; (B) Asymmetric vesicles formed by the sequential deposition of individual monolayers based on single emulsion templates. Image modified from the indicated references. (82, 144)

3.1.3.3 Emulsion-Templating with Double Emulsions

Water-in-oil-in-water double emulsions can be routinely generated with excellent monodispersity and 100 % encapsulation efficiency using microfluidics. (145) Double emulsions are recognised as ideal templates for forming vesicles by having

building blocks dissolved in the membrane cores. In addition, double emulsions and vesicles share similar core-shell structures; thus, double emulsion droplets prepared by droplet-based microfluidics can be used to shed light on the development and generation of vesicles.

Glass capillary microfluidic devices, developed by Weitz group were used to prepare lipid vesicles (39) and polymeric vesicles (146) transformed from double emulsion templates. In the oil phases, build blocks (phospholipids/block copolymer) were dissolved in the organic solvent mixtures to realise dewetting-induced bilayer formation. In Figure 3.6(A), lipid stabilised double emulsion were continuously produced in the device. As extra oil phases were removed from the membrane, owing to the dewetting process (stated detailed in Chapter 2), two lipid monolayers at the internal oil-water interface and external water-oil interface came together into a bilayer, eventually forming a vesicular shape.

In order to reduce the toxicity and improve the biocompatibility of bilayer, Arriaga et al. demonstrated a novel microfluidic design based upon microcapillaries which can prepare double emulsions with ultrathin shells, implying relatively less organic solvent is trapped in the membrane, Figure 3.6(B). (147) The idea behind the microfluidic device is that a biphasic flow occurs in the injection capillary where inner aqueous phase flows in the centre of the capillary surrounded by the oil phase carrying phospholipid molecules (and which moves along with the inside wall of the injection capillary due to affinity of hydrophobic nature of surface). This enables the formation of double emulsions with nanoscale shells, and provides a promising platform for vesicles generation (with the potential to broaden their application in biomedical research areas).

Recently, Deshpande et al. reported the formation of monodisperse, cell-sized (5 – 20 μm) unilamellar lipid vesicles via the formation of double emulsion drops with lipid molecules dissolved in 1-octanol as the intermediate phase. After the one-step formation of double emulsion drops in a flow-focusing microfluidic geometry, the double emulsion drops spontaneously develop a Janus geometry with a side-

connected 1-octanol pocket because of dewetting. The 1-octanol segment eventually splits off, yielding fully assembled liposomes within 1 - 5 minutes that do not contain any non-desirable organic solvent in the bilayer, Figure 3.6(C). (148)

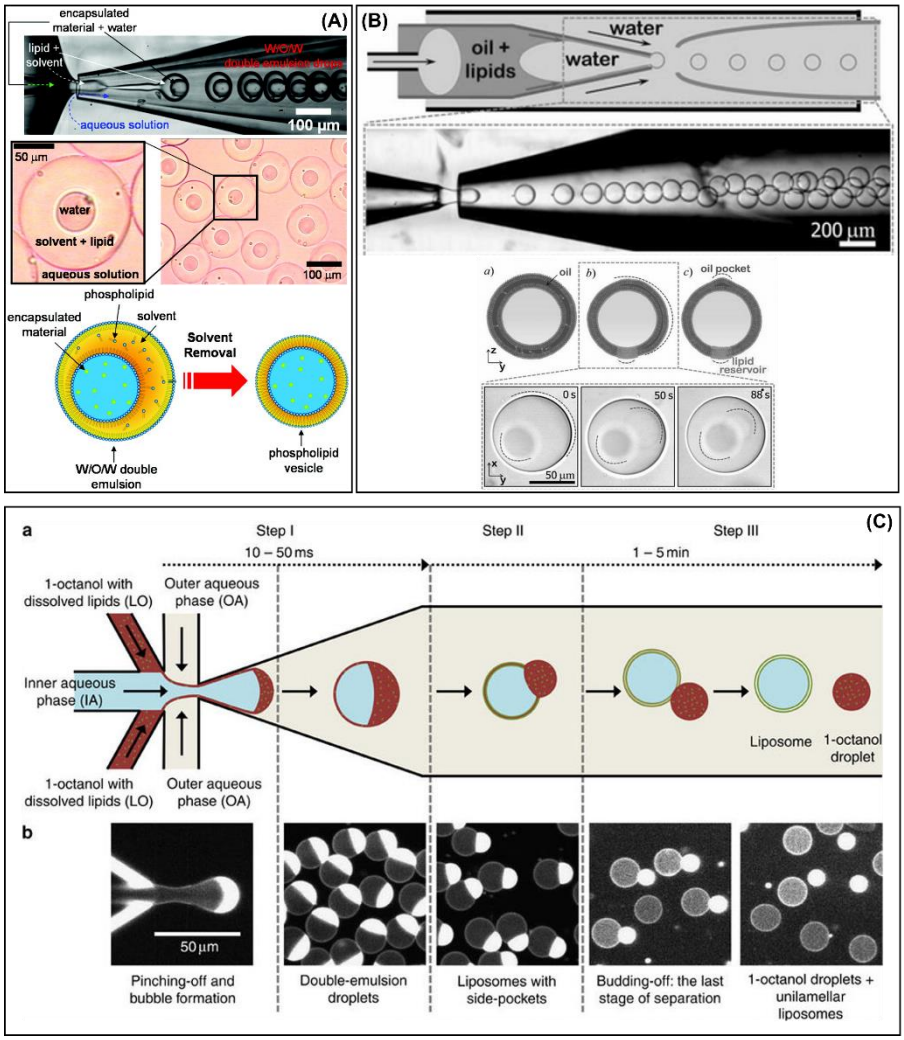

Figure 3.6 (A) Microfluidic fabrication of phospholipid-stabilised double emulsions in a glass capillary device. Optical images of double emulsions with solvent shell containing phospholipid molecules and schematic of dewetting process for solvent removal from the shell; (B) Microfluidic preparation of double emulsion drops with ultrathin shells. Optical images of collected double emulsion drop template; the formation of lipid bilayer via dewetting process; the resultant lipid vesicle; (C) Schematic of working principle of microfluidic device. Fluorescence images showing steps corresponded to each of step described in the working principle. Temporal-resolution sequences showing the separation of the 1-octanol droplet from the lipid vesicle.

3.1.4 *In Vitro* Transcription and Translation in Artificial Cell Models

Transcription and translation is a conserved biochemical process shared across all life classes. The transcribing of a DNA template to messenger RNA (mRNA), followed by translation to a defined protein sequence is integral to all life, and thus has become known as the central dogma of molecular biology, (149, 150) as shown in Figure 3.7. Thus, to demonstrate the potential and to prove emulsions templated vesicles' compatibility with biomolecules and their applications as artificial cell models, it is of importance to show that they can perform this process. (16, 151-153)

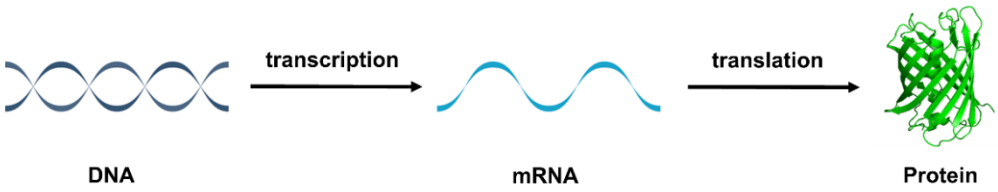

Figure 3.7 The central dogma of molecular biology. DNA is first transcripted to messenger RNA. mRNA is translated to yield a protein with defined amino acid sequence.

It has been demonstrated that the individual components for transcription and translation can be extracted from bacterial cells and then purified. (154) During an incubation period of several hours, these components can only be reacted with a DNA templates, either in plasmid vectors form from cloning or as a liner PCR (polymerase chain reaction) fragments for cell-free protein synthesis, especially those that are toxic to cells. However in recent years, cell-free expression machinery as an alternative to *in vitro* expression has expanded its use to *in vitro* compartmentalisation in synthetic biology, especially in artificial cell engineering. (155)

Cell-free protein synthesis technology has been known about since 1961 and was first used by Nirenberg and Matthaei to decipher the genetic code. (156) Cell-free translation system containing ribosomal machinery and reagents required for protein

synthesis in conjugation with DNA sequence are increasingly being considered as viable alternatives for translation of essentially every protein. Using cell-free systems, activation of biological machinery can be achieved without cell integrity for protein expression to occur. In particular, the open reaction environment allows for the addition or removal of substrates for protein expression, as well as precise, online reaction monitoring. Importantly, the nature of cell-free protein synthesis enables shortened protein production timelines and increased flexibility for the addition or removal of natural or synthetic components compared with *in vivo* methods. Overall, cell-free protein synthesis holds promise to be a powerful technology platform for a new and rapidly developing field of synthetic biology – building synthetic cells. (13, 115)

Given that the concept that translation is one of the central cellular processes required for life, and the product of the cell-free expression system, proteins which are main component of the multiple cellular function, cell-free protein synthesis system (cell-free transcription-translation) have been broadly utilised in the development of synthetic cellular system. (115) Yu demonstrated the first liposome compartmentalised cell-free expression to synthesise a green fluorescence protein (GFP) within liposomes with binary compositions (egg phosphatidyl choline; cholesterol) in the bilayer. (157) As fluorescent proteins are readily detected using basic fluorescence microscopy, other GFPs such as red-shifted GFP and enhanced GFP (EGFP) have been created effectively to be exploited in the cell-mimetics. Following this first attempt of protein expression within liposome, synthesis of GFP in artificial cellular entities, it has demonstrated that the cell-mimetic environments (liposomes, water-in-oil single emulsions, water-in-oil-in-water double emulsions, coacervates) are compatible with biomolecules and can satisfy the prerequisite for constructing functional cell, which is *in situ* generation of complex biological structures. (16, 151-153, 158-163) Cooper and his team performed cell-free protein synthesis within water-in-oil single emulsions, (164) water-in-oil-in-water double emulsions (165) and polymersomes respectively (112) to study the preference to localisation of an actin-like bacterial cytoskeletal protein MreB at the membrane interface as well as osmotic-pressure triggered release of protein from polymersomes.

Additionally, cell-free protein translation machinery has been successfully compartmentalised in synthetic cells to express membrane proteins, such as nanometre-size pores, (16, 82) and ion channels and transporters. (166-168) Having these complex membrane proteins expressed in the interior of compartments and reconstituted into membranes, the functioning synthetic cellular system can be eventually achieved realising idea of mimicking cells exist in nature.

3.2 Materials and Methods

3.2.1 Materials

Double emulsion droplets templated vesicles were prepared using a capillary microfluidic device comprised of three cylindrical glass capillaries of 1 mm in outer diameter (World Precision Instruments, Inc., IB100-6, USA) tapered and nested within a square capillary of 1.05 mm inner dimension (AIT Glass, USA).

Cylindrical injection capillary was treated with Sigmacote (Sigma-Aldrich, USA) while the cylindrical collection capillary was treated with 2-[Methoxy(polyethyleneoxy)propyl]-trichlorosilane, (Fluorochem Ltd.).

The innermost aqueous solution contained a cell-free protein synthesis solution (PURExpress, New England Biolabs) and plasmids coding for EGFP and α-hemolysin respectively. The middle oil phases were a mixture of chloroform (Sigma, USA) and hexane (Sigma, USA) with a volume ratio of 36:64 with 5 mg/ml of 1,2-dioleoyl-*sn*-glycero-3-phosphocholine (DOPC) (Sigma-Aldrich, USA) or triblock copolymer poly(2-methyloxazoline-*b*-dimethylsiloxane-*b*-2-methyloxazoline) (PMOXA-*b*-PDMS-*b*-PMOXA) (Polymer Source, Canada). The continuous phase was watery solution of 10 wt% PVA (Mw = 13000-23000, Sigma-Aldrich, USA) and 0.5 M NaCl with 1100 mOsm/l while collection buffer was an aqueous solution of 0.55 M NaCl which balances the osmolarity as inner aqueous phase. A water-soluble green dye - calcein (Sigma, USA) was used as a model active material for the dye release experiments. The pore-mediated dye leakage was conducted using α-

hemolysin from Staphylococcus aureus (Sigma). Osmolarities were measured using an osmometer (3300 Micro-Osmometer, Advanced Instruments, Inc., UK). Fluids were manipulated by syringe pumps (Harvard Apparatus, USA).

The generation of double emulsion droplets was observed using a high-speed camera (Vision Research Inc.). The expression of EGFP and the triggered release of the calcein by incorporating with nano-pore forming protein were evaluated by a confocal laser scanning microscope (LSM 510 META, Carl Zeiss, Germany).

3.2.2 Preparation of Solutions

In order to prove the vesicles' compatibility with biomolecules as cell mimics, double emulsion droplets templated vesicles were used as cell-like bioreactors to perform *in vitro* transcription and translation (IVTT). Vesicles filled with cell-free gene expression solutions were created using mixtures of PURExpress cell-free reagents and plasmids as inner water phase. This innermost aqueous phase was kept on ice until it was loaded into the syringe. Membrane building blocks, either as phospholipid or triblock copolymer, were dissolved in a mixture of chloroform and hexane (36:64 vol%) at a concentration of 5 mg/ml for the middle phase of double emulsion droplets. Prior to loading middle phase into the glass syringe, the solution was sonicated for 30 minutes to assure amphiphiles were dissolved in the organic solvent mixture. A 10 wt% PVA aqueous solution was used as the continuous phase of double emulsions.

3.2.3 Fabrication of Microfluidic Device

The microfluidic devices were based on coaxial assemblies of cylindrical and square glass capillaries on glass slides demonstrated by Weitz group. (52, 169) Two cylindrical glass capillaries of 1 mm in outer diameter and 0.58 mm in inner dimension were tapered by axially heating and pulling the capillary using a pipette puller (Sutter Instrument Co, Model P-97, USA) to have precise orifices with size of 40 μm. The inner dimeter of two tapered capillaries were polished using 3000 grade

sand paper to obtain inner dimensions of around 100 and 200 μm for the injection tube and collection tube respectively.

The capillaries were assembled within a square capillary of 1.05 mm and the distance (ca. 100 μm) between the inner and collection capillary was controlled manually under optical microscope. Before nesting within the square capillary, the cylindrical injection capillary was dipped in with Sigmacote for 30 minutes to make it hydrophobic, while the round shape collection capillary was treated with 2-[Methoxy(polyethyleneoxy)propyl]-trichlorosilane to render its surface hydrophilic.

Both of the two cylindrical capillaries were inserted into the square capillary from its two opposite ends, which was placed on a glass slide. Another circular capillary was pulled to form two long and thin pipettes to obtain an outer diameter of around 200 μm. One pulled capillary with small size tip was inserted into the open end of the cylindrical injection capillary and aligned using the optical microscope. Lastly, dispensing needles used as inlets of fluids were glued to the glass slide using a transparent 5 Minutes Epoxy (Devcon).

3.2.4 Lipid/Polymer Vesicles Preparation

Ultrathin shell double emulsion templated liposomes or polymersomes were prepared using a glass capillary microfluidic device. The injection capillary with smaller size of tip was used to inject the purified *E. coli* extract, required for protein synthesis, with plasmids coding for different types of proteins; this formed the inner aqueous core of the vesicles. As middle phases, a mixture of chloroform and hexane was used with either DOPC or triblock copolymer (PMOXA-*b*-PDMS-*b*-PMOXA). This mixture was injected through the interstices between two injection capillaries forming the plug-like water in oil droplets. The continuous phase was a water phase of 10 wt% PVA and 0.5 M NaCl pumped through the interstices between the injection capillary and outer square tube.

The innermost, middle and outer phases were injected into the microfluidic device at flow rates of 500, 400 and 3000 μl/h respectively. Double emulsion droplets with thin membranes were collected in a glass vial containing water solution of 0.55 M NaCl solution.

3.2.5 Cell-Free Proteins Expression within Vesicles

The plasmids containing EGFP and α-hemolysin sequences respectively were kindly provided by Mr. Ross Eaglesfield. Single plasmid of EGFP were used for protein expression both in bulk and in vesicles. Experiments in bulk were useful to examine the design of the synthetic plasmid.

A novel cell-free transcription-translation system named PURExpress (154) (New England Biolabs, USA) was used in all *in vitro* transcription and translation experiments in this thesis. The system was reconstituted from the purified components necessary for *E. coli* protein expression. It is a one-step reaction which simply requires mixing of two tubes of solutions with the template DNA. Conducting IVTT within cell-mimetic systems by means of using PURExpress system is becoming desired in the research of building synthetic cells.

According to the protocol of PURExpress system, preparation of the cell-free protein synthesis solution is depicted in Figure 3.8. For individual experiment, 30 μl of solution B was added to 40 μl of solution A. 8 μl of plasmid, and 2 μl of RNase inhibitor (New England Biolabs, USA) were then added. Lastly, 20 μl of nuclease-free water was added to the mix up to 100 μl total volume. The prepared solution was gently mixed by pipetting up and down three times.

The solution was kept on ice until it was either loaded into a 100 μl glass syringe (Hamilton, CH) or incubated in a 96-well plate (Fisher Scientific, USA) in plate reader (Synergy HT, BioTek) with a standard shaking incubation at 37 °C for 210 minutes. When double emulsion droplets were produced, they were collected into a glass vial for solvent evaporation for 10 – 30 minutes. Afterwards, 150 μl of the suspension of

vesicles was pipetted into a well on the glass slide (Marienfeld, Germany) and covered by a cover slip (20 × 20 mm) for incubating at 37 °C for 3 hours in a temperature controlled pad (Tempcontrol 37-2 Digital, Meyer Instruments).

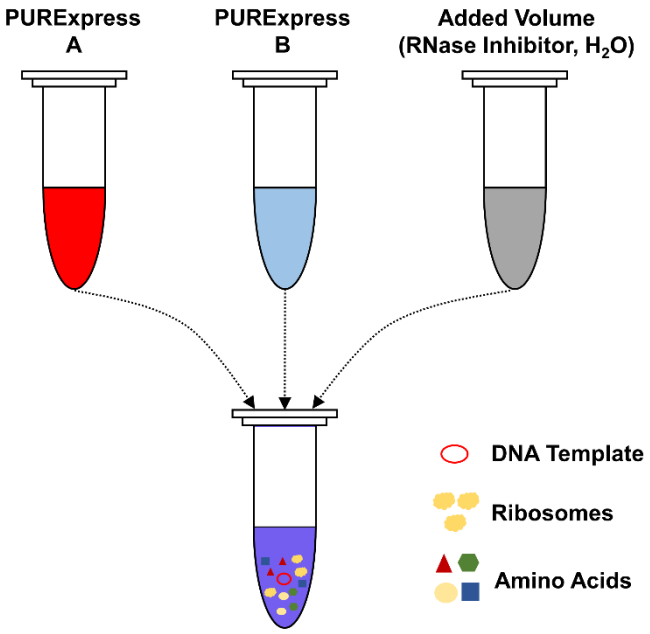

Figure 3.8 Schematic illustration of preparation of cell-free protein synthesis. This was made of designed plasmid coding for proteins of interest, PURExpress solutions A and B, supplements and nuclease-free water.

3.3 Results and Discussion

3.3.1 Lipidic/Polymeric Vesicles Generation

A glass capillary microfluidic device was used to fabricate double emulsion drops with ultrathin membranes, as illustrated in Figure 3.9(A). We used innermost smaller capillary to inject aqueous phase of 8 wt% PEG and 2 wt% PVA, into the left tapered capillary; the PEG enhanced the contrast between inner and outer aqeous phases as well as the viscosity of the solution, while the PVA enhanced the stability of the double emulsion drops. We treated the left tapered injection capillary to be

hydrophobic, thus preventing wetting of the innermost aqueous phase on the capillary wall. We used this tapered capillary to inject the middle oil phase, DOPC dissolved in a mixture of chloroform and hexane in which their volume ratio was 36:64; the total lipid concentration was 5 mg/ml. We injected innermost aqueous phase and middle oil phase at flow rate of 500 µl/h and 400 µl/h, respectively; under these conditions the innermost aqueous phase formed large water in oil emulsion drops within the left tapered capillary, as exemplified in the schematic illustration in Figure 3.9(A). We then injected the outer aqueous phase, a 10 wt% PVA solution, through the interstices between the left tapered capillary and the square capillary, at flow rate of 3000 µl/h. We treated the right tapered capillary to render its surface hydrophilic, therefore preventing wetting of the middle oil phase on its wall. To prevent osmotic stresses, we collected the double-emulsion droplets in a glass vial containing 50 mM NaCl solution having the same osmolarity as the inner watery cores. Importantly, the unwanted residual oil droplets formed within the device due to the excess lipid phases between two water-in-oil droplets can be easily removed from lipid vesicles samples by exploring the density differences in the solution systems, Figure 3.10.

Highly uniform thin-shell double emulsions were prepared using the microfluidic device at high-throughput, and then collected and imaged as shown in Figure 3.9(C). The thin shelled double emulsion droplets were featured with the enhanced stabilities as a result of reducing the thickness of the middle layer until reaching the lubrication regime. (170) Thus, lipid vesicles produced by transforming from ultrathin shell double-emulsion droplets at a higher yield ratio compared to the liposomes prepared by thick membrane double emulsions. (147) These double emulsions have two concentric interfaces which enable the direct formation of a bilayer. The formation

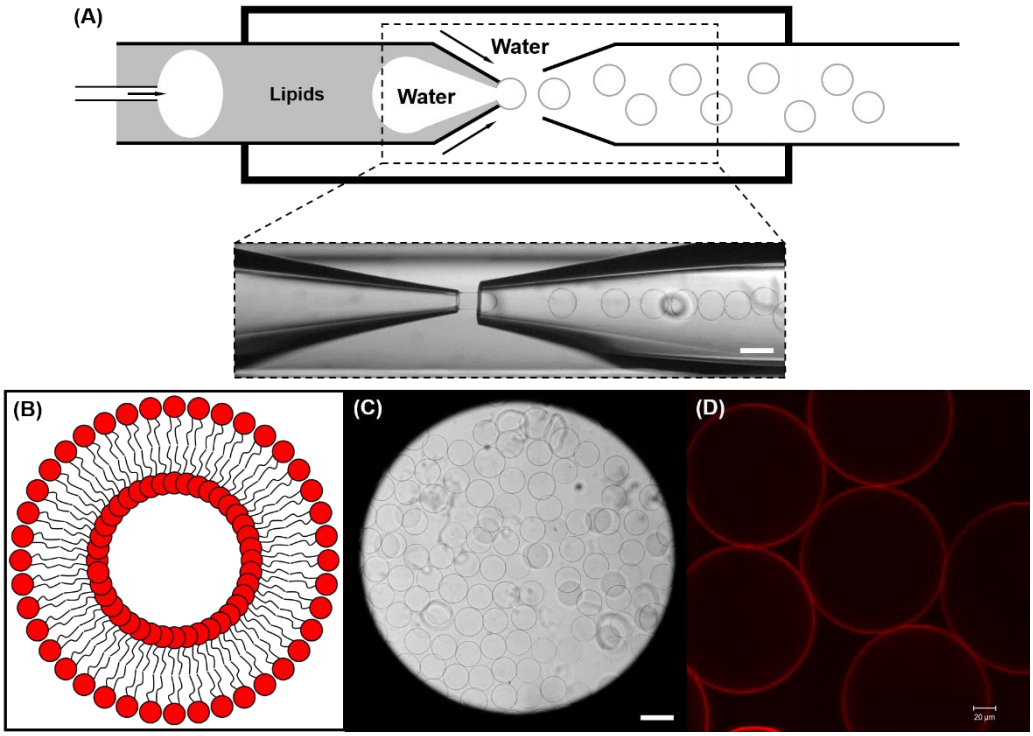

Figure 3.9 Microfluidic production of lipid vesicles from thin-shell double emulsion templates: (A) Schematic illustration of microfluidic device for fabrication of double-emulsion droplets with thin shells. Scale bar is 200 μm; (B) Schematics of a produced lipid vesicle; (C) Optical microscope image of the microfluidically prepared double emulsions. Scale bar denotes 200 μm; (D) CLSM image of as-formed lipid vesicles with bilayers labelled with Rhodamine-PE. Scale bar is 20 μm.

of the bilayer was induced by the dewetting process. The lipid molecules were dissolved in middle oil phase consists of a mixture of highly volatile good solvent (chloroform) for lipids and a less volatile poor solvent (hexane), double emulsions exhibited dewetting of the middle phase containing the lipids during evaporation.

Initially, in membranes of double emulsion, lipid molecules occupied both inner and outer interfaces, which helped to keep the construct intact. As the good solvent preferentially evaporated, the poor solvent was concentrated and was expelled from the dense array of lipid molecules at the inner and outer interfaces, resulting in two lipid monolayers stick together forming a lipid bilayer membrane, Figure 3.9(D). The

expelled poor solvent droplets floated in the glass vial due to their lower density and were easily removed by pipetting as shown in Figure 3.10. Importantly, the middle layers of double emulsion templates were very thin, complete dewetting transition required a shorter time.

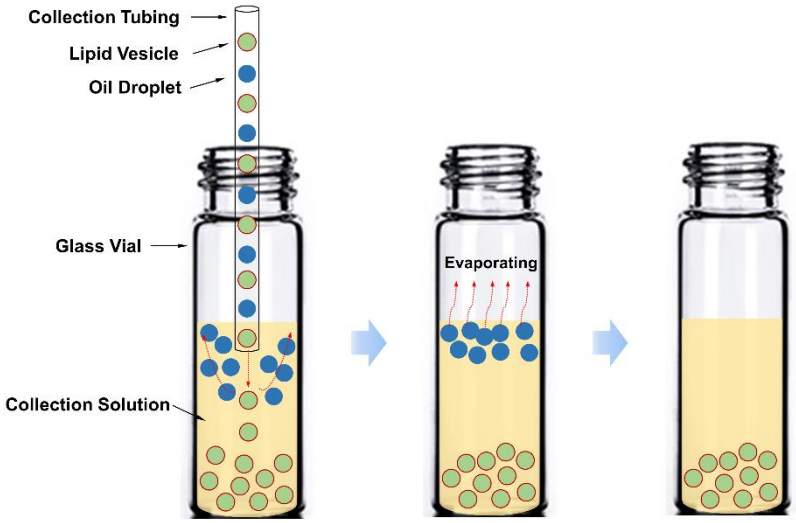

Figure 3.10 Oil removal from lipid vesicles samples by applying density differences of solutions. Density: Lipid vesicles > Collection solution > Oil droplets.

Polymersomes are alternative cell mimicking models, Figure 3.11(A). The triblock copolymer, PMOXA-PDMS-PMOXA, has been widely studied to form polymeric flat membranes and vesicles as a result of fluidity nature of PDMS for mimicking cell membrane. (171, 172) In between two hydrophilic blocks is the hydrophobic central block, forming the similar membrane structure as the membrane comprised by lipid chain groups. Due to molecular structure of the triblock copolymer, it can have two morphologies in the resultant membrane, depending on the disposition of the two hydrophilic parts on the two sides, I-Shape, Figure 3.11(C) or on the same side of the hydrophobic layer, U-Shape, Figure 3.11(D). (173, 174) By utilising the same microfluidic strategy, Figure 3.12(A), thin-shell double-emulsion templates for constructing polymersomes were produced. The double emulsions were

monodisperse in size and efficiently encapsulate the fluorescent dye (calcein) as shown in Figure 3.12(B, C). The typical coefficient of variation (CV), in size is lower than 4 %. In Figure 3.12(C, D), there was the cross talk occurred between calcein and Nile Red as the overlap in their spectrums of two fluorophores originated by the setting of fluorescence filters.

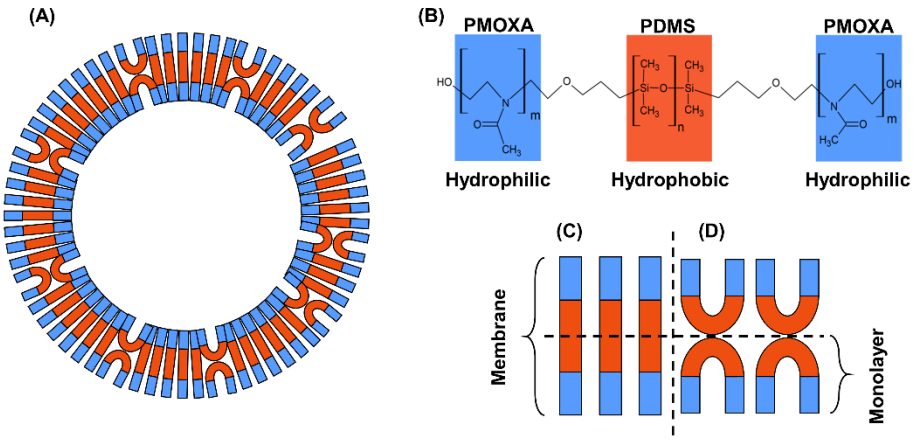

Figure 3.11 Cell-like structure in the form of polymersome: (A) Schematics of polymeric vesicular structure; (B) Membrane building block: PMOXA-PDMS-PMOXA, triblock copolymer as an analogy to lipid molecules. Two PMOXA chains are 'water loving', in between is the PDMS block which is hydrophobic; (C) Membrane in I-shaped conformation; (D) Membrane in U-shaped conformation.

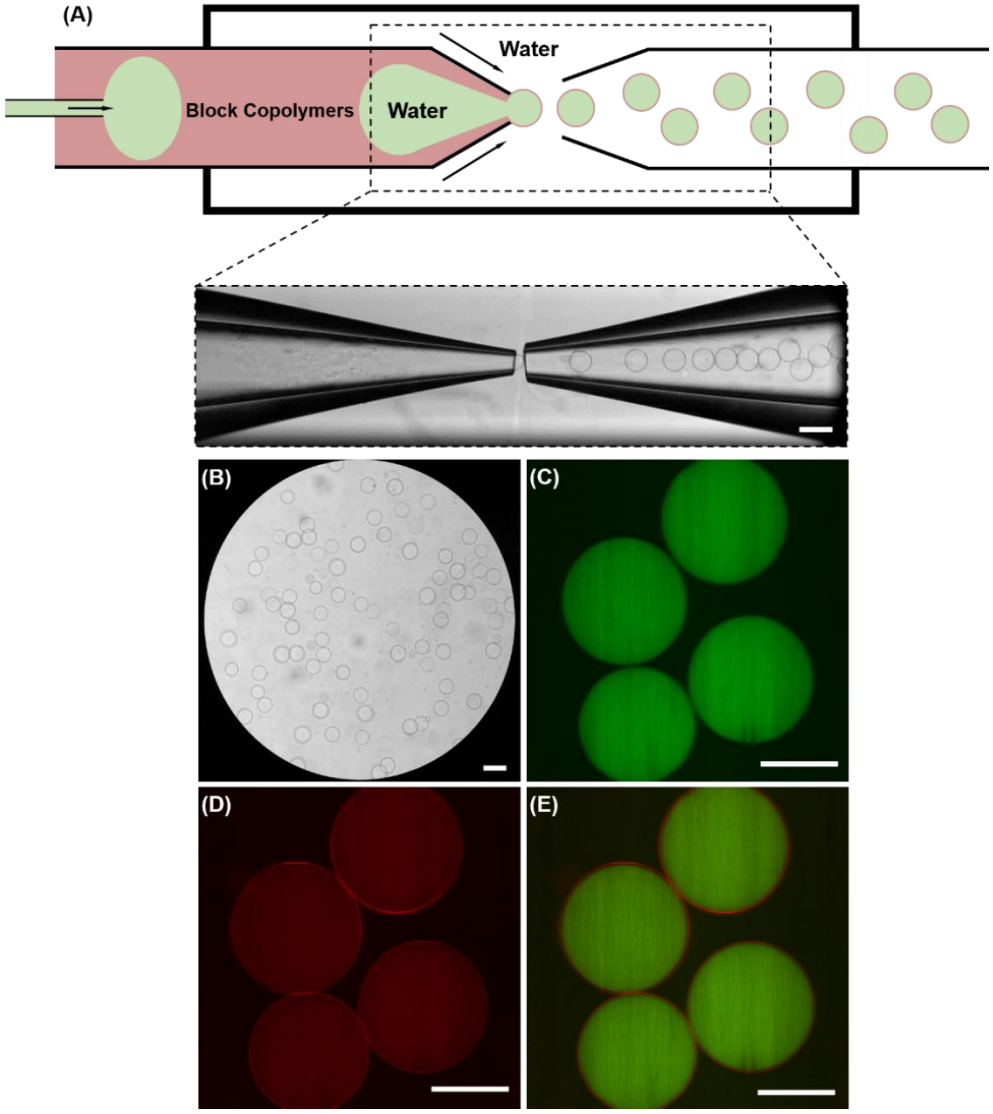

Figure 3.12 Production of polymersomes from thin shelled double emulsion droplets: (A) Schematic demonstration (top) of microfluidic approach for making double emulsions with ultrathin membranes. Optical micro-image (bottom) of generation process. Scale bar is 200 μm; (B) Optical microscope image of monodisperse double emulsion droplets. Scale bar denotes 200 μm; (C-E) CLSM images of as-formed polymersomes. Scale bars are equal to 100 μm; (C) Green channel: calcein encapsulated inside polymersomes; (D) Red channel: polymeric bilayers labelled with 0.5 mol% Nile Red; (E) Merged channel: interior aqueous phase enclosed by a polymeric membrane.

3.3.2 Protein Expression in Lipid Vesicle Based Artificial Cells

This microfluidic method enables exceptional robustness, flexibility and controllability, and results in monodisperse artificial cell chassis. To demonstrate the potential as cell-mimic systems and to prove their biocompatibility, we performed the *in vitro* transcription and translation within both liposomes and polymersomes.

Prior to microfluidic encapsulation of synthetic plasmids for targeted proteins together with cell-free expression solution to undertake gene-directed protein synthesis in lipidic or polymeric microcompartments. The water-soluble fluorescent protein EGFP was expressed in bulk solution to validate successful plasmid design by monitoring fluorescent protein synthesis using a plate reader. This was done to investigate if the signal was intense enough to be detected when showing IVTT in a vesicle format. To do this, the cell-free protein synthesis mix was prepared as previously described. The synthetic plasmid was added into IVTT solution respectively, and pipetted into a well on a 96-well plate. One more portion of cell-free mix solution without the plasmid used as a control was added into another well as well. The plate was incubated at 37°C for 210 minutes, and the expression levels of EGFP synthesis were read every 5 minutes using a standard FITC filters.

Increase in EGFP fluorescence indicated successful expression of the protein by cell-free synthesis, as shown in Figure 3.13. In the first 2 hours, fluorescence signal curve of EGFP shows an increasing trend with time. After 2-hour expression, the fluorescence signal reached a plateau.

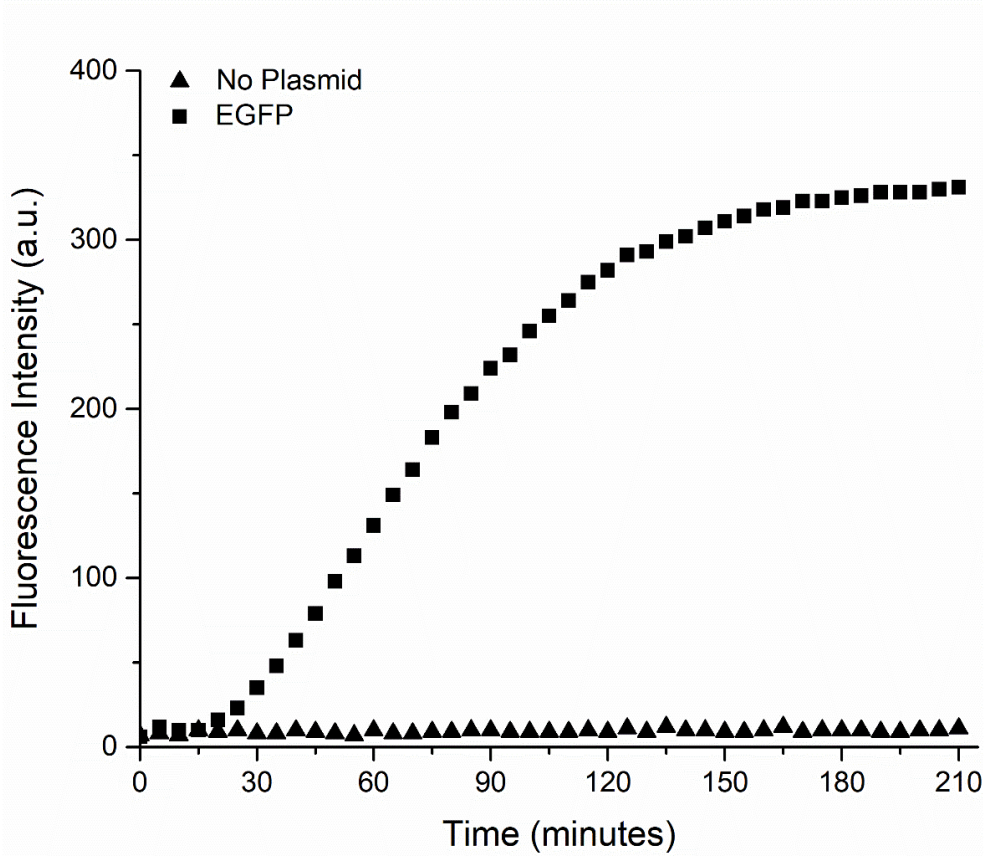

Figure 3.13 The expression kinetics of the IVTT of EGFP in bulk recorded by a plate reader.

The ultrathin shell double emulsions templating route to form a large number of monodisperse lipid vesicles with high encapsulation efficiency provides excellent models entrapping biomolecules which could be cell-free expression systems within membrane-bound compartments, mimicking the 'cytosol' of artificial cells. Lipid vesicles were employed as cell-like bioreactors to perform *in vitro* transcription and translation (IVTT). Lipid vesicles filled with PURExpress cell -free gene expression solutions were successfully created as inner water phase to prepare loaded liposomes. The collected double emulsion droplets were left at room temperature for 10 – 30 minutes in order to allow the complete dewetting transition and sedimentation of liposomes, and then they were incubated at 37°C and monitored for 3 hours by confocal laser scanning microscopy (LSM 510 META, Zeiss). Images were captured

every 5 minutes in which expression levels were analysed by the supplied Zeiss software. As Figure 3.14(A1 – A3) shows, the fluorescence intensity of EGFP in liposomes notably increased from 0 to 85 minutes. In the first 85 minutes, Figure 3.14(B), the fluorescence signal increased linearly and then reached a plateau after 3-hour expression, probably because of exhaustion of the nutrients required for the protein synthesis. This data was consistent with other kinetic studies performed on PURExpress cell-free protein formation. (152) A difference in reaction kinetics can be seen in between bulk and cell-like compartments might due to the macromolecular crowding within the aqeous phase that facilitates the recation rate of the cell-free expression. As such we demonstrated that our lipid vesicles can act as compartments for cell-free gene expression which is a step forward in making an artificial cell from bottom-up.

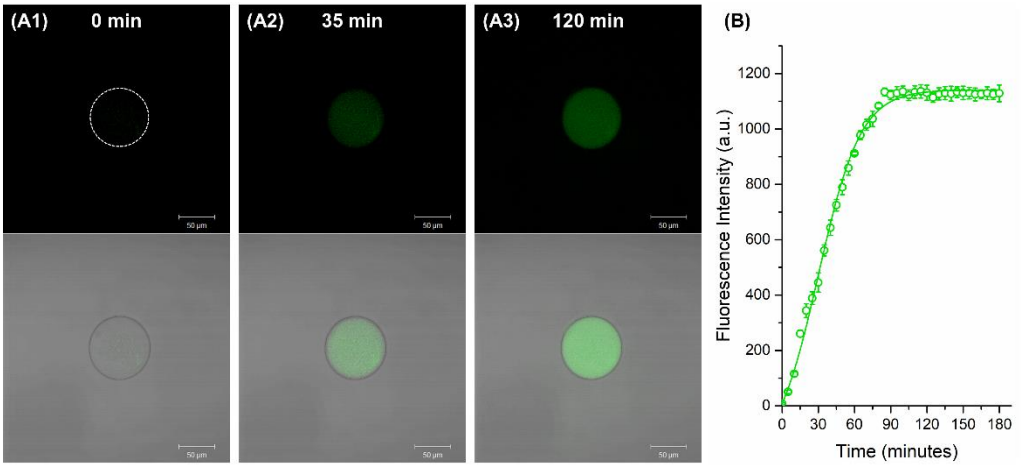

Figure 3.14 IVTT of EGFP in lipid vesicles: (A1 – A3) Sequence images show expression of EGFP inside the liposomes; (B) The corresponding expression kinetics. (n = 15).

3.3.3 Protein Insertion into Polymersomes

In order to demonstrate that the membranes of polymersomes formed in our method can be a promising analogues to lipid bilayers and to show the feasibility of engineering the properties of such membranes, we performed cell-free expression of

a pore-forming protein, α-hemolysin (αHL), (175) and the pore-mediated transport of molecules across polymeric boundaries.

We first prepared polymersomes loaded with PURExpress cell-free expression solutions with the synthetic plasmid coding for αHL and 10 μM of calcein fluorescent molecules, and observed the fluorescence intensity in polymersomes over time, Figure 3.15(A). The performance of IVTT was measured in the same manner as lipid vesicles. The αHL-induced transport is shown in Figure 3.15(B1 – B3). Once the monomers of αHL were expressed inside polymeric compartments and assembled nanopores in the membranes, the dye in the polymersomes rapidly diffused into the external environment.

In Figure 3.15(C), we observed that the membrane proteins were incorporated into the membranes from 60 – 65 minutes since the incubation started, which caused the dramatic decrease of fluorescence intensity. While a slight decay in fluorescence was found in the first hour which was a consequence of photobleaching. To further confirm the incorporation of membrane proteins into the polymersomes, αHL (20 μg/ml) was added into the suspension of as-formed polymersomes loading calcein (10 μM) within inner aqueous phase, and observed the fluorescence intensity leakage over the time course, Figure 3.16(A).

In Figure 3.16(B1 - B3, C), we similarly observed fluorescent molecules leakage over ~20 minutes since the addition of αHL at 5 minutes. In contrast, in the absence of αHL, there was no significant reduction of the fluorescence intensity can be seen. Consequently, these results demonstrated the biological relevance of these polymeric bilayers with thicker membranes compared with lipid bilayers in supporting insertion and assembly of a pore-forming membrane protein. Additionally, loading the vesicles with genetic materials and *in vitro* transcription and translation system provided evidence that corroborates the produced polymeric microcompartments can serve as the synthetic cell models on which to display the integration of highly functional membrane proteins.

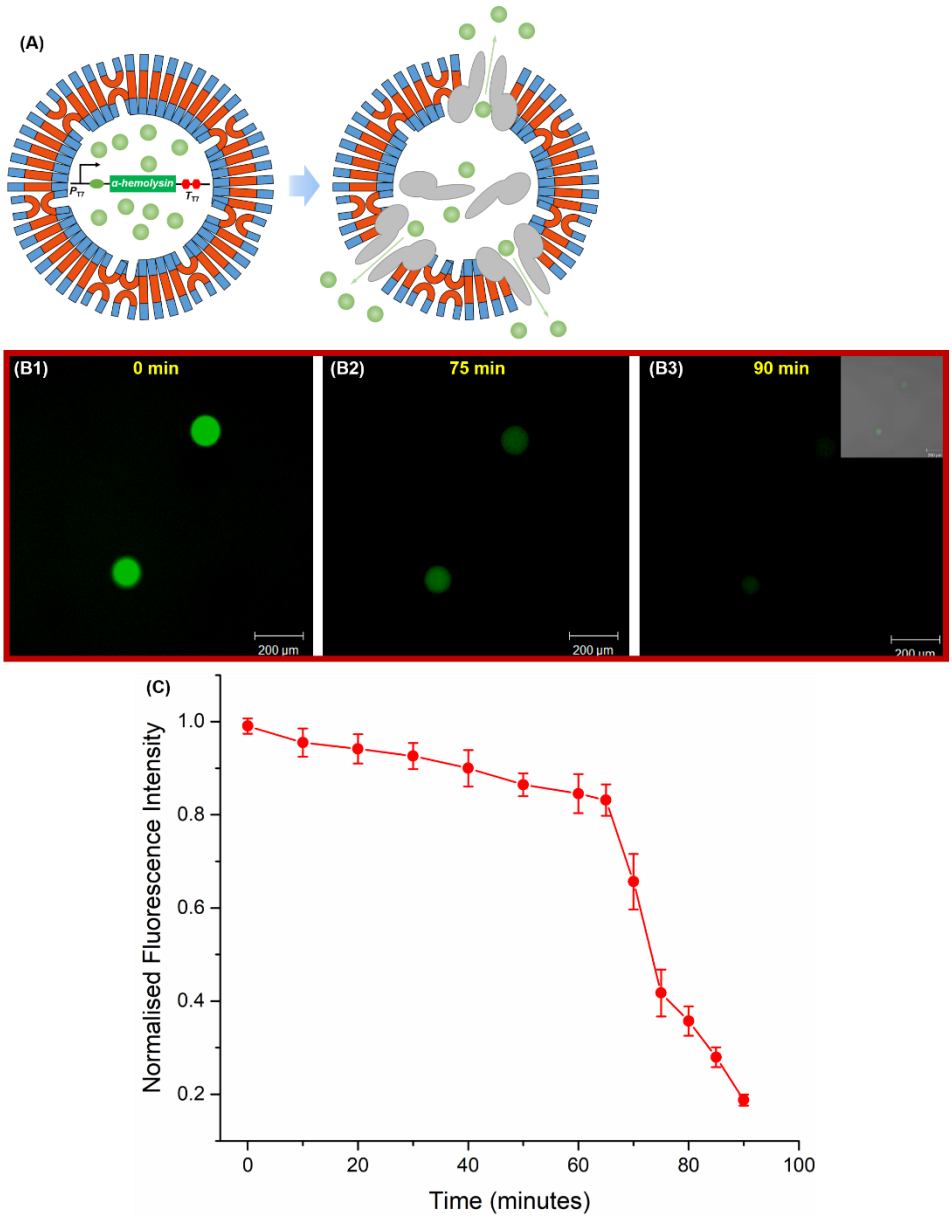

Figure 3.15 Membrane protein synthesis and function in polymersomes: (A) Schematic diagram and (B1 – B3) confocal image series show polymeric vesicles loaded with DNA that encodes the αHL gene, cell-free expression solution, and calcein were incubated to allow an IVTT of αHL monomers, membrane incorporation of monomers and pore assembly and function; (C) Kinetics of time-dependent loss of calcein fluorescence due to the expression of αHL (n = 4).

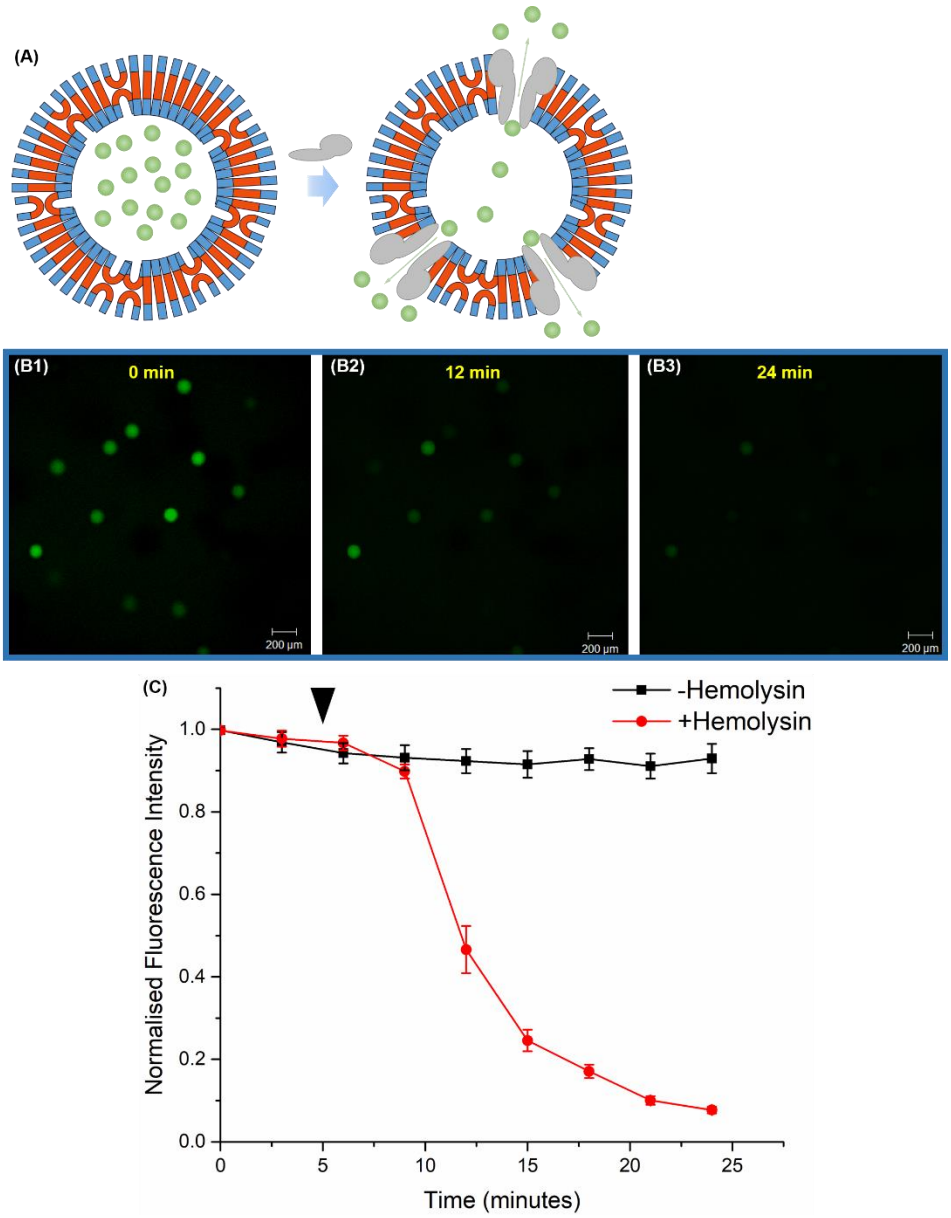

Figure 3.16 Reconstitution of nano pore-forming protein into polymersomes: (A) Schematic diagram and (B1 – B3) confocal image series show αHL pore-mediated transport of fluorescent molecules; (C) Kinetics of time-dependent release of calcein fluorescence (n = 7).

3.4 Conclusion

In this Chapter, we have shown a microfluidic route based on glass capillaries to form monodisperse liposomal and polymersomal structures by using ultra-thin shell

double emulsion droplets as the templates. These thin-shelled double emulsions droplets were constructed with thin layer of organic solvent in the membranes as a result of the biphasic flow mechanism in the injection capillary. By inducing the dewetting transition in the membranes, the organic solvent evaporated, assisting to form either lipid bilayers or polymeric bilayers.

It was shown that IVTT can take place within the produced vesicle-based artificial cell models. EGFP, the water-soluble fluorescent protein was cell-free expressed inside lipid vesicles. The linear increase of fluorescence intensity caused by expressing EGFP was clearly seen, which confirmed that the constructed lipid vesicles were successfully applied as bioreactors to perform the protein synthesis that is a key reaction occurs in natural cells.

Polymeric vesicular compartments were also formed by using the same microfluidic technique. To the best of this author's knowledge this is the first generation of polymersomes composed of PMOXA-*b*-PDMS-*b*-PMOXA, which were widely studied as the best candidate to produce polymersomes using conventional methods. (176) To further investigate the polymeric membrane property, a pore-forming protein induced fluorescent molecules diffusion across the polymeric boundaries was shown, which relied on the incorporation of the membrane proteins into polymeric membranes. IVTT was also performed in our polymeric compartments. The synthesis of αHL within the aqueous core of the polymersomes inserted into the polymersomes and triggered a remarkable decrease of fluorescence intensity that was consistent with the assembly of pores in the bilayers by adding monomers into the external solution. These experiments showed that vesicle-based artificial cells, liposomes and polymersomes, produced by microfluidics offered the great models to deepen our understanding of certain functions of living cells, like cell-cell and cell-environment commutations via functional membrane-associated proteins.

Chapter 4 Mapping Viscosity in Thin-Shell Double Emulsion Templated Lipid Vesicles by FLIM

Chapter 4 describes the use of the molecular rotor based on *meso*-substituted boron-dipyrrin (BODIPY) in combination with fluorescence lifetime spectroscopy for mapping viscosity within artificial bilayers of lipid vesicles fabricated by microfluidics. The aim is to investigate the viscosity of the artificial membrane environment generated from microfluidic interfaces as model lipid bilayers. This will enable us to visualise the membranes of the synthetic cell chassis using fluorescence lifetime image microscopy (FLIM), determining their associated viscosity values. In the future such data may enable us to determine the potential of using these systems to build functional cell-mimetic systems by incorporating channels into artificial bilayers.

4.1 Introduction

4.1.1 Membrane Fluidity

The cell membrane (or plasma membrane) is made up of a complex fluid-like structure of various phospholipids, proteins and cholesterol. (177, 178) It fulfils two important roles during the entire of lifespan of the cell in: (i) maintaining the physical integrity of the cell i.e. to mechanically delimitate the cell from its external microenvironment; and (ii) control the movement of particles (endocytosis and exocytosis of large of particles) and thereby regulate the exchange of substances between internal and external media. (179) One of the key physical parameters of the biomembrane is its fluidity, which determines the ease with which phospholipids are able to travel in the plane of the bilayer. (180-182) It is widely accepted that membrane fluidity acts a pivotal part in cellular functions, such as endocytosis, membrane fusion and cell signalling. (183) Also, changes of this intrinsic property of the biomembrane have been linked to various diseases. (182, 184-190)

4.1.2 Conventional Methods to Measure Membrane Fluidity

There are various techniques for determining the membrane fluidity, which is the intrinsic property of fluid-like structure by observing either the rotational or lateral mobility of a tracer molecule incorporated into the membrane. Typically, membrane

fluidity can be measured with nuclear magnetic resonance spectroscopy (NMR), electron spin resonance (ESR) and fluorescence-based approaches.

The measurement of micro-viscosity in vesicular bilayer has been studied by ESR spectroscopy. (191) In ESR, stable nitroxyl radicals as reporter molecules (spin probes) are widely used to characterise the bilayers microenvironment and membrane dynamics by measuring the rotational correlation time of the spin probes. (191) In addition, ESR is used as a means for quantifiable viscosity values in the bilayer environment at high spatial resolution, with the aim of exploring the significant area of liposomes in drug delivery. (192, 193)

Similar to ESR, deuterium NMR spectroscopy, has been also commonly applied to examine membrane fluidity with deuterated lipids are conjugated into a membrane. (194, 195) In NMR spectroscopy, quantifiable information of membrane micro-viscosity is acquired through the specific spectroscopic features result from the average carbon-deuterium bond orientation of the deuterated lipids. (178) In particular, with ^{2}H-NMR the residual quadrupolar couplings are related to the segmented order parameters of the flexible phospholipid molecules in a liquid-crystalline membrane system. (196) By utilising NMR, the structural and fluid information of a membrane can be simultaneously, non-invasively revealed at atomic precision. As a consequence of the heterogeneous nature of biomembranes, both ESR and NMR offer no insight into lateral differences in membrane viscosity values due to the fact that spectroscopy characteristics depend upon observation of the rotational dynamic of the tracer molecule.

Lateral motions of molecules within the membrane can be probed by a number of fluorescence based methods. These techniques reply on incorporating of a selection of suitable fluorescent molecules with a broad range of wavelengths. (197, 198) Fluorescence recovery after photobleaching (FRAP) has been used to determine the diffusion coefficients or micro-viscosity in biological membrane. (199, 200) In a FRAP experiment, a membrane is fluorescently labelled with fluorescent probes as the first step, and then imaged with weak laser illumination. Subsequently a small

region, termed as the Region of Interest (ROI) is photobleached using an intense laser pulse. The bleached area is then imaged over time with a significantly reduced laser illumination to record the recovery of fluorescence signals, which results from the lateral diffusion of the phospholipid molecules into the photobleached spot. By monitoring the kinetics of fluorescence recovery with time, the diffusion coefficient of the fluorescent lipid or tracer probe within the membrane can be determined and corresponded to the lateral motion in the bilayer environment.

FRAP is a simple and powerful technique for the analysis of lipid mobility in the larger membrane and generation of the maps of diffusion coefficient in a single spot. However, FRAP suffers from its lack of spatial resolution information which is of significance when investigating the membrane as a whole. (201, 202)

Another ideal technique to study the lateral organisation of the membrane can be found in Fluorescence Correlation Spectroscopy (FCS). (203-205) Similar to FRAP, the application of FCS requires fluorescent labelling of the molecules of interest, and the measurement of membrane lateral heterogeneities are based on the fluctuations, which are given rise by the mode of lateral diffusion of the probe, in fluorescence intensity acquired from a diffraction limited observation volume. Positioning the tiny focal volume to the plane of the bilayer allows direct measurement of the translation mobility coefficient of a low concentration of fluorescent probes. (206) Recent research demonstrated that FCS equipped with higher spatial resolution ($>$ 500 nm) is available that go beyond the resolution limit. (207) In spite of the fact that many technically-demanding FCS-based techniques are able to investigate the membrane lateral dynamics, in the most of cases only a tiny observation spot readout is possible and spatially-resolved information is inaccessible.

4.1.3 Molecular Rotors

The definition and prospect of molecular rotors was coined by the pioneer in nanotechnology Richard Feynman in his talk "There's Plenty of Room at the Bottom" at an American Physical Society meeting in 1959. (208) Very recently, molecular

rotors have emerged to be a promising probe to shed light on quantifying the micro-viscosity in biological systems, such as living cells and biomimetic cell models. (209-212)

The molecular rotors, specifically exploited in this thesis, are a class of synthetic viscosity-sensitive fluorophores in which fluorescent parameters, such as their quantum yield and fluorescence lifetime, are strongly correlated to the micro-viscosity of their immediate environment. (75, 212) The sensitivity to viscosity of the molecular rotors originates through altering the non-radiative deactivation rate of the excited state in a viscous surrounding medium. This typically occurs due to a viscosity-dependent intramolecular structure change, such as twisting or rotation. (212) Upon exaction, the double bond decreases in bond order producing a bond of 1, which becomes flexible to rotation. In the excited state that is barrierless for rotation, the rate of rotation can be described according to the Stokes-Einstein-Debye relationship.

$$k_{rot} = \frac{1}{\theta_r} = \frac{k_B T}{4\pi r^3 \eta} \tag{4.1}$$

Where k_{rot} is the rate of rotation, θ_r is the rotational-correlation time, k_B is the Boltzmann constant (1.3806×10^{-23} m^2 kg s^{-2} K^{-1}), T is the absoluate temperature, r is the radius of the molecule in metres and η is the solvent viscosity in N s m^{-2}.

As reviewed in Chapter 2, the fluorescence lifetime is correlated to the sum of radiative and non-radiative rate constants. The most widely adopted class of molecular rotors are featured with Twisted Intramolecular Charge Transfer (TICT) excited states. (213) In the case of this particular type of rotors, intramolecular rotation is the leading basis of the non-radiative decay. Assuming $k_{nr} = k_{rot}$, then Equation (4.1) can be rewritten by integrating Equation (2.1) to give Equation (4.2):

$$\tau = \frac{1}{k_r + \frac{k_B T}{4\pi r^3 \eta}} \tag{4.2}$$

In the above relationship τ is the fluorescence lifetime and k_r indicates the radiative decay rate constant, and this relation delivers a connection between the fluorescence lifetime and the values of temperature and viscosity of the media. In additional to Equation (4.2), a more practical relationship between viscosity and fluorescence lifetime was described by Förster-Hoffmann model shown below. (214)

$$\tau = C_m \times \eta^{\gamma} \tag{4.3}$$

where C_m is the concentration-temperature constants and γ is the dye dependent molecular parameter, which is calculated from the slope of a straight line yield from a plot of a function of logarithm of fluorescence lifetime vs logarithm of viscosity.

These values are obtained by measuring the lifetime of the molecular rotor in solutions with different mixture ratios, for example methanol-glycerol mixtures of increasing glycerol content corresponds to a higher viscosity. Various of fluorescent molecules highlighted with viscosity-sensitivity characteristic have been reported, such as retinol palmitate, (215) Hoechst 33258, (216) DCVJ, (213) and di-4-ANEPPDHQ. (217) A type of fluorophore, *meso*-substituted boron-dipyrrin (BODIPY), has attracted scientists' attention can act as a molecular rotor featured with strong correlation with the viscosity with sharp variations in its fluorescence quantum yield and lifetime. (209) The combination of this class of viscosity sensitive fluorophores with Fluorescence Lifetime Imaging Microscopy (FLIM) opens the door to highly resolved spatial mapping of local micro-viscosity in biological membranes. (209, 210, 212, 218)

4.1.4 Giant Unilamellar Vesicles

The cell is an active and exquisitely complex system and is difficult or even impossible to fully understand due to the wide variety of processes occurring, in

partnerships, at any one time. A variety of idealised systems and cell models have been created and synthesised to circumvent this problem. A promising candidate is a giant unilamellar vesicle (GUV), which provides cell-like structure with a confined volume of aqueous media. It can be used to study biochemical reactions as well as physical nature of the membrane. Membranes or bilayers in the form of giant vesicles have been utilised as controlled and flexible platforms for membrane research. Engineering of giant vesicles in wide range of size can be performed using electroformation, gentle hydration, extrusion or microfluidics. An example of compounds for self-assembly of bilayer and the categories of giant vesicles are treated in detail in Chapter 3.1.1.

4.2 Materials and Methods

4.2.1 Materials

The phospholipids for experimentation were from stock samples purchased from Sigma Aldrich. 1, 2-dioleoyl-*sn*-glycero-3-phosphocholine (DOPC) was purchased as lyophilised powders and subsequently dissolved in chloroform at 25 mg/ml. For microfluidically produced thin-shell lipid vesicles, DOPC was diluted at 5 mg/ml into a solvent mixture of chloroform and hexane with a volume ratio of 36:64 (Sigma). Microfluidic lipid vesicles were fabricated and collected using similar inner (PEG and PVA) and outer (PVA) aqueous solutions, and collection solution (50 mM NaCl) presented in Chapter 3.

4.2.2 BODIPY Based Molecular Rotor

The molecular rotor applied in the membranes in this study was a kind gift from Dr. Marina Kuimova who is from Imperial College London. The fluorescent molecule was synthesised as described in previous work by Dr. Marina Kuimova group. (210, 219, 220) The molecular rotor, which is a substituted boron dipyrromethene (BODIPY) derivative, is depicted in Figure 4.1. The fluorescence spectrum is presented in Figure 4.2 and shows that the excitation and emission wavelengths are 490 nm and 520 nm, respectively.

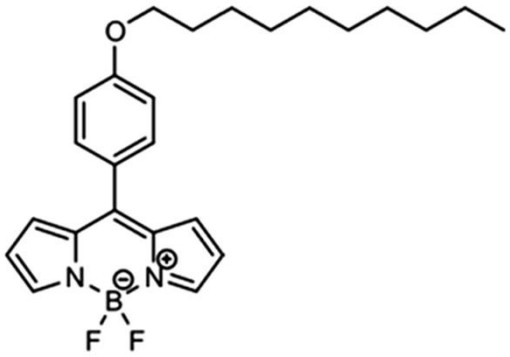

Figure 4.1 The chemical structure of the *meso*-substituted BODIPY molecular rotor (BODIPY-C10).

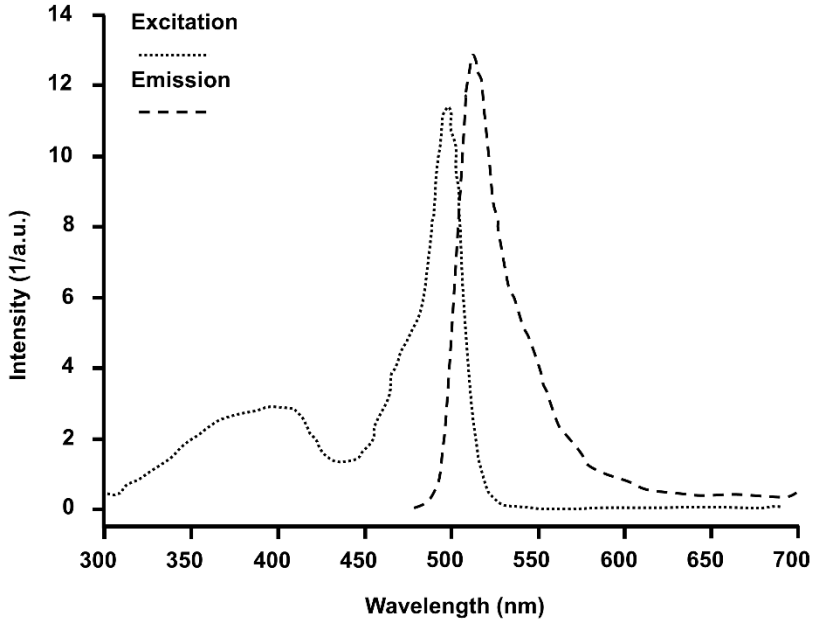

Figure 4.2 The fluorescence spectrum of the BODIPY-C10 molecular rotor with phospholipid in chloroform.

4.2.3 Preparation of Giant Unilamellar Vesicles

4.2.3.1 GUV Electroformation

The most popular method for GUV production is an electroformation technique firstly outlined by Miglena Angelova et al. (35) The underlying theory of creation of GUVs via electroformation relies upon applying an alternating electric field across hydrating lipid layers, leading to lipids reorganising into membrane buds and forming vesicular structures. Electroformation for the preparation of giant vesicles adopted was based on a standard protocol. (221) The desired lipid was made up to a final concentration of 3.75 mg/ml which used to generate a uniform lipid coating. The lipid was initially diluted at a concentration of 25 mg/ml in a solution of chloroform. The mixture was made up to a 1 ml solution of chloroform and acetonitrile with a volume ratio at 95:5. Prior to form the lipid films, the solution was stored in the freezer at -20°C for a few days.

Clean indium tin oxide (ITO)-coated slides (30 × 30 mm) for electroformation were prepared by connecting with one copper wire secured with conductive paint to provide electrical contact. The conductivity of the ITO slides was obtained with a multimeter to measure the resistance, between the ends of the wire and the centre of the slides, and only those with $< 40\ \Omega$ were used. These slides were then rinsed with methanol and blow dried using compressed nitrogen. The lipid solution was then spin-coated onto the conductive surface of the ITO slides, at a speed of 300 rpm for 30 seconds to produce an even lipid coating across the entire slides. After spin-coating, the lipid-coated slides were dried under vacuum for at least two hours to ensure the removal of all residual solvent exists within the lipid film.

The ITO slides coated with lipid sheets were then separated from the conductive surface of another uncoated ITO by a rubber gasket, either a rubber O-ring or a PDMS block with an excised centre, and sealed with vacuum grease to form a sealed chamber for electroformation. The set-up for electroformaion was assembled as depicted in Figure 4.3(A).

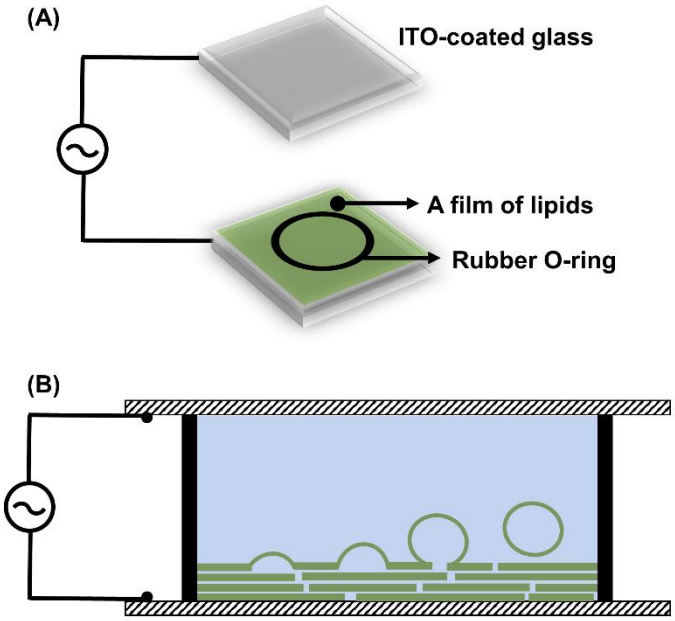

Figure 4.3 (A) Electroformation set-up. Two surfaces of ITO slides (one with a lipid sheets) were separated by a rubber O-ring forming a chamber for electroformation. The chamber was filled with inner buffer of 100 mM sucrose, and an AC-field was applied to the surfaces of ITO slides to initiate electroformation; (B) Schematic of electroformation apparatus for the construction of DOPC GUVs. DOPC vesicular structures formed by budding off from the film of the conductive substrate.

The electroformation experimentation requires two solutions which were used to control pH values and osmotic pressure as well as to provide a density gradient between inner and outer GUV environment. An interior buffer consisting of 100 mM sucrose was used and an exterior collection buffer of 90 mM glucose and 10 mM HEPES (pH adjusted to 7.4 using 25% KOH) was used to provide a sugar density gradient, which ensured that GUVs settled to the coverslip surface for investigation by optical microscopy. 300 μl of inner buffer (100 mM sucrose) was added into the chamber before sealing the ITO slides. For single phase (DOPC) GUVs electroformation, an AC-field electroformation pulse sequence was applied across the interior buffer-filled electroformation chamber, as displayed in Figure

4.3(B), and electroformation parameters used for DOPC GUVs was outlined in Table 4.1.

Table 4.1 Electroformation pulse applied into the electroformation chamber. The voltage was ramped from 0.1 to 1.6 Vpp over the duration of 60 minutes, then maintained at 1.6 Vpp for a further 60 minutes, at the frequency of 10 Hz. This pulse sequence stimulated vesicles growth from the lipid-coated ITO slides. The 2.0 Vpp pulse applied for 60 minutes, at a frequency of 4 Hz with the aim to the detachment of GUVs from the slides.

Pulse frequency (Hz)	Pulse voltage (Vpp)	Pulse shape	Time (minutes)
10	0.1	Sine	10
10	0.5	Sine	20
10	1.0	Sine	30
10	1.6	Sine	60
4	2.0	Square	60

Once detached the DOPC GUVs were transferred into the 1 ml of glucose buffer at a concentration of 90 mM associated with 10 mM HEPES. This provided adequate distribution of DOPC vesicles over the surface of a coverslip to investigate single vesicle without interaction with other GUVs. For study of GUVs using FLIM the vesicle solution was gently pipetted to a microscope slide with a well and then sealed with a square coverslip which can cover the well space to ensure no evaporation of the buffer and no movement of solution caused by convection.

4.2.3.2 Microfluidic Generation of GUVs

DOPC vesicles templated by double emulsion droplets and thin shell were produced according to the detailed protocol described in Chapter 3. The inner aqueous phase of PEG and PVA was pumped into the small injection capillary; and the BODIPY-C10 molecular rotor was dissolved in the lipid middle phase at a concentration of 0.1

mol% (1:1000 molecular rotor : lipid), which was injected in the another injection glass tube. 10 wt% of PVA solution as outer fluid was pumped into microfluidic device through the interstice between the injection capillary and the square capillary. A glass vial containing collection solution was used to store the produced double emulsion droplets, in which dewetting process occurred aids the transformation of as formed lipid vesicles from double emulsion templates.

For the exploration of membranes of as formed GUVs using FLIM, the vesicles were pipetted gently to a dished microscope slide with the tip-cut pipette tips reducing the shear forces applied to the GUVs. A coverslip was then sealed onto the microscope slide securing the vesicles within the well for the observation.

4.2.4 Fluorescence Lifetime Data Analysis

All fluorescence lifetime data for this chapter was acquired and analysed using Becker & Hickl SPCImage data analysis software package. To generate fluorescence lifetime images, all fluorescence decays recorded in each pixel were fit with either mono or bi-exponential decay models according to Equations (4.4) and (4.5), respectively, with the goodness of fit regulated by the reduced chi-squared, χ^2, test.

$$I(t) = I_0 \exp\left(\frac{-t}{\tau}\right) \tag{4.4}$$

$$I(t) = \alpha_1 \exp\left(\frac{-t}{\tau_1}\right) + \alpha_2 \exp\left(\frac{-t}{\tau_2}\right) \tag{4.5}$$

where I is the fluorescence intensity, t is the time, I_0 is the fluorescence intensity immediately after exaction and τ is the fluorescence lifetime. In Equation (4.5), $\alpha_1, \alpha_2, \tau_1$ and τ_2 are the amplitudes and lifetimes of the two exponentially decaying components. These fractional contributions and lifetimes of the two fitted decay components were plotted as functions of time, and the mean lifetime (τ_{mean}) was calculated according to Equation (4.6). For all fluorescence lifetime images, the goodness of fit parameter χ^2 values for various pixels between 0.8 – 1.3 indicated as

a good fit. For lifetime imaging all images were gathered until a maximum signal in the peak channel of 100 counts was recorded.

$$\tau_{mean} = \frac{\alpha_1\tau_1^2 + \alpha_2\tau_2^2}{\alpha_1\tau_1 + \alpha_2\tau_2} \tag{4.6}$$

To obtain a complete model, the instrument response function (IRF) for a FLIM system needs to be taken into account, due to the impact that IRF gives rise to the decay function. The IRF is the function the FLIM system would record when it detects the laser pulse directly, which describes the shape of the excitation pulse and the measurement method.

In order to achieve accurate fitting, it is necessary to deconvolve the measured fluorescence decay data from the IRF. Artificial IRFs can be adopted to the fitting, however, these would not elucidate any unique aberrations induced by reflections or misshaping of laser pulses in the FLIM set-up. In addition, artificial IRFs cannot be used to investigate data which may have a shorter lifetime than the provided IRF.

Real (measured) IRF data was acquired by parking the laser beam at the centre of the optical axis and removing the selective filters before the detector. Neutral density filters were positioned before the pinhole for reducing the optical density to protect the detector from damage. Measurement of IRF was conducted under the same conditions as acquisition of FLIM data. All parameters affecting the timing and the time scale (ADC Resolution, TAC and CFD) were held constant for both IRF and lifetime measurements. The electronic slider for controlling the laser power was also maintained as it can have an effect on the shape of the laser pulse. The real IRF data must be reasonably free of fluorescence, so the fluorescent sample was replaced with a non-fluorescent scattering object, for example, a glass cover slip, and the resultant signal was recorded for one second with a maximum signal in the peak channel of 50000 counts allows the IRF to be considered as practically noise-free.

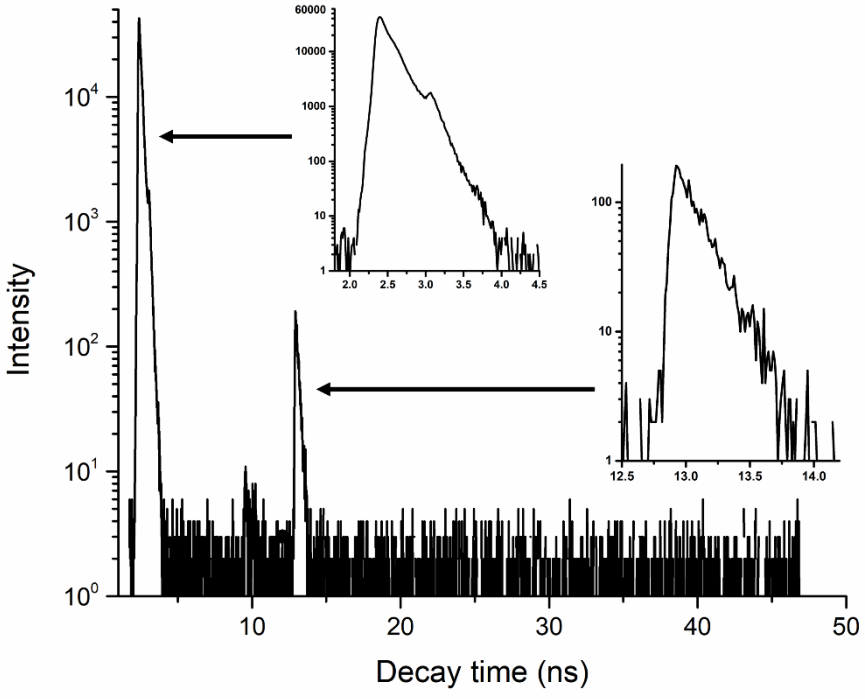

Figure 4.4 IRF recorded using 473 nm laser at a repetition of 20 MHz. The first peak corresponds to initial laser pulse recorded from a glass scattering sample and the second peak related to optical reflection within the FLIM system.

In Figure 4.4, a typical IRF was measured using the 473 nm laser line at a repetition rate of 20 MHz with a glass cover slip as a scattering target. It can be seen that a secondary pulse exists which is two orders of magnitude lower in intensity than that of original laser pulse occurs 11 seconds earlier. The most likely source of this pulse originates from reflections within the optical path of the detection system.

4.3 Results and Discussion

4.3.1 Effect of Measured IRF on Fluorescence Decay Fitting

To determine the impact of the measured IRF, especially the secondary pulse on the fluorescence decay curves, rhodamine was used as the fluorescent calibration solution of known lifetime. Rhodamine B aqueous solution is known to have a

fluorescent lifetime (measured at 20°C) of 1.74 ns. (222) The fluorescence decay of the fluorophore can be fitted with a simple single-exponential.

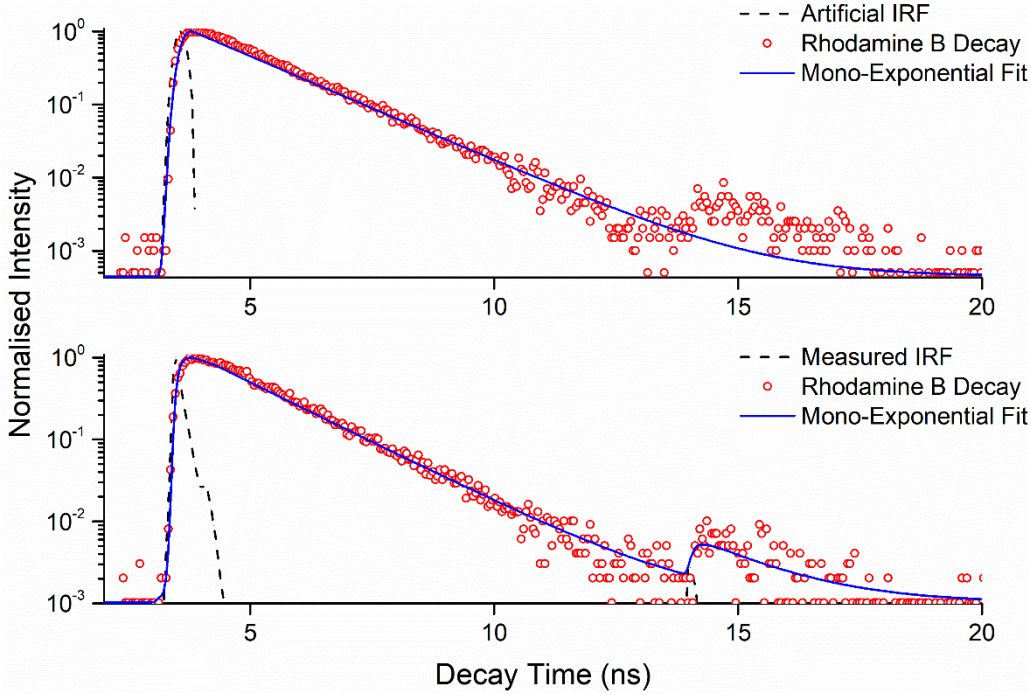

Figure 4.5 Fluorescence decay profiles for Rhodamine B aqueous solution at a temperature of 20°C analysed with both an artificial IRF (top) and a real IRF (bottom).

In Figure 4.5, it can be seen that the artificially generated IRF provide a defective fit to the measured rhodamine B fluorescence lifetime data as indicated by a high χ^2 value of 6.83 with a corresponding lifetime value of 1.98 ns. The lifetime value acquired from the data is greater than that of rhodamine B calibration solution. The secondary pulse of the IRF contributes to the exaggerated lifetime value. A good mono-exponential fit was obtained when analysing the fluorescence data with the real IRF, showing a lifetime value of 1.72 ± 0.02 ns with a χ^2 of 1.3 ± 0.1.

4.3.2 Calibration of Viscosity Probe

Prior to using the molecular rotors mapping, the viscosity within the artificial membrane, the relationship between the fluorescence lifetime and viscosity for BODIPY based viscosity-sensitive fluorophore were determined in a series of methanol and glycerol solutions of varying concentrations of glycerol, Figure 4.6. Acquisition of data on the calibration of molecular rotors was under kind help by Dr. Niall Geoghegan.

The obtained relationship plot was also used for the purposes of the calibration of the molecular rotors and quantitative measurement of viscosity values from converted lifetime. The viscosity probe was initially dissolved in the methanol at a concentration of 2.5 μM before glycerol was added to adjust the viscosity. Concentrations varied from 50 vol% to 90 vol% glycerol where measured at temperatures between 10°C and 60°C to produce the calibration graph. Temperature was controlled using a peltier heater coupled to a thermocouple controlled by a PID board to maintain the temperature to be constant in this calibration experimentation.

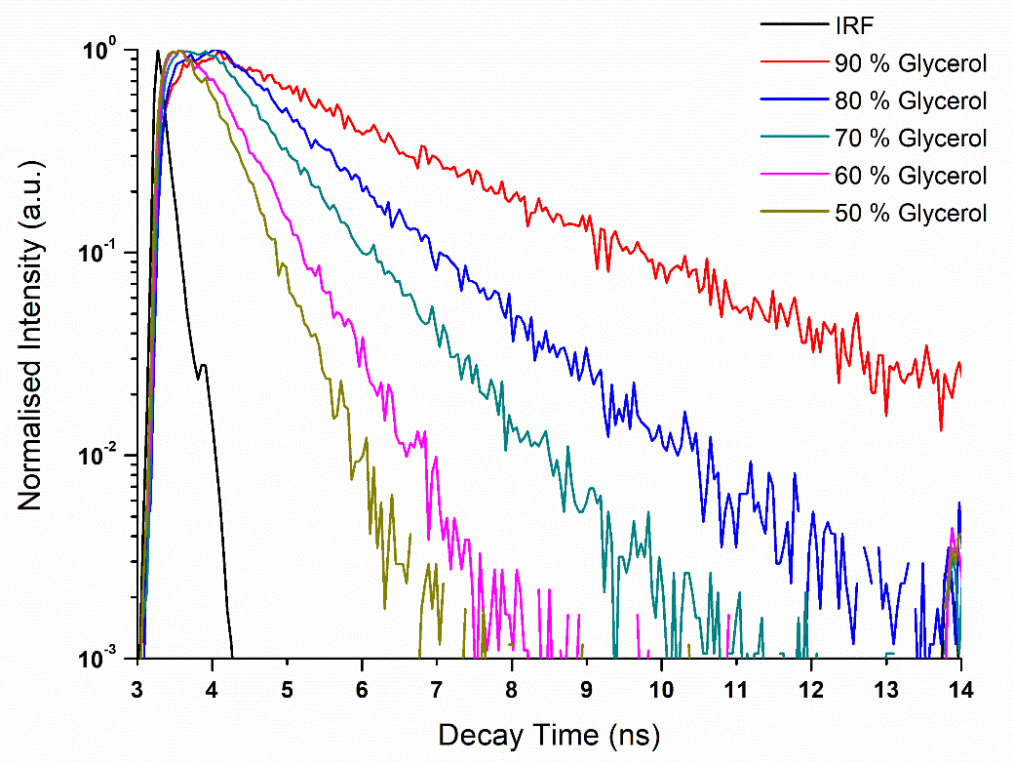

Figure 4.6 Selected fluorescence decay traces for BODIPY-C10 recorded in methanol and glycerol mixtures (50 vol% - 90 vol% glycerol) of different viscosity.

As the concentration of glycerol increases, the fluorescence lifetime of the viscosity probe varies markedly as a function of viscosity in accordance with the aforementioned theory. The fluorescence decay profiles for each solution mixture were mono-exponential indicating only one population of the molecular rotor in each solution. Furthermore varying the temperature for each solution determined the calibration curve in Figure 4.7.

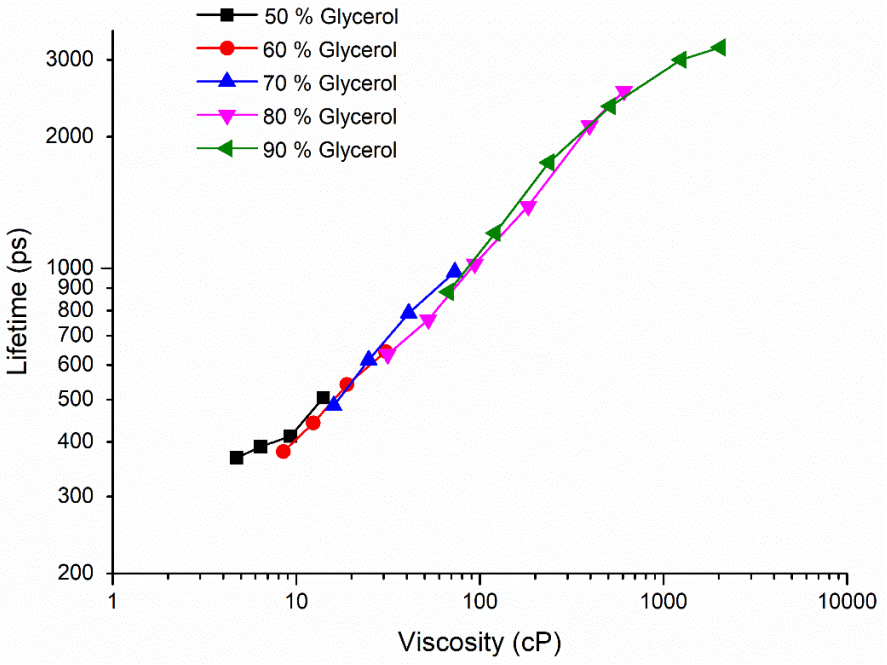

Figure 4.7 Fluorescence lifetime of BODIPY-C10 recorded in methanol/glycerol mixtures of various compositions, plotted against viscosity. The data were taken over temperature range of 283 K – 333 K.

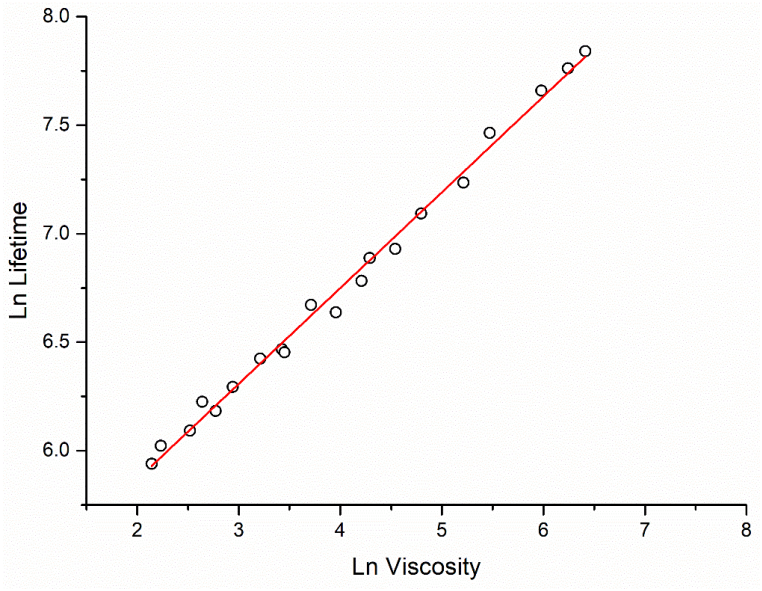

Figure 4.8 A plot of Ln fluorescence lifetime vs Ln viscosity for BODIPY-C10 yields a straight line with a gradient of 0.44 (R^2 = 0.99) in accordance with the Föster-Hoffmann equation (viscosities range from 10 cP to 1000 cP).

The calibration of the molecular rotors was also performed to investigate the viscosity alteration by the temperature shown in Figure 4.7. Importantly, it can be concluded that the temperature increase does not have any influence on the photophysics of BODIPY-C10 or its function as a molecular rotor, apart from the alteration of the viscosity of the solution. In Figure 4.8, a linear relationship was observed between the Ln lifetime vs Ln viscosity over two decades of viscosity values, which shows good agreement with the modified Förster-Hoffmann equation, Equation 4.7, within this viscosity range. Two viscosity dependent constants, C_m and γ were derived by fitting a linear function to the Ln-Ln plot of lifetime vs viscosity. The obtained values of C_m = 4.98 and γ = 0.44, which are consistent with previously reported values. (210) The results of BODIPY-C10 calibration corroborate previous literatures in which similar compounds were calibrated over the same range of viscosity. (210, 219) The generated calibration plot allows us to use molecular rotors lifetimes to determine an unknow viscosity.

$$\ln(\tau) = \ln C_m + \gamma \ln(\eta) \tag{4.7}$$

4.3.3 Lipid Vesicles Generation

4.3.3.1 Microfluidic Method

A glass capillary microfluidic device was used to fabricate double emulsion drops with ultrathin membranes, (147) as illustrated in Figure 4.9. We used innermost smaller capillary to inject aqueous phase of 8 wt% PEG and 2 wt% PVA, into the left tapered capillary. The inner surface of the left tapered injection capillary was rendered to be hydrophobic, thus preventing wetting of the innermost aqueous phase on the capillary wall. We used this tapered capillary to inject the middle oil phase, DOPC dissolved in a mixture of chloroform and hexane which volume ratio is 36:64; the total lipid concentration is 5 mg/ml. The viscosity probe BODIPY-C10 was added into DOPC solution at a concentration of 0.1 mol%.

We injected the innermost aqueous phase and middle oil phase at flow rate of 500 μl/h and 400 μl/h, respectively; under these conditions the innermost aqueous phase formed large water in oil emulsion drops within the left tapered capillary, as shown in the schematic illustration in Figure 4.9. We then pumped the outer aqueous phase, a 10 wt% PVA solution, through the interstices between the left tapered capillary and the square capillary, at flow rate of 2000 μl/h. We treated the right tapered capillary to modify its surface hydrophilic, thus preventing wetting of the middle oil phase on its wall. To prevent osmotic stresses, we collected the highly monodispersed double emulsion drops in a 50 mM NaCl solution having the same osmolarity as the inner water cores.

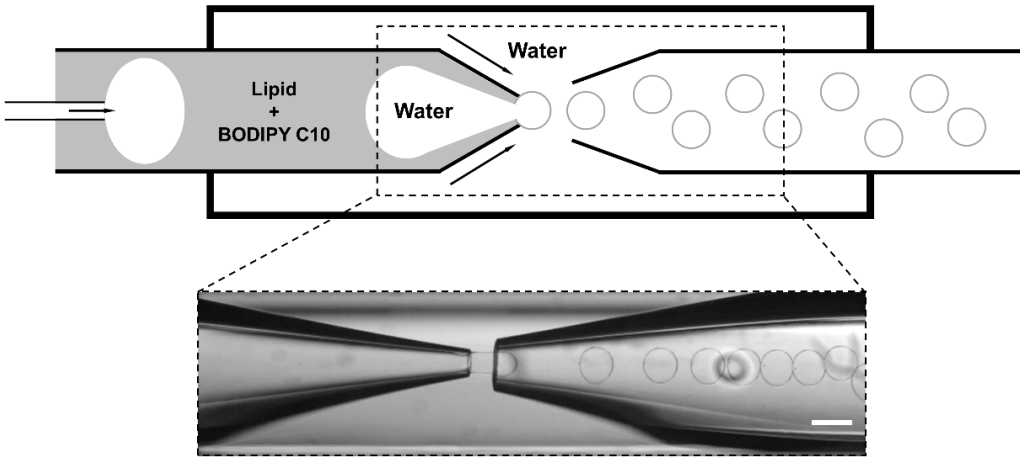

Figure 4.9 Schematic of preparation of thin-shell double emulsions in a glass capillary microfluidic device; high speed camera snapshot of the formation process of double emulsions. Scale bar denotes 200 μm.

Monodispersed water-in-oil-in-water double emulsions were successfully generated using this device. The double emulsion droplets were incubated at the room temperature in the 50 mM NaCl collection buffer. In the similar fashion of the formation of lipid vesicles described in the Chapter 3, chloroform the good solvent for the lipids rapidly diffused from the thin shells of double emulsions to the surrounding medium. The reduction in the solvent quality induced two lipid monolayers, which subsequently came together, forming a lipid bilayer membrane.

As a consequence, the stable lipid vesicles were completely transformed from microfluidically produced the double-emulsion templates with ultrathin shells. As shown in Figure 4.10, owing to the precise control over the size of the double-emulsion templates, as-formed lipid vesicles are extremely uniform with the mean diameter of lipid vesicles is 178.5 ± 6.3 μm, Figure 4.10(A).

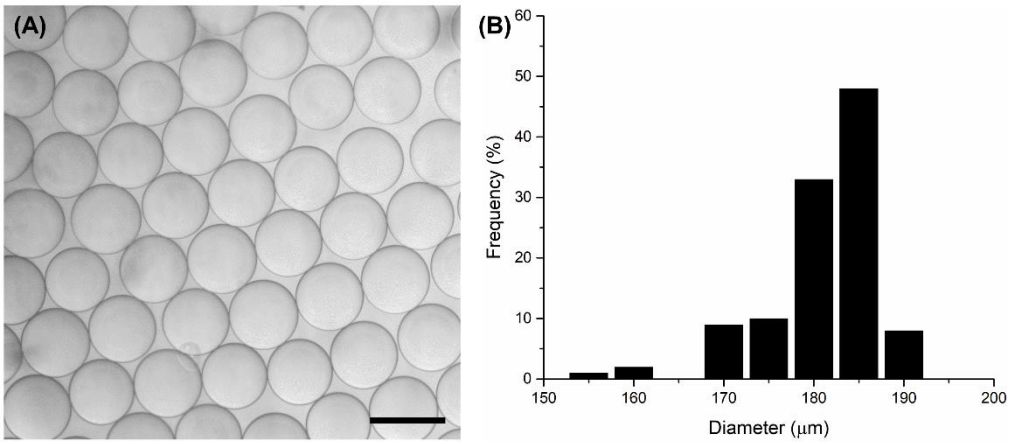

Figure 4.10 (A) Optical microscope image of the resultant monodisperse lipid vesicles producing using flow rates equal to 500 μl/h, 400 μl/h and 2000 μl/h for respectively inner, middle and external phase. Scale bar represents 200 μm; (B) Size distribution (diameter) of the measured lipid vesicles (n = 111).

Figure 4.11 shows as-prepared lipid vesicles with their bilayers stained by BODIPY-C10 molecular rotors. The resultant liposomes were highly monodispersed, in which the molecular rotors distributed homogeneously in the lipid vesicles boundaries.

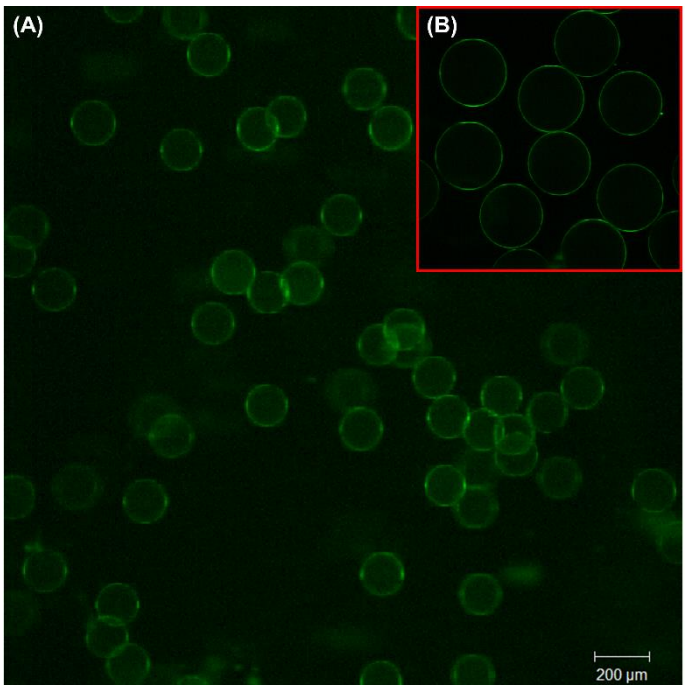

Figure 4.11 Confocal laser scanning microscope image of lipid vesicles with BODIPY-C10 entrapped in bilayers produced by microfluidics: (A) Confocal images of as-formed uniform lipid vesicle observed under a 5x objective lens. Scale bar is 200 µm; (B) Inset in (A) is confocal image of lipid vesicles imaged by a 20x objective lens.

4.3.3.2 Electroformation Method

High quality of giant unilamellar vesicles (GUVs) incorporated with BODIPY-C10 were produced at high yield using electroformation as shown in Figure 4.12.

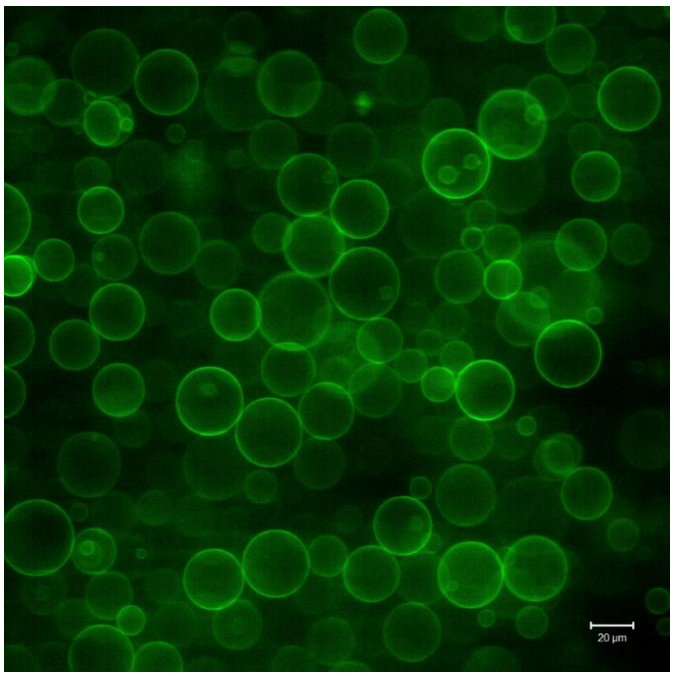

Figure 4.12 Confocal laser scanning microscope image of DOPC GUVs within electroformation chamber that were labelled with 0.5 mol% molecular rotors, showing the high yield possible using electroformation. Scale bar is 20 µm.

Owing to the mechanism of the electroformation method, the organic solvent used to dissolve lipid molecules was degassed for several hours ensuring that the solvent-free environment resulted in the self-assembly of the lipids into several stacks of bilayers on the ITO slides surface. A complete rehydration with an aqueous solution was initiated in the presence of an AC electric filed. Growth and detachment of GUVs within the electroformation chamber was obtained by gradually reducing the AC frequency in a stepwise fashion. As a consequence, the electroformed GUV compartments were enclosed by a single lipid bilayer without any organic solvent.

4.3.4 Viscosity Studies in DOPC Bilayers – GUVs and Microfluidic Fabricated Lipid Vesicles

Lipid vesicles templated from thin-shell double emulsion droplets were produced by microfluidics, providing a useful model system to mimic the biomembranes of cells. The resultant lipid bilayers were formed as a result of the dewetting process, which

was with the assistance of an organic solvent mixture, chloroform and hexane. However, the viscosity of artificial biomembranes as well as biocompatibility were strongly influenced by the presence of organic solvent. The combination of FLIM and the viscosity-sensitive molecular rotors pave the way to monitor the dewetting-induced artificial bilayer formation, Figure 4.13, through comparing the viscosity within microfluidic prepared membranes with the solvent-free membrane environment formed via electroformation.

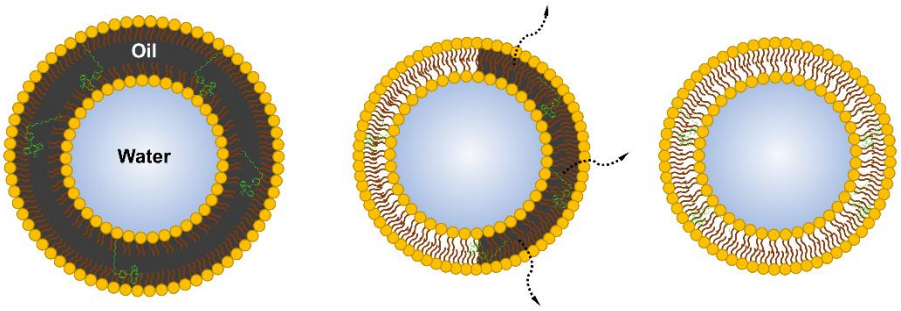

Figure 4.13 Schematic demonstration of fluorescence lifetime measurement of dewetting-induced bilayer formation with incorporation of BODIPY-C10 rotor in the membrane.

The fluorescent lifetime of the molecular rotor BODIPY-C10 was measured in both lipid bilayers formed by microfluidics and electroformed lipid bilayer over a course of time, at ambient (room) temperature. Lipid vesicles were prepared in both methods only composed of DOPC, which is presented for the fluid phase at 20°C. In terms of lipid vesicles produced by microfluidics, the fluorescence lifetime measurement started from the collection off-chip, and were tested at another two time points, 20 minutes and 40 minutes respectively. The electroformed liposomes were characterised in the same fashion. FLIM was used to determine the lifetime value, and therefore the viscosity of two types of vesicles.

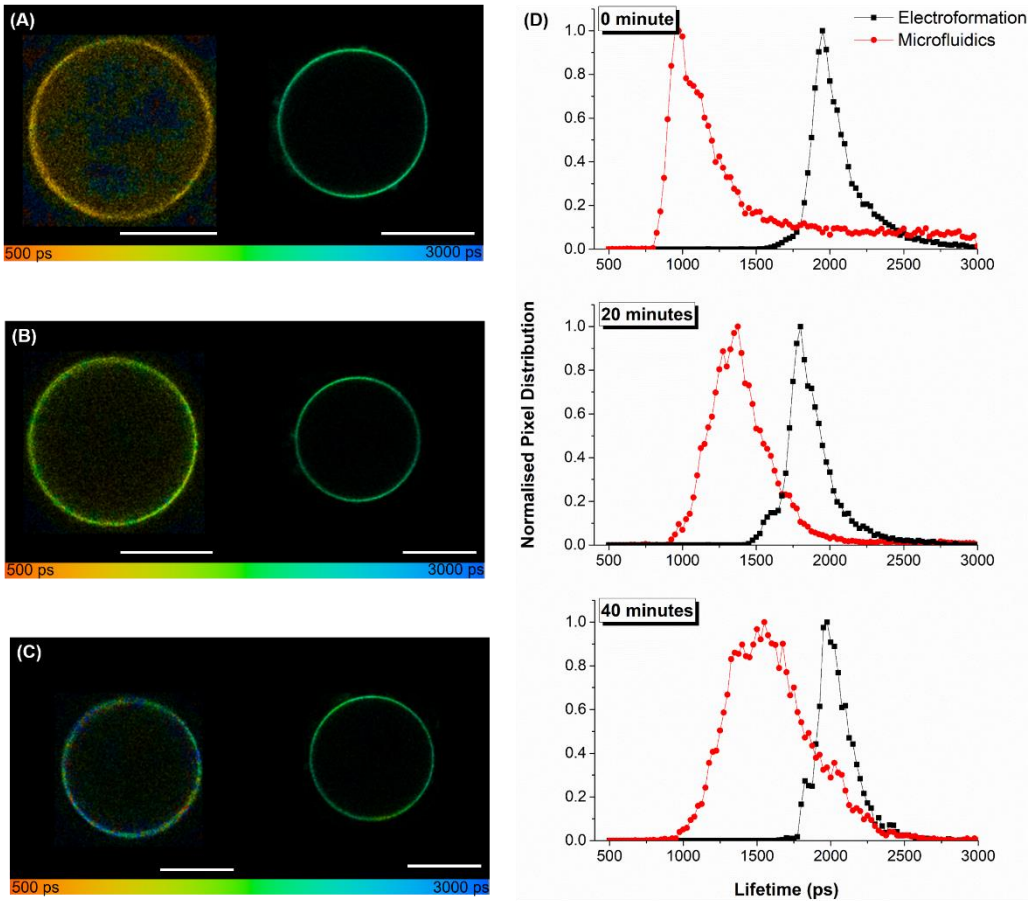

Figure 4.14 Representative fluorescence lifetime images of two kinds of lipid vesicles imaged with BODIPY-C10 rotor and the corresponded lifetime values: (A) FLIM image of a microfluidic produced lipid vesicle (left) and a electroformed liposome (right) at 0 minute; (B) Both two types of vesicles imaged at 20 minute after preparation; (C) Fluorescence lifetime images of two vesicles at 40 minute; (D) The corresponded lifetime histograms of two vesicles measured at 0, 20 and 40 minutes. The fluorescence lifetime range 500 – 3000 ps. Scale bar for microfluidic fabricated and electroformed lipid vesicles are 100 μm and 20 μm, respectively.

In Figure 4.14, the lifetime images for BODIPY-C10 in DOPC were best fit to a bi-exponential decay. This is in contradiction to the reported mono-exponential decays in fluid phase bilayer, for example DOPC bilayers, for BODIPY based viscosity-sensitive rotor. (210, 212, 223) In comparison with fluid phase bilayer fit with a mono-exponential decay, the source of the second decay component occurred in both vesicle generation methods may originate from the aggregation of BODIPY-

C10 rotor which may form during the electroformation process and/or the dewetting process, respectively. As can be seen from the representative lifetime images in Figure 4.14 (A-C), which were plotted in the same colour scale, the lifetimes of microfluidic constructed lipid vesicles gradually increased. In contrast, the lifetimes of electroformed liposomes measured at three time points with 20-minute interval remained constant.

Further, both trends of lifetime alteration over time for two different vesicles are shown in Figure 4.14(D) in which lifetime distributions and the average lifetimes of double-emulsion templated lipid vesicles at 0, 20 and 40 minutes were 975 ps, 1375 ps and 1550 ps are displayed. This showed a significant, 59% increase in the average lifetime value, while the average lifetimes of electroformed liposomes showed little change (at around 1950 ps - presenting an unperturbed state of lifetimes over 40 minutes).

The increase of lifetimes of microfluidics-artificial bilayer results, perhaps result from the dewetting process occurring in the membranes over the period of the measurements (as a result of evaporation of volatile solvent (chloroform) and the diffusion of hexane into surrounding aqueous phase). As depicted in Figure 4.13, during the dewetting process, the tail groups of the lipid molecules gradually stick together where fatty acid chains tangle resulting in a more viscosity membrane environment compared with organic solvent existed membrane.

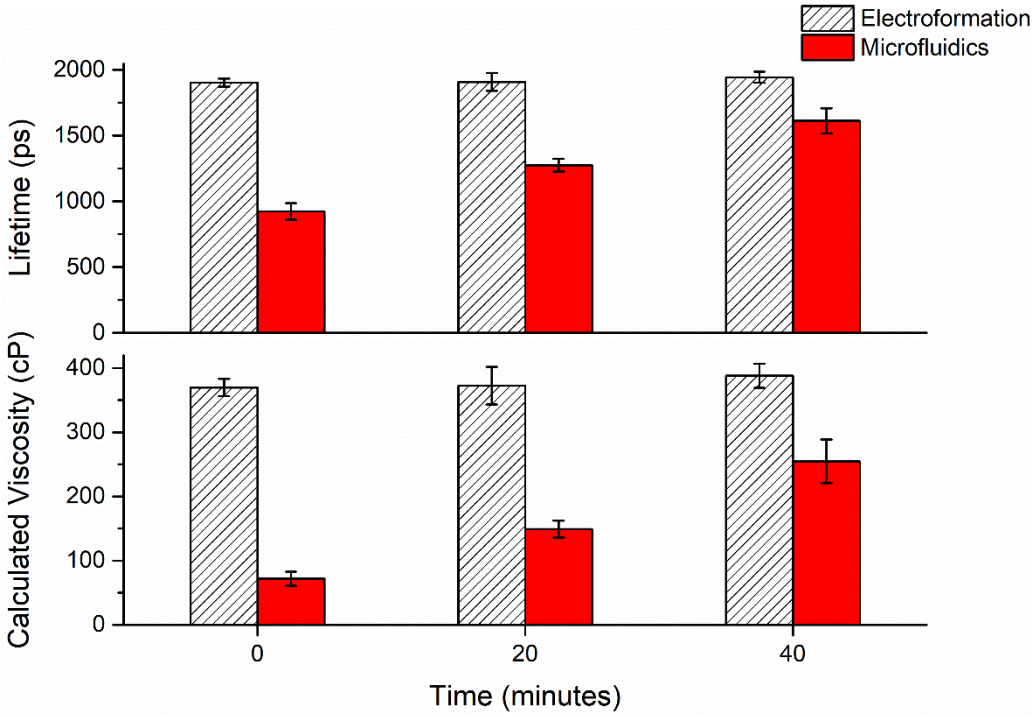

Figure 4.15 Comparison of lifetimes and viscosities measured in two population of vesicles made by microfluidics (red data) and electroformation (patterned data). Error bars represent the standard deviation (n = 3 – 4).

As discussed above, based upon the lifetime value obtained from the single vesicle during 40 minutes, the lipid vesicles' bilayers tend to be more viscous, whereas no significant alteration can be seen in electroformed vesicles over the range of lifetimes measured. In order to further quantitatively explore the membrane viscosity of lipid vesicles, 3 – 4 vesicles were imaged and characterised by FLIM for both fabrication approaches. In Figure 4.15, the lifetimes measured by FLIM for two types of vesicles are shown, demonstrating a good agreement with the trends shown in Figure 4.14(D). A similar significant rise in calculated viscosity of microfluidic-based liposomes are presented in Figure 4.15. At the beginning of FLIM measurement, the target membrane was in fact, thin-shell double emulsion membranes where solvent mixture homogenously entrapped, resulting in a less viscos membrane (71.96 ± 10.88 cP). As dewetting-assisted bilayer formation occurred the calculated viscosities of semi-formed bilayer at 20 minutes was 149.02 ± 13.06 cP, and 254.63 ± 33.82 cP at

40 minutes. The more viscous membrane was, the less organic solvent encapsulated in the bilayers. The viscosities of electroformed liposomes for 0, 20 and 40 minutes were 369.80 ± 13.57 cP, 372.47 ± 29.35 cP and 387.96 ± 18.75 cP respectively, indicating these solvent-free bilayers were good biomembrane references used to be compared with vesicles built by the microfluidic technology.

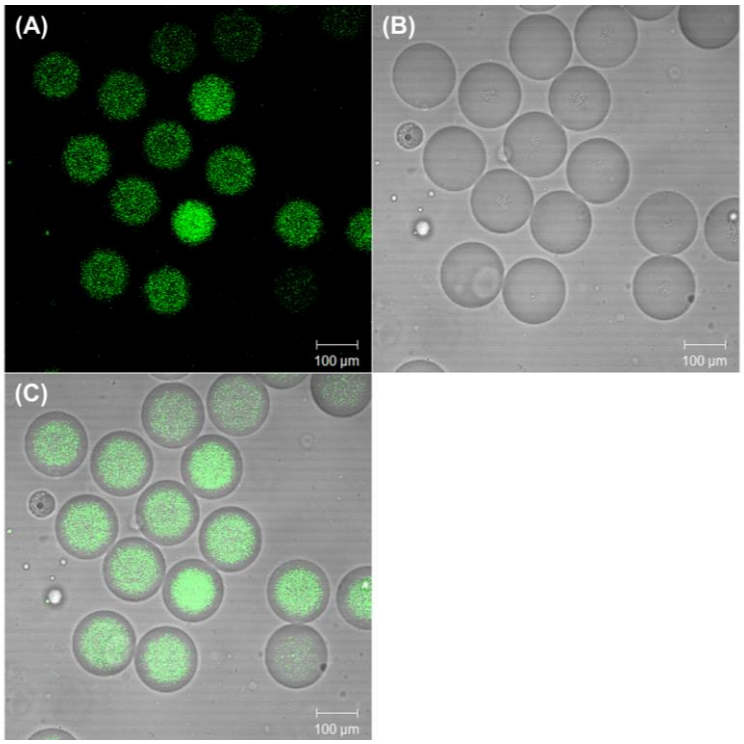

Figure 4.16 CLSM image of the localisation of BODIPY-C10 molecular rotors after 60 minutes: (A) Green channel of as-formed lipid vesicles with concentrated BODIPY-C10 forming an oil pocket at the top; (B) Bright field of lipid vesicles; (C) Merge channel of double emulsion templated lipid vesicles.

Imaging of microfluidic-based vesicles was also performed using FLIM at 60 minutes, however the remaining solvent was less dense than the inner aqueous core, and an oil pocket formed at the top of the resultant lipid vesicles. (147) BODIPY-C10 is an oil soluble fluorophore, and it partitioned upward to the top of vesicles, leaving less rotors in the bilayer for the lifetime signal acquisition, Figure 4.16. For this reason the values of calculated viscosity at 60 minutes were not able to record.

In future, increasing the concentration of the molecular rotor in the membrane, for instance to 0.5 mol% as the maximum rotor concentration to prevent dye aggregation, (210) may be a reasonable approach to obtain the long-time viscosity measurement. Additionally, a surfactant-controlled complete dewetting through adjusting interfacial energies by using a triblock copolymer surfactant has been demonstrated, and this may enable such measurements to be made. (151) The precise control of interfacial energies can facilitate the entire dewetting process shortly after the collection of the double emulsion templates forming the oil-free lipid vesicles, which would be helpful to accommodate the rotors within the bilayers rather than aggregating in the oil pockets at the top of the lipid vesicles.

4.4 Conclusions

In this chapter, the BODIPY-based molecular rotors were used to image viscosity in artificial lipid bilayers, in order to assess the utility of lipid vesicles to be synthetic cell models, which templated from ultrathin shell double emulsions produced by microfluidics, and to investigate the effects of dewetting-assisted bilayer formation on membrane viscosity.

The fluorescence lifetimes of the BODIPY-C10 rotors were first determined in methanol/glycerol mixtures of known viscosity in order to calibrate the rotors using a Förster-Hoffmann plot. In order to investigate whether temperature affected the fluorescence lifetimes of the rotors, the fluorescence lifetimes of BODIPY-C10 in methanol/glycerol were measured at 283 K – 333 K, which gave similar linear relationships between lifetimes and viscosities while conducting at a series of temperatures, implying that BODIPY lifetime is not strongly affected by temperature.

By a mean of microfluidic strategy, monodisperse lipid vesicles were produced in a high-throughput format. The lipid vesicles were transformed from templates that were in the form of double emulsions with ultra-thin shells. With assistance of the dewetting, two independent lipid monolayers "zipped" along the entire interface

forming a lipid vesicle. In addition, high qualities of GUVs were produced by an electroformation approach by which efficiently avoid organic solvent persisted in the biomembranes.

The BODIPY-C10 rotors were then incorporated into microfluidic-based lipid vesicles and electroformed GUVs, in order to investigate viscosity within lipid bilayers with an increasing time of 20 minutes. By performing the FLIM measurements and comparisons between two kinds of bilayers, our hypothesis regarding on the shift of lifetimes towards the value of the electroformed GUVs was confirmed. A 59% increase of lifetimes can be seen in microfluidic configuration after 40 minutes since the vesicles were prepared. This rise in reported lifetimes was due to the dewetting process at water-oil and oil-water interfaces which forced the membranes to be solvent free.

We then proceeded to determine membrane viscosity within two configurations of vesicles and showed: (i) a significant rise in calculated viscosity within microfluidic-based vesicles from 71.96 ± 10.88 cP to 254.63 ± 33.82 cP; and (ii) that there was no notable change in electroformed vesicles' bilayers at a range of time points. These experiments showed that microfluidic-based lipid vesicles can serve as novel cell-like architectures, especially their bilayer environments were featured similar qualities in terms of fluidity property as pure bilayers manufactured using a solvent-free method.

Chapter 5 Microfluidic Generation of Asymmetrical Bilayer Vesicles as Artificial Cells

Chapter 5 describes a novel integrated microfluidic approach for fabrication of monodispersed giant unilamellar vesicles with asymmetric bilayers as artificial cell models. The vesicles are continuously assembled in two distinct steps within a microcapillary microfluidic device, giving an "on-demand" defined composition, depending upon the flow rates of fluids. In the first step, water-in-oil droplets are stabilised with the first phospholipid phase to form the inner leaflet within an injection capillary. These dispersed droplets then flow through a second injection channel where a continuous reagent replaces the first monolayer solution to produce uniform water-in-oil-in-water double emulsions.

By controlling the continuous aqueous phase flow rate in the device, the diameter of the double emulsions can be varied from 350 μm to 187 μm. We have evaluated membrane asymmetry by using fluorescence quenching assays. To demonstrate the versatility of the approach, we also engineered hybrid asymmetric bilayer vesicles with an independent phospholipid inner-leaflet and diblock copolymer monolayers at the outer layer. Our strategy demonstrates the high-throughput fabrication of asymmetric bilayer vesicles in an integrated synthesis, with potential applications in researching the physical properties of membranes and vesicle drug delivery systems. The work described in this chapter has been presented at *EMBL Microfluidics* (Heidelberg, Germany, July 2016).

5.1 Introduction

5.1.1 Membrane Asymmetry

In 1972, Mark Bretscher first reported the existence of partial lipid asymmetry in the membranes, which experimentally proved phosphatidylcholine (PC) and sphingomyelin (SM) are abundant within exterior layer of the lipid bilayer. (224) Five years later, Rothman and Lenard developed the concept of lipid asymmetry in plasma membranes, and the degree of lipid species differences between the interior and exterior leaflets of the membrane was firmly established. (225) Of the glycerophospholipids, phosphatidylcholine (PC) tends to locate in the outer-leaflet,

and the aminophospholipids phosphatidylserine (PS) and phosphatidylethanolamine (PE) are concentrated in the inner-leaflet. The sphingolipids, sphingomyelin (SM) are also confined to the outer-monolayer, (226) as shown in the Figure 5.1. In the membranes of cells, the compositional asymmetry can have important consequences for such features as membrane permeability, (227) transmembrane protein orientation and localisation, (228) and membrane shape as well as stability. (229, 230) Additionally, this transmembrane lipid asymmetry provides the two leaflets of membranes with different biophysical properties and influences numerous cellular functions. For instance, membrane-bound enzymes, like protein kinase C and Na^+ and K^+-ATPase are affected by PS which is located in the inner-leaflet and which is an essential co-factor to these enzymes functions, (231) whereas the outer-monolayer concentrated PS works as a recognition site for phagocytes. (232) In general, the transbilayer phospholipid asymmetry provides a significant property that merits detailed study.

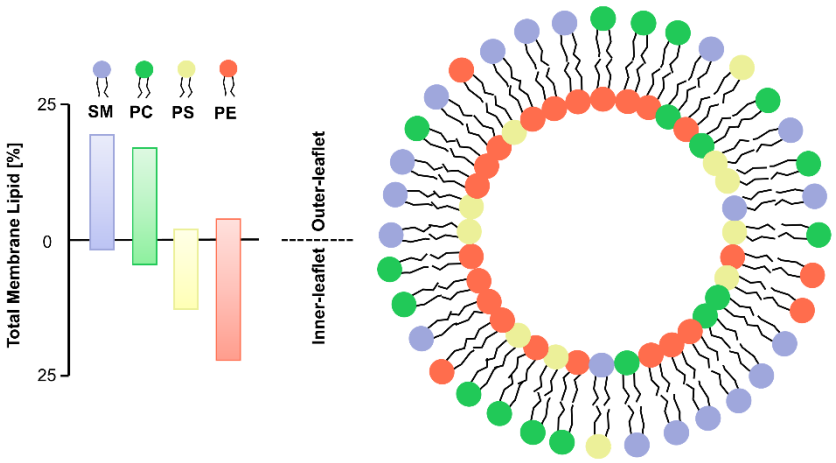

Figure 5.1 Schematically illustration of transbilayer distribution of phospholipids in human red blood cells. (226, 233)

5.1.2 Measurement Methods of Phospholipid Bilayer Asymmetry

Various methods of determining the lipid *sidedness* across a bilayer exist, determining this property by either direct or indirect methods. Commonly used direct methods for studying the lipid asymmetry fall into five general categories: chemical labelling, (234) modification by phospholipases, (226) immunochemical methods, (235) protein-mediated phospholipid translocation (236) and physicochemical techniques, for instance, nuclear magnetic resonance (NMR), electron spin resonance (ESR) and X-ray analysis. (235, 237) However, all these direct methods are valid only if the reagent, for example, enzymes or chemical probes, which face the outer-leaflet reacts only with the lipid on the outer-monolayer and not with the inner layer. It is also important that the process of measurement does not induce alterations in the original asymmetric lipid arrangement of membranes.

The rates of chemical or biochemical reactions are often of a different order compared to the rate of phospholipid translocation, making many of the direct methods, described above, unsuitable for dynamic studies of transmembrane asymmetry. Indirect methods have therefore been developed to assess transbilayer lipid asymmetry. Annexin V binding is a new fluorescent probe that can be used for the detection of cells with PS exposed on the cell surface, (142, 238, 239) as annexin V binds only to the PS on the outer-leaflet of bilayer membranes.

However, the most widely used method for readily visualising membranes with two different leaflets, and studying the dynamics of lipid movement between the two monolayers, is to use a variety of phospholipid analogues (as phospholipid probes). These membrane probes include fluorescent analogues of natural lipids, as well as lipophilic organic dyes that have little structural resemblance to natural biomolecules. Most of the analogues incorporate a reporter group to the head group or to one fatty acid chain of the phospholipid. This can then be easily integrated into the outer-leaflet of the bilayer and then rapidly quenched by the addition of membrane-impermeant reagents to indicate the asymmetric arrangement of membranes and

assess the movement of phospholipids between the inner-leaflet and outer-leaflet. (40, 82, 142)

5.1.3 Construction of Asymmetrical Bilayer Vesicles

Vesicles are aqueous lumen enclosed by bilayer membranes composed of either phospholipids (liposomes) (240, 241) or block copolymer (polymersomes) (128, 131). They have attracted interest as artificial cell chassis for studying cellular membrane biology. (168, 242, 243) However, the majority of existing research relies on well-characterised symmetrical bilayer vesicles rather than vesicles with an asymmetrical bilayer, which much better represents natural cells in terms of complexity and reality.

Thus, membrane researchers are looking for novel and facile ways of producing vesicles with asymmetrical bilayers in order to accurately mimic cells as they exist in nature. In the last decade, David A. Weitz and co-workers created a phase transfer method to fabricate asymmetrical bilayer vesicles, Figure 5.2(A), (81) which leaves inverted micelles transfer the second lipid phase via density gradient between inner aqueous solution and lipid phase to achieve resultant asymmetrical bilayer vesicles in final watery solution. In Figure 5.2(B), Noah Malmstadt and his team synthesised asymmetric giant lipid vesicles by means of a combination of phase transfer methods and microfluidic techniques. This method introduced the concept of using microfluidics, already a well-developed technology in analytical sciences, as a method for preparing vesicles, (39, 162, 244, 245) for complex artificial cell research. (142)

The production yield of vesicles built using these methods remained low, and the methods originally used made the control of the size of the resultant vesicles difficult. In Brian M. Paegel's lab, a new approach based on layer-by-layer assembly within microfluidic device, as depicted in Figure 5.2(C) was detailed. (82) Uniform-sized asymmetric vesicles were produced in the microfluidic device, but the collection of the vesicles for off-chip experimentation was unreliable due to fragile nature of phospholipid membrane.

Recently, Paul R. Chiarot's lab, Figure 5.2(D), and Ocsar Ces's group, Figure 5.2(E), reported new approaches on microfluidic fabrication of vesicles that have asymmetric bilayers. (40, 246). The devices used for building up vesicles were, however, difficult to design and operate in practical experiments. In addition to the complexity of the devices, the materials the devices were constructed from, polydimethylsiloxane, PDMS, is a delicate elastomer that reacts with organic solvents, such as toluene and chloroform, which are essential reagents for dissolving both phospholipids and block copolymers. Exposure to these reagents results in swelling of the PDMS device, collapsing channels within it, and degrading the performance of vesicles formation. (247)

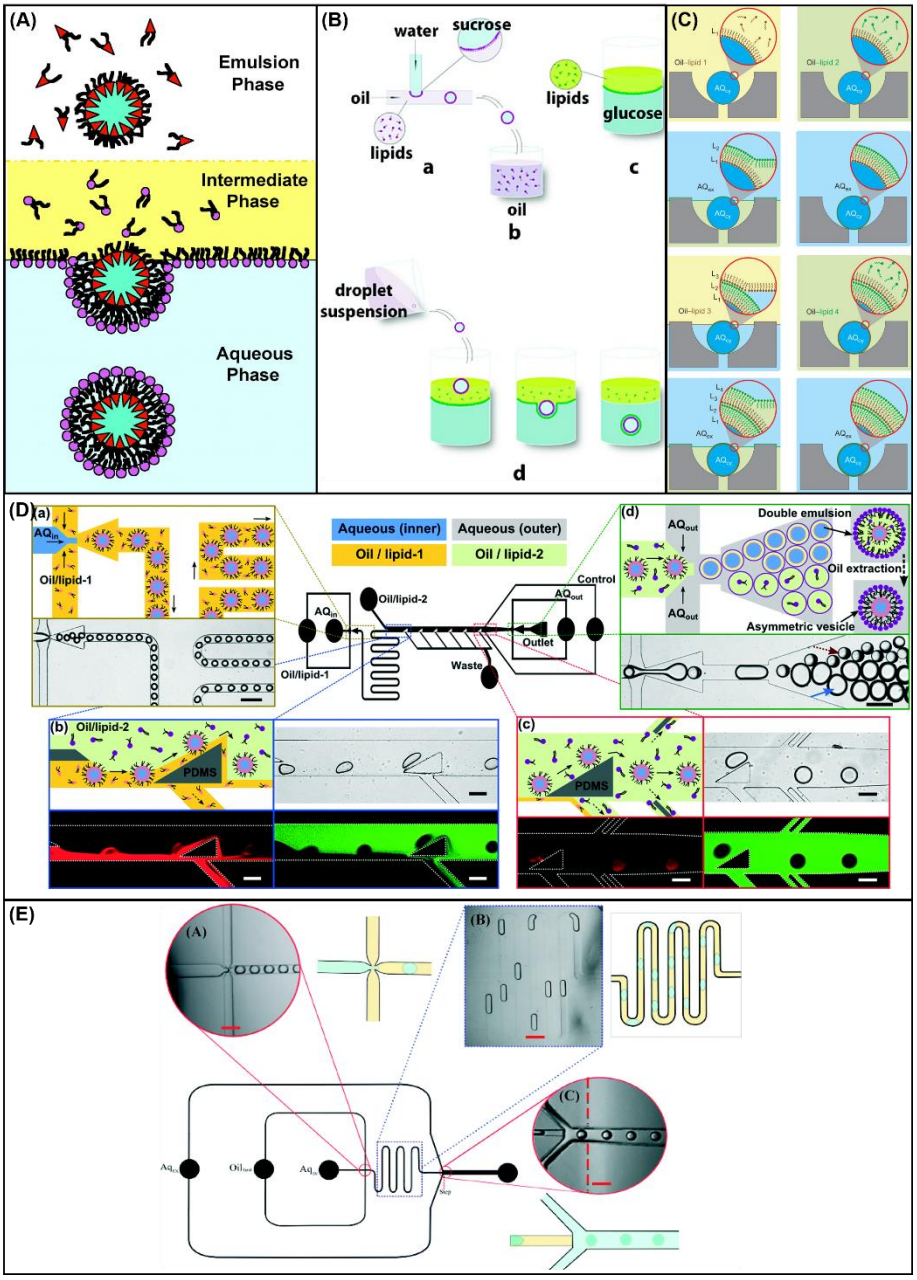

Figure 5.2 Methods of producing vesicles with asymmetric bilayers: (A) Schematics of phase-transfer technique uses to engineer asymmetric bilayer vesicles; (81) (B) Single droplets are formed in microfluidic chip, and then by using phase-transfer method to form the second distinct lipid outer-leaflet; (142) (C) Layer-by-layer approach showing the generation of asymmetric liposome through trapping single droplets, and then flowing different lipid oil phases assembling the asymmetric bilayers; (82) (D) Schematic illustration of total synthesis of asymmetric vesicles by using a similar layer-by-layer method within a PDMS microfluidic device; (40) (E) 2D schematics of the microfluidic set-up for constructing asymmetric vesicles. (246)

5.2 Materials and Methods

5.2.1 Materials

Experiments were conducted with the following phospholipids: 1,2-dioleoyl-*sn*-glycero-3-phosphoethanolamine (DOPE), 1,2-dioleoyl-*sn*-glycero-3-phosphocholine (DOPC) (Sigma), 1,2-dipalmitoyl-*sn*-glycero-3-phosphoethanolamine-N-(biotinyl) (Biotinyl-PE) and cholesterol (Avanti Polar Lipids, Inc.). Diblock copolymer, poly(butadiene-*b*-ethyleneoxide) (PB-*b*-PEO) was acquired from Polymer Source (Canada). As tracer lipids, we used (n-(Texas Red sulfonyl)-1,2-dihexadecanoyl-*sn*-glycero-3-phosphoethanolamine,triethylammoniumsalt) (TR-PE), 2-(12-(7-nitrobenz-2-oxa-1,3-diazol-4-yl)amino)dodecanoyl-1-hexadecanoyl-*sn*-glycero-3-phosphocholine (NBD-PC) (Life Technologies), (n-(7-nitrobenz-2-oxa-1,3-diazol-4-yl)-1,2-dihexadecanoyl-*sn*-glycero-3-phosphoethanolamine, triethylammonium salt) (NBD-PE) (Avanti Polar Lipids, Inc.). Streptavidin used for modifying the surface property was purchased from Sigma. Phosphate-buffered saline (PBS) (Sigma) buffer was utilised to prepare streptavidin solution.

To dissolve phospholipids and diblock copolymer, a solvent mixture of chloroform and hexane (Sigma) was prepared. For the watery phases, we dissolved poly(ethylene glycol) (PEG, Mw = 6000 Da, Sigma) and poly(vinyl alcohol) (PVA, Mw = 13,000-23,000 Da, Sigma) in deionised (DI) water to 10 wt% as inner aqueous solution; 10 wt% PVA solution was produced as the continuous aqueous phase. A 50 mM NaCl (Sigma) solution was used to collect double emulsion drops. Osmolarities of all aqueous phases were measured using an osmometer (3300 Micro-Osmometer, Advanced Instruments, Inc., UK). For fluorescence quenching assay, sodium dithionite (Sigma) was dissolved in 50 mM NaCl solutions.

5.2.2 Preparation of Solutions

The inner-leaflet and outer-leaflet lipid solutions (DOPE or DOPC 70 mol% and cholesterol 30 mol%) were solubilised in an organic solvent mixture (chloroform 36

vol% and hexane 64 vol%) to a total lipid concentration of 5 mg/ml. All fluorescent lipid probes were additionally added to each lipid phase at 0.5 mol% for fluorescence imaging and fluorescence quenching assay. In fluorescence quenching assay, 15 wt% of Biotinyl-PE was also added to the outer-leaflet solution for both configurations. A polymeric outer monolayer of hybrid bilayer was prepared by dissolving PB-*b*-PEO in the solvent mixture to make it 5 mg/ml. To form the inner watery solution, PEG and PVA were dissolved to 10 wt%. 10 wt% of PVA solution was used as the outer aqueous phase to ultimately form double emulsions. The collection phase was 50 mM NaCl. Sodium dithionite was dissolved in the collection solution at 0.1 M as the quenching reagent. All aqueous solutions were filtered through 0.25 μm syringe filter (Life Technologies).

5.2.3 Fabrication of Microfluidic Device

The microfluidic device was assembled by microcapillaries. The microfluidic device platform was made of two glass slides. Glass slides were glued together for 5 minutes using epoxy (Devcon) as in Figure 5.3(A, B). The device consists of four circular glass capillaries. The innermost injection round capillary with 580 μm inner diameter, 1 mm outer diameter (WPI), was tapered by a gas torch and the tip was adjusted by sand paper to 40-60 μm inner diameter. This innermost capillary was inserted into the untapered opening of the middle injection circular glass capillary, whose inner and outer dimensions are 200 μm and 1 mm (WPI), to create a biphasic flow within the middle injection capillary and forming a stable water jet as shown in Figure 5.3(C, E, F)

The outermost injection cylindrical glass capillary, with inner diameter 1.17 mm (Harvard Apparatus), was pulled by a micropipette puller (P-97, Sutter Instrument, Inc.) and sanded to shape the tip into 100 μm. To make the inner wall hydrophobic, the glass capillary was treated with Sigmacote (Sigma) for 30 minutes and then washed with isopropyl alcohol. Next, a round collection capillary of the same dimension as the outermost injection capillary and with a 200 μm tapered tip was

dipped into 2-[Methoxy(polyethyleneoxy)propyl]-trichlorosilane (Fluorochem Ltd.) to render the glass capillary surface hydrophilic. It was then rinsed with DI water.

After dripping and rinsing the capillaries, the remaining fluids were then removed with compressed air prior to assembly. To complete the fabrication of the suite of injection capillaries, the middle injection tube was inserted into the unprocessed end of the last injection capillary. The tips of the outermost injection capillary and the collection tube were coaxially aligned inside a square glass capillary (VitroCom) under an optical microscope at 10x magnification. These were then glued to the platform as in Figure 5.3(D). Lastly, dispensing needles, used as inlets of fluids, were connected at either the junctions between capillaries or their ends by using 5 minutes epoxy as illustrated in Figure 5.3(G). Figure 5.3(H), shows a digital image of the fabricated microfluidic device used for manufacturing vesicles with transbilayer asymmetry.

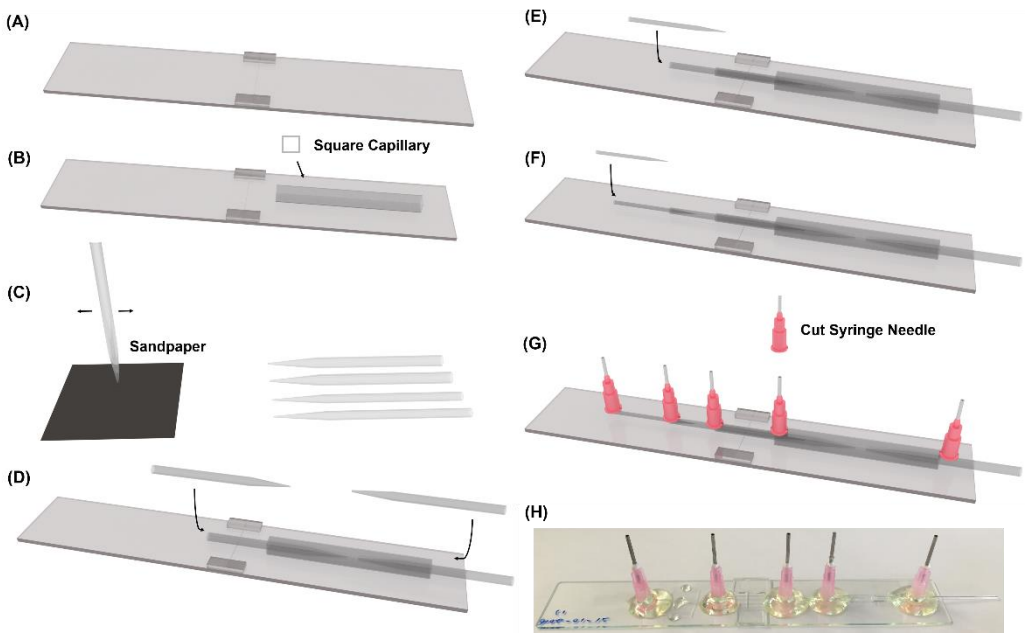

Figure 5.3 Step-by-step instructions on building a microfluidic device for the fabrication of asymmetric bilayer vesicles: (A, B) A square capillary was glued to the device platform made of two glass slides; (C) Four tapered cylindrical capillaries were polished to modify the diameter of the orifices; (D) The two glass capillaries with the largest outer dimeters were opposingly inserted inside the square capillary and glued to the device platform; (E) The middle injection glass capillary was inserted into the opening end of the lager

injection tube; (F) The last injection capillary was positioned such that the tip was slightly inserted into the middle injection glass tube and glued to the glass slide; (G) Syringe needles were cut and glued onto the device and serve as the inlets of the microfluidic device; (H) Digital image of a fabricated microfluidic device for the preparation of vesicles with asymmetric agreements within the membrane.

5.2.4 Operation of Microfluidic Device

The inner and outer aqueous phases were loaded into 10 ml and 20 ml plastic syringes (BD) respectively and lipid or polymer phases into 5 ml glass syringes (SGE). All reagents were injected into the microfluidic device using syringe pumps (Harvard Apparatus) through silicone tubing with inner and outer diameters of 1 mm and 3 mm respectively (VWR). The tubing was used in all connections between syringes and dispensing needles on the device. The flow rates of the innermost aqueous phase, lipid 1, lipid 2/polymer and the continuous aqueous phase were typically tuned to be 2500, 400, 600 and 3000 μl/h, respectively. The formation process of emulsion droplets was monitored by using a Zeiss Axio Imager. A2 microscope (Carl Zeiss MicroImaging) equipped with a Phantom V1611 high-speed camera (Vision Research Inc.). Once produced, double emulsion drops were collected into a vial called the collection bath, that contained a 50 mM NaCl solution.

5.2.5 Surface Treatments

For fluorescence quenching assays of the asymmetry of microfluidically-synthesised membrane, it was imperative that the vesicles remained stationary at the bottom of the observation chamber (μ-Slide 4 Well, Ibidi) for the duration of the measurements. This was achieved through a well-established coupling method of biotin-streptavidin interaction displayed in Figure 5.4, as it has been demonstrated to maintain immobilisation of vesicles on the surface of support substrates. (248, 249)

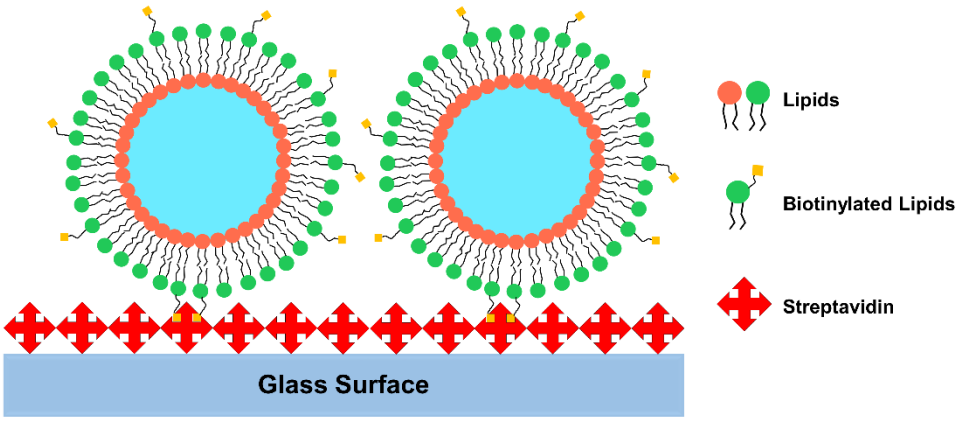

Figure 5.4 Schematic describing the biotin-streptavidin binding utilised in fluorescence quenching assay. Asymmetric bilayer vesicles with biotin conjugated lipids on the outer-leaflet anchor to the streptavidin-coated surfaces.

The observation chambers were sonicated in DI water for 30 minutes followed by drying under N_2, then plasma treatment was applied to the chambers rendering surfaces hydrophilic. Streptavidin was dissolved in PBS buffer at 1 mg/ml first, and thereafter diluted to be 0.1 mg/ml for surface modification. 0.1 mg/ml streptavidin solution was added into each well of observation chambers followed by incubation at 4°C for 2 hours resulting in physical adsorption of streptavidin on the surfaces. Prior to conducting assay with the chambers, they were gently flushed 3 times with 50 mM NaCl solution.

5.2.6 Fluorescence Quenching Assay Experiment

To validate the asymmetry of the lipid vesicle membranes, fluorescence quenching assay was applied. Lipid vesicles with NBD fluorophore in either inner-leaflet or outer-leaflet were measured as soon as the vesicles were transformed from double-emulsion templates. Firstly, a 200 µl suspension of vesicles with only the outer monolayer labelled with NBD-PC was added to an observation chamber where fluorescence images were taken. 50 µl of the fluorescent quencher sodium dithionite

was added into the chamber as a 1 M solution dissolved in DI water. The fluorescence emission of the asymmetric lipid bilayer vesicles was measured before and after addition of quencher solution.

Vesicles that were stained with NBD-PE on the inner-leaflet were measurement conducted in the same fashion. Multiple images of each vesicle were taken throughout the fluorescence quenching assay using the time-series function of the confocal laser scanning microscopy (Zeiss LSM 5 Live). Quantitative fluorescence comparisons were made by normalising the average fluorescence intensities of each type of vesicles (n = 3) over the entire quenching assay experiment.

5.3 Results and Discussion

5.3.1 Asymmetric Bilayer Vesicles Assembly

Asymmetric bilayer vesicles were fabricated utilising a two-step emulsification process with two types of phospholipids within a single microfluidic device. The strategy is schematically demonstrated in Figure 5.5(A). First of all, a stable aqueous coaxial jet at the centre of the capillary surrounded by a lipid phase, which was flowing along the inner surface of innermost injection capillary due to the hydrophobic nature of the capillary wall, (60) was formed in the middle injection capillary through injecting the inner aqueous phase into the lipid 1 phase. The formation of the stable water phase jet rather than plug-like water-in-oil droplets is a result of the degree of increasing interfacial confinement due to the decreasing inner diameter of the injection tube, Figure 5.5(B). This water jet was well coated with lipid 1 phase to form the inner-leaflet of bilayer, which implies that there was no excess lipid 1 phase flowing into the next injection capillary that could then emulsify at the orifice of the middle tube, resulting in the production of a train of separate water-lipid 1-lipid 2 and lipid 2 drops in the last injection capillary as exemplified in Figure 5.5(A). The middle injection capillary was designed to avoid interfere between the two lipid phases and to ensure that each leaflet is assembled independently. Next, in the outer injection glass capillary, only lipid 2 solution was delivered in order to

assemble the outer-leaflet of the asymmetric bilayer. These drops flowed along the outer injection capillary and re-emulsified at the tip in the discontinuous dripping regime, resulting in monodisperse double emulsions with two distinct phospholipid phases on each interface in the bilayer. As Figure 5.5(C) shows, which was acquired by high-speed camera, uniform spherical double emulsions were ultimately collected in the glass collection capillary. Subsequently, the double emulsions were collected in a glass vial containing 50 mM NaCl.

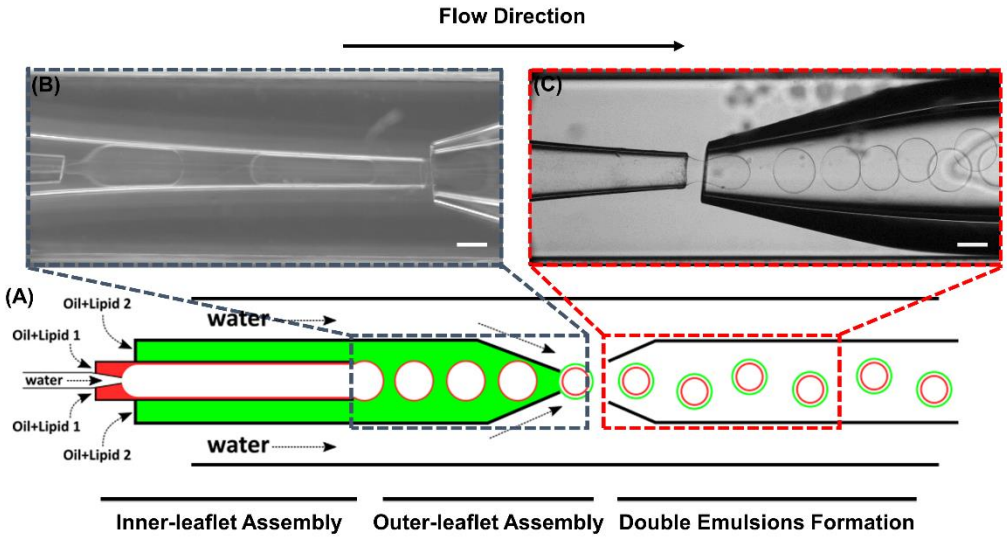

Figure 5.5 Microfluidic fabrication of water-lipid 1-lipid 2-water double emulsions: Here (A) Schematic of a glass capillary microfluidic device for fabrication of asymmetric bilayer vesicles; (B) Optical microscope image showing the emulsified water-lipid 1 jet by the continuous lipid 2 phase within the outer injection capillary; (C) High-speed optical microscope image of continuously produced water-lipid 1-lipid 2-water double emulsions with ultrathin shells. Scale bars denote 200 μm.

The highly monodisperse double emulsions were used as templates to form the eventual lipid vesicles with asymmetric bilayer by removing the organic solvent from the intermediate layer of the double emulsion, which is known as the dewetting method and depicted in Figure 5.6(A-D). (39, 243, 250) Chloroform is a good solvent

for phospholipid dissolution and more soluble in aqueous phase than hexane fraction of organic solvent mixture, (251) enabling chloroform fraction started to evaporate and diffuse into external environmental aqueous phase rapidly right after collection, therefore leaving the shell of double emulsion to be hexane concentrated, which is a bad solvent. The depletion in quality of solvent induced attractive interaction between internal and external lipid leaflets forcing them into a closer contact, and as a result, the hexane fraction was excreted out of the membrane, and two lipid monolayers zipped together along the interfaces forming an unilamellar asymmetric lipid bilayer membrane.

As shown in Figure 5.6(A, B) double emulsion droplets were contained in a glass vial with collection solution immediately after formation in the microfluidic device. The membranes of double-emulsion templates possessed solvent mixture, resulting in the translucency of the vesicle membranes. After 2 hours, vesicle membranes became transparent due to the solvent (chloroform) evaporating and hexane dewetting, so leading to the transformation from double emulsions to vesicles with compact asymmetric bilayer formed.

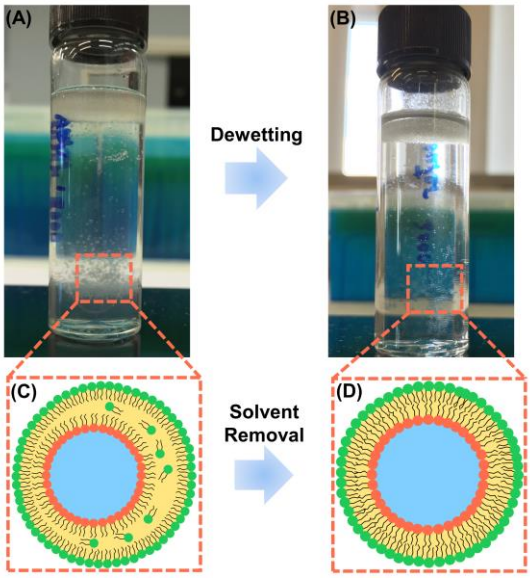

Figure 5.6 Transformation of double emulsion drops to asymmetric lipid bilayer vesicles induced by dewetting process: (A) Digital image of double

emulsion templates collected right after generation by microfluidic device; (B) Digital image of asymmetric lipid bilayer vesicles contained in the glass vial. Schematic illustrations of a double emulsion drop with organic solvent remaining in the membrane (C); a well-formed lipid vesicle with asymmetric bilayer after the action of dewetting (D).

Figure 5.7(A) exhibits a bright field optical microscope image of monodisperse double emulsion droplet templates a few minutes after generation, representing asymmetric bilayer lipid vesicles on the bottom of the collecting vial. The asymmetric membrane lipid vesicles are uniform. Figure 5.7(B) shows that the mean diameter of lipid vesicles is 336 μm and its coefficient of variation is 2.73%, demonstrating the high monodispersity of the as-formed double-emulsion droplet templates (n = 120 vesicles were measured).

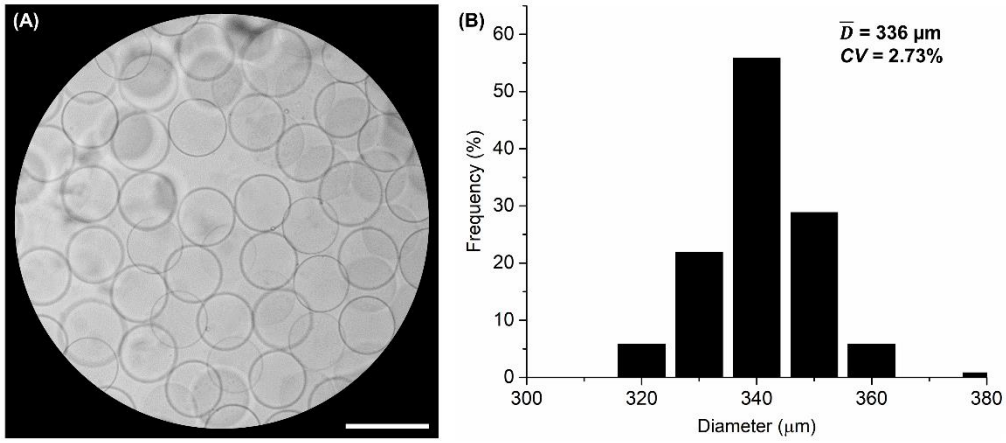

Figure 5.7 Monodisperse double emulsions collected into a vial: (A) Optical micrograph of uniform-sized double emulsions that are the templates of asymmetrical lipid bilayer vesicles produced using flow rates at 2500 μl/h, 400 μl/h, 600 μl/h and 3000 μl/h for respectively inner, lipid 1 phase, lipid 2 phase and external phase; (B) Size distribution of double emulsion droplets. Scar bars are 500 μm.

The composite asymmetric bilayer vesicles with phospholipid on the inner-leaflet and diblock copolymer on the external leaflet were produced in the same fashion, but with the lipid 2 phase replaced by diblock copolymer solution delivered in the

outer injection capillary. At the middle injection tube, the lipid phase covered the aqueous phase quickly, forming the aforementioned water-DOPE jet. Afterwards, the stable jet was coated with diblock copolymer solution in outer injection capillary, and re-emulsified to be pinched off at the orifice. The diblock copolymer floated freely in the double emulsion membranes, and arranged itself at the outer interface to form the outer robust polymeric layer. With dewetting, a transition process taking place, (243) which ultimately induced the attraction of the inner lipid leaflet and outer block copolymer leaflet forming the final composite asymmetric bilayer of the vesicles.

5.3.2 Diameter of Asymmetric Bilayer Lipid Vesicles

Generation of double emulsions in the dripping regime at the injection tube orifice within co-flowing glass-based microfluidic devices was subject to capillary force, which holds the drops in the capillary, and a drag force that draws drops to be pinched off. (252) Drop growth and separation is governed by the two aforementioned forces. As the drag force, which is proportional to the velocity of the exerted flow, exceeds the interfacial tension, (63) it was possible to control the size of the drops by varying the velocity of the continuous aqueous phase. The inner watery phase and two lipid phases were maintained as constant while adjusting the velocity of outer flowing phase (Q_o) as 2, 4, 6, 10 and 20 ml/h, respectively. The diameters of the double-emulsion templates decreased by raising the outer flow rate because of higher drag force employed. Accordingly, the diameters of the resultant asymmetric bilayer lipid vesicles monotonically reduced from 350 ± 11.1 μm to 187 ± 10.6 μm (as a power law Equation (5.1)) with increased flow rate of continuous phase, as plotted in Figure 5.8. While the velocity of the continuous aqueous phase varied, the inner phase and all lipid phases were held at constant flow rates. Images inserted in Figure 5.8 show that all the resulting lipid vesicles produced by the corresponding outer flow rates remained highly uniform in size.

$$D = 451.63\,(Q_o)^{-0.276} \tag{5.1}$$

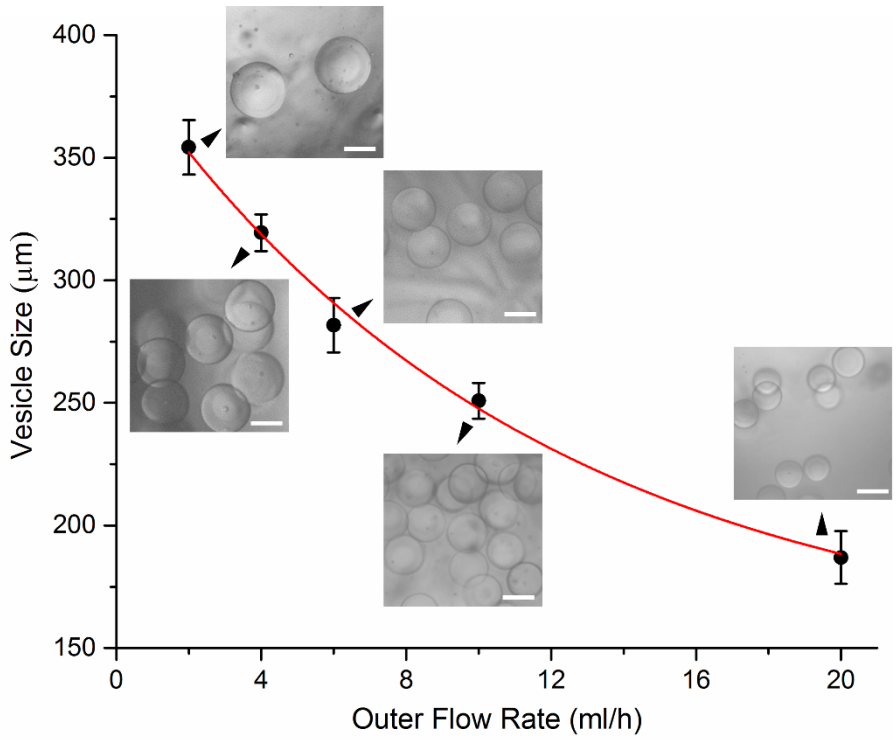

Figure 5.8 Size of the asymmetric bilayer lipid vesicles as a function of flow rate of continuous phase. The data was fitted with a power function (R^2 = 0.96). (Inset) optical microscope images of monodisperse lipid vesicles prepared at the values of outer flow rates (2 ml/h, 4 ml/h, 6 ml/h, 10 ml/h and 20 ml/h). Scale bars are 200 µm.

5.3.3 Characterisation of Lipid Membrane Asymmetry

We firstly evaluated the asymmetry of lipid vesicle bilayer by confocal laser scanning microscopy (LSM 5 Live, Zeiss). Two fluorescent lipids were used as probes to distinguish the inner-leaflet from outer-leaflet. The inner layer made of DOPE was stained with TR-PE, which is shown in Figure 5.9(C), and the outer DOPC leaflet that was labelled with NBD-PC is exhibited in Figure 5.9(D). The merged dual-channel confocal microscopy image of the synthetic asymmetrical bilayer lipid vesicle was exemplified in Figure 5.9(E). The fluorescence intensity profile, Figure 5.9(F) taken along the dotted line validated two tracer lipids localised on inner and outer-leaflet respectively, which confirmed the potential for asymmetry.

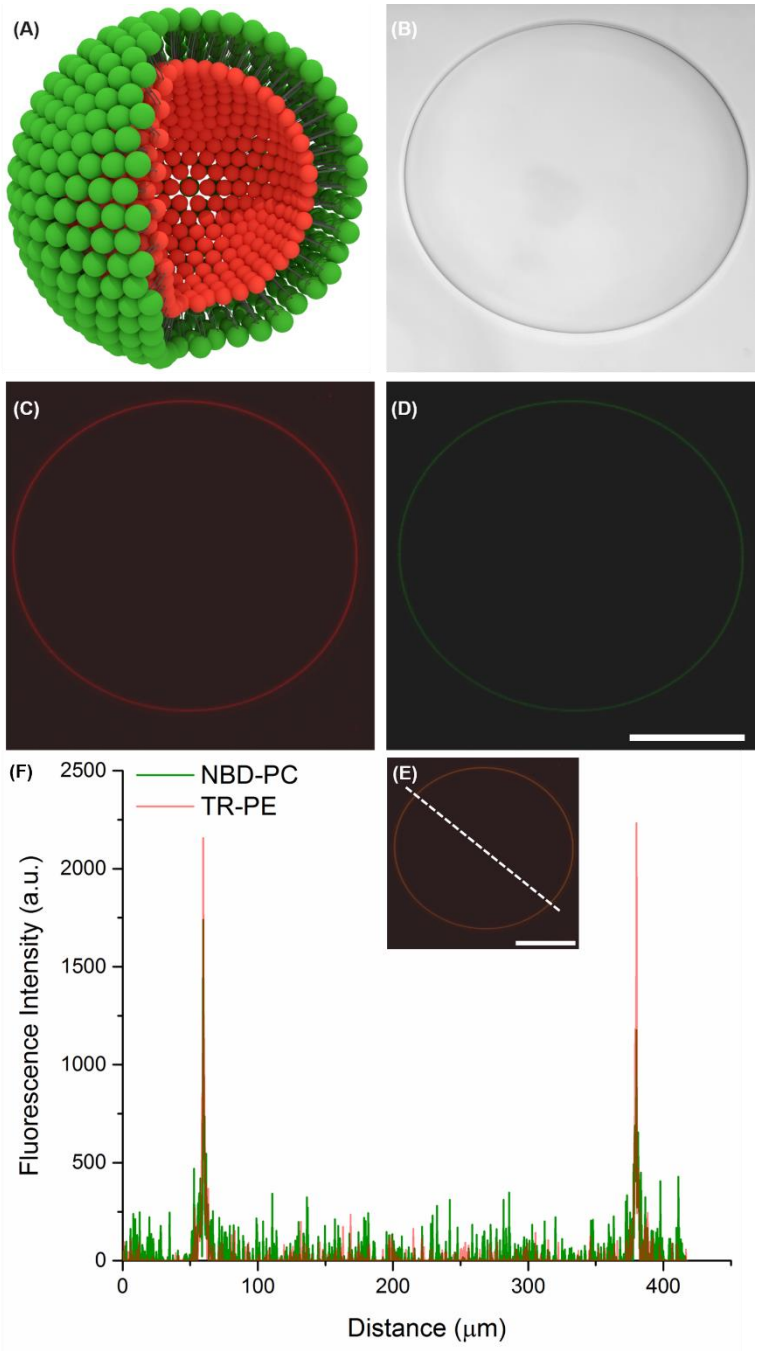

Figure 5.9 CLSM images of a produced asymmetric bilayer lipid vesicle: (A) Schematics of an asymmetric bilayer lipid vesicle; (B) As formed vesicle in bright field; (C) Fluorescence of TR-PE labelled of inner-leaflet; (D) Fluorescence of NBD-PC labelled of outer-leaflet; (E) Merged channel of TR-PE and NBD-PC; (F) Profile of fluorescence intensity of the dotted white line crossing the asymmetric bilayer lipid vesicle in (E). NBD fluorophore signal represented in green and Texas red displayed in red. All scale bars denote 100 μm.

Asymmetrical lipid bilayers were also verified by a fluorescence quenching assay, used to investigate the distribution of tracer lipid between the inner and outer monolayer of the bilayer. (253) NBD-PE and NBD-PC were used as probes in the inner-leaflet and outer-leaflet, respectively. Sodium dithionite was applied as the fluorescence quenching reagent to reduce the fluorescence of the NBD-lipid. As the quencher molecule cannot diffuse across the lipid bilayer, only the tracer lipid labelled at the outer monolayer of bilayer of the vesicle can react with the quencher molecule. (253) The fluorescence quenching assay was performed directly after vesicle generation. Two types of asymmetric lipid bilayer vesicles were adopted for this assay. Firstly, we only labelled the NBD-lipid probe with the inner-leaflet, and left outer-leaflet with no fluorophore. The fluorescence emission of this type asymmetric bilayer vesicle was measured before and after addition of quencher solution, as shown in Figure 5.10(A, B). Secondly, we conducted the assay again using vesicles with outer monolayers tagged with NBD-lipid probe, and measured the fluorescence signal before and after incorporation of quencher molecules in the suspension of vesicles, as illustrated in Figure 5.10(C, D). A high degree of asymmetry of the lipid bilayer was synthesised by our device. Figure 5.11 shows the kinetics of the quenching, which is dominated by the diffusion of the quencher in the outer phase. The reaction between asymmetrical lipid bilayer vesicles with sodium dithionite solution can be seen in the normalised fluorescence intensity as a function of time. In the scenario of inner-leaflet incorporating with NBD-lipid, the fluorescence intensity dropped by 4%, which demonstrated that 96% of NBD-lipid remained within the inner monolayer of the lipid bilayer upon the addition of quencher solution after 240 seconds. In contrast, when NBD-lipid was added to the outer-leaflet, 96% of total fluorescence intensity was rapidly quenched on addition of the quencher. The time constant, $\tau = 51.9 \pm 1.83$ s, of the exponential decay was slower than reported, (81) due to the use of a highly viscos outer phase (10 wt% PVA). These results confirmed that a high degree of asymmetry of the lipid bilayer was successfully and readily achieved using our technique.

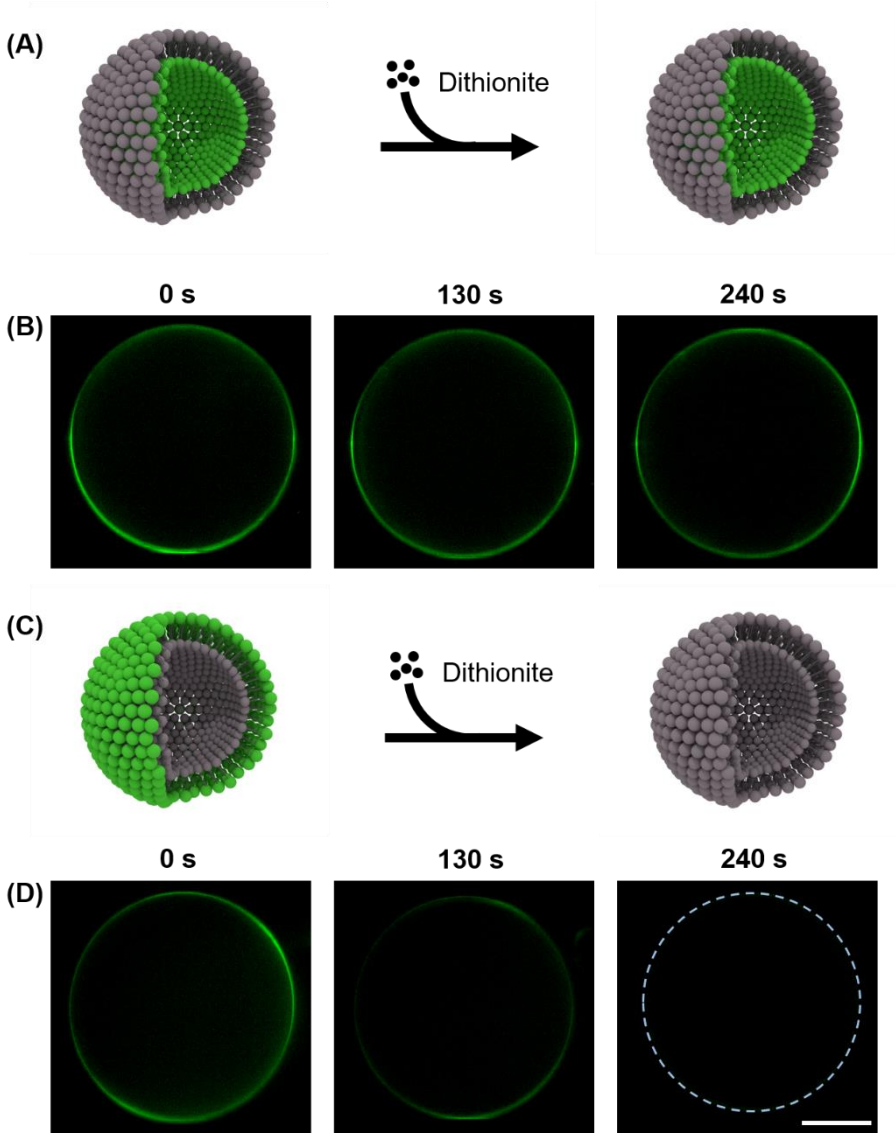

Figure 5.10 Fluorescence quenching assay to demonstrate bilayer asymmetry: (A) Schematic of quenching assay test on asymmetric bilayer vesicles with only inner-leaflets tagged with NBD fluorophore; (B) An image series (0, 130, 240s respectively) of inner monolayer labelled vesicles display fluorescence signal maintains with reacting to the quencher; (C) Schematic of quenching assay test on asymmetric bilayer vesicles with only outer-leaflets tagged with NBD fluorophore; (D) An image series (0, 130, 240s respectively) of outer-leaflet labelled vesicles show reduction of fluoresce signal when exposed to the quencher solution.

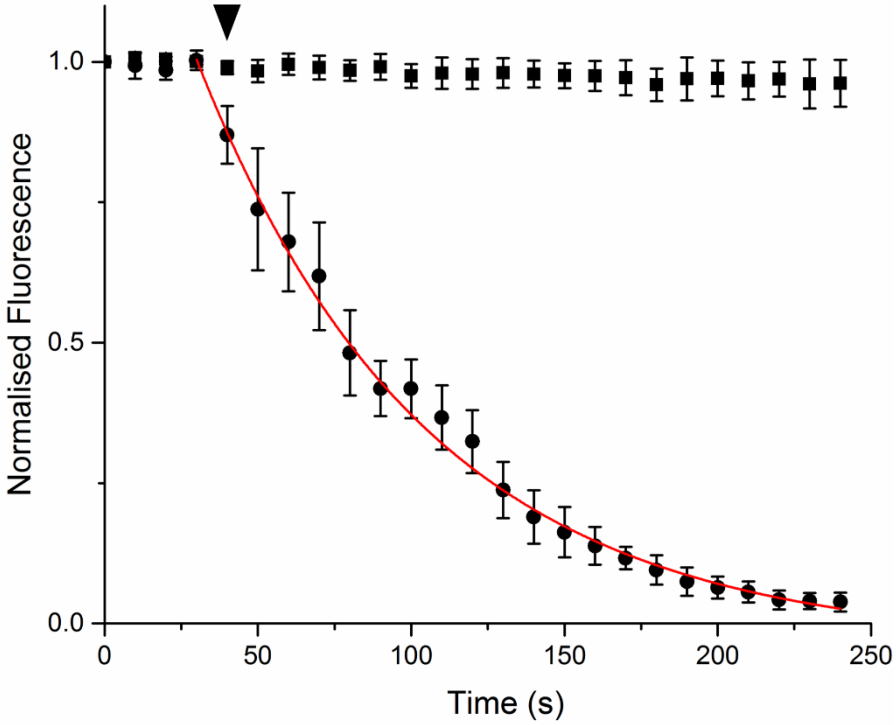

Figure 5.11 Treating asymmetric bilayer lipid vesicles assembled with NBD fluorophore in either the inner-leaflets (squares) or the outer-leaflets (circles) with quenching agent (inverted triangle) (n = 3). Solid red line represents an exponential decay with $R^2 = 0.99$; R indicates the correlation coefficient. Scale bar is 100 µm and applies to all images.

5.3.4 Increased Robustness with Block Copolymers

In the context of real-life applications, lipid bilayers have often been very fragile, especially mechanically. (128) To increase the robustness of the vesicles, we have developed a new structure where one of the leaflets is made out of a block copolymer. Using our microfluidic system uniquely enables us to control the specific contents of each individual leaflet. Block copolymers can be constructed to be amphiphiles in which one block of molecules is hydrophilic and the other is hydrophobic. Block copolymer can aggregate in aqueous medium producing vesicular structure in the same fashion as phospholipids, but the polymeric bilayers have better mechanical properties due to the large chains available. (128, 131) Contrary to the control provided by our method, previous strategies to reinforce vesicles using block

polymers resulted in mixtures of lipids/polymers across leaflets, such that both leaflets contained some polymer and some lipids. (254, 255) We created asymmetric composite vesicles by replacing one of the lipids with PB-*b*-PEO. The membranes can then be formed when the diblock copolymer arranges at the outer interface. After dewetting, this ultimately led to the aggregation of an inner lipid leaflet and an outer block copolymer leaflet, forming the final composite bilayer, Figure 5.12(A).

Similarly to the lipid-lipid bilayers, we characterised the asymmetry of the lipid-polymer bilayer by confocal laser scanning microscopy (LSM 5 Live, Zeiss), Figure 5.12(B-D). Figure 5.12(C) shows a calcein dye (green fluorescence) encapsulated within the vesicle, surrounded by the DOPE inner-leaflet that was stained by 0.5 mol% of TR-PE, Figure 5.12(D). This analysis confirmed the presence of a full lipid leaflet, that will be supported by a copolymer outer leaflet.

The composite bilayer structures offer the capability to control the functionality of each leaflet independently. For example, an inner lipid leaflet carries biocompatibility that would benefit encapsulation of biologically-active components, while the outer polymeric leaflet allows a stronger structure. It could also advantageously enable to orient membrane spanning elements (proteins and channels) based on specific affinity.

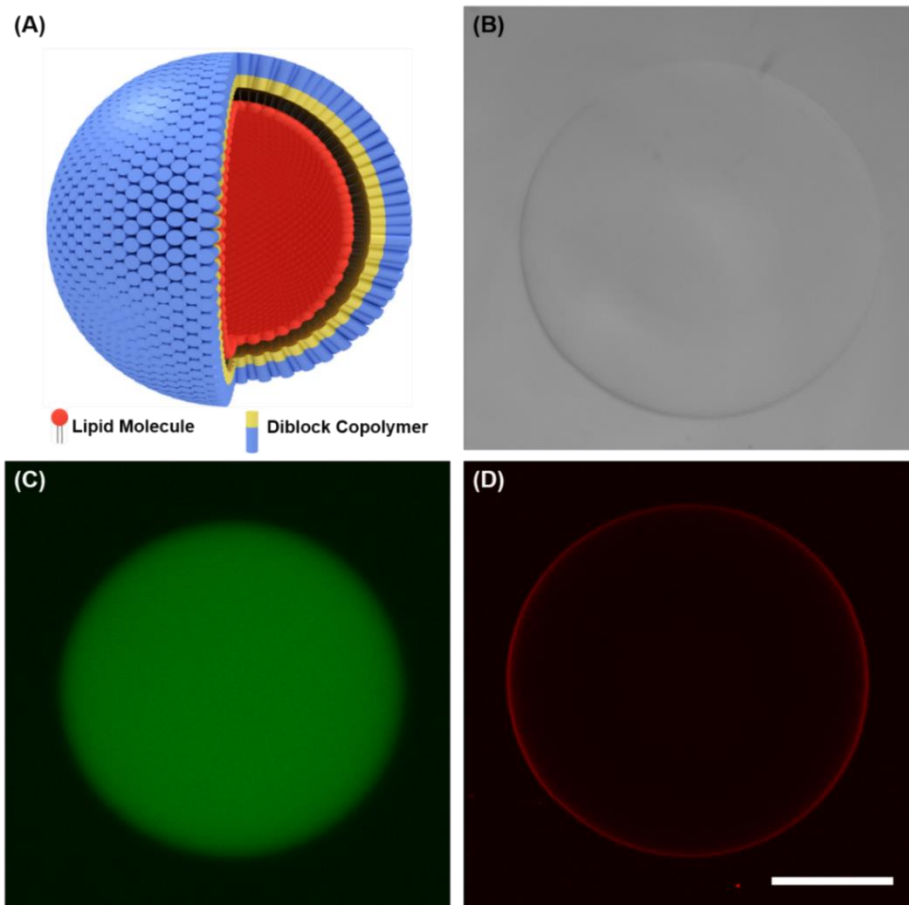

Figure 5.12 A produced hybrid bilayer vesicles: (A) Schematic illustration of hybrid bilayer vesicles with lipid-coated inner-leaflet and diblock copolymer-coated outer-leaflet; (B) Bright filed optical microscope image of a synthetic hybrid bilayer vesicle; (C) CLSM image of copolymer reinforced vesicle with encapsulation of calcein dye in the aqueous phase; (D) CLSM image of lipid-coated inner-leaflet of a hybrid bilayer vesicle. Scale bar is 100 μm.

5.4 Conclusion

A novel capillary microfluidic device presented in this Chapter provides not only a facile, but also robust approach to continuously produce monodisperse asymmetric bilayer vesicles with tailored bilayer composition at high-throughput. By adjusting the flow rate of the continuous fluid in the microfluidic device, the diameter of asymmetric bilayer vesicles was simply controlled, ranging from 187 μm to 350 μm. As-formed asymmetric bilayer lipid vesicles were examined by fluorescence

microscopy and fluorescence quenching assay to confirm the asymmetric arrangement within the bilayer. Asymmetric lipid bilayers showed as high as 96% degree of asymmetry when treated with quenching agent during the assay. Furthermore, we engineered a new type of bilayer, in which phospholipid (DOPE) formed the inner-leaflet and diblock copolymer (PB-*b*-PEO) coated to form the external leaflet. To the best of this author's knowledge this is the first time polymer reinforced bilayer vesicles have been synthesised in a microfluidic device. The asymmetric bilayer vesicles produced by our strategy hold the potential to be used as artificial cell chassis to explore membrane biology and as cargo carriers for drugs.

Chapter 6 Conclusions and Future Perspectives

In living systems the basic building unit, cells, are the highly advanced microreactors in which all complicated biochemical reactions occur, driving the processes of life from birth to death. Their complexity has inspired not only biologists, but also engineers and physicists to think about building a living cell from scratch. This task has attracted attentions of scientists from all over the world, amongst whom from Europe have recently created an initiative aiming to meld the efforts together and speed progress toward the ambition: Engineering of Synthetic Life. (256) Accomplishing this goal of constructing a cell from the bottom up would not only provide insight into the fundamental process in natural cells but also pave the way for real-world application, for example better drug tests, patient-tailored medicine.

Prior to synthesis of a synthetic cell that displays biological functionality as a mimic of certain aspects of living cells, building the boundaries of cell-like mimics is the most important step. This membrane is a semipermeable barrier not only delineates the interior from exterior, but also permits small molecules to pass into the cellular space. Furthermore, the membrane plays a crucial role in evolution as it separates (257) different genomes from one another reducing the problem of inactive parasites.

In this thesis, the overarching goal was to develop and fabricate droplet-based microfluidic devices in which artificial membranes were synthesised. In other words, the overall findings obtained during the research underpin the bottom-up construction of vesicle-based synthetic cell compartments and related membrane properties for the investigation of incorporating with membrane proteins. In the preceding chapters we reached several key breakthroughs towards achieving this goal.

6.1 Summary of Findings

Chapter 3 aimed to offer new routes to the construction of cell-like compartments using droplet-based microfluidic technique. These vesicular structures were transformed into artificial cells by performing in vitro transcription and translation. Further, highly functional artificial cell chassis were produced based on these artificial

cell constructs with certain types of membrane proteins incorporated into the bilayers.

Chapter 4 is concerned with introducing FLIM instrument into the characterisation of boundary systems of artificial cell mimics with the assistance of the molecular rotors. By taking advantage of microfluidic technique, the molecular rotors dissolved with phospholipid molecules in the volatile oil phase formed bilayers of double emulsion droplets. The combination of FLIM with molecular rotors shed light on the measurement of dewetting-induced viscosity change within artificial cell membranes through detecting the alteration of the lifetime of viscosity-sensitive molecules during the time course. In addition, we proposed this method was capable of tracking the amount of oil trapped in the bilayer gives the evidence of microfluidically fabricated vesicle-based synthetic cells are excellent models for the investigation of cell features.

In Chapter 5 we demonstrated a new capillary-based microfluidic strategy so as to producing vesicles featured with asymmetric arrangement in their bilayers. Initial attempts with the devised microfluidic device was to generate asymmetric bilayer lipid vesicles which are able to be used as more accurate cell-mimicry models in terms of lipid bilayer composition between two independent lipid monolayers. By characterising the asymmetric bilayers using confocal laser scanning microscopy and the fluorescence quenching assay, it can be seen that bilayers equipped with high degree of asymmetry was readily acquired using our device. Importantly, an advanced geometry of bilayer was constructed within the microfluidic device, is hybrid asymmetric bilayer namely as lipid stabilised the inner-leaflet and outer-leaflet was coated with block copolymer molecules.

6.2 Future Work and Outlook

The experimentation works presented in this thesis have opened up several avenues which could be explored in future. The directions of the potential studies fall into two parts. The first is exploring the potential application in building a cell from the

bottom up. The second involves developing a better understanding of the artificial cell modes developed in this thesis.

6.2.1 Microfluidics-Assisted Division of Cell Models

Several key advancements of engineering of cell model chassis using microfluidics for high-level functionalities have been accomplished in this thesis. As the models for mimicking cells, reproduction through cell division is a key signature of protocells. Apart from bringing biological machinery to constrict and divide the cell-mimic models, it is also intriguing to explore this process by applying physical forces. Recently Zhao et al. has demonstrated a passive three-dimensional splitting method based on capillary systems. Droplets flowed into a θ-shaped glass capillary with identical subchannels, resulting in a symmetric division of droplets. (258) Thus, a microfluidics-assisted approach which is the integration of a capillary-based lipid vesicles generator and the splitting device, could accomplish this task, as shown in Figure 6.1.

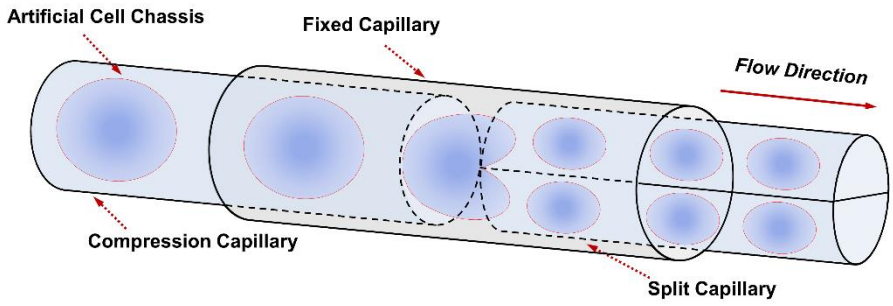

Figure 6.1 Scheme of the splitting process. Lipid vesicles generate at first stage and then flow into a compression capillary for aligning lipid vesicles with the split capillary.

Double emulsion droplets templates can be produced using the same protocol described in Chapter 3. The re-injection of as-formed lipid vesicles can be performed by connecting the outlet of the double emulsion generator and inlet of the splitting

device using a tubing. By carefully selecting the dimension of the compression capillary in which lipid vesicles will be well aligned in the centre of the capillary for the next step splitting process. A θ-shaped capillary will be employed as a splitter in this device providing passive force for droplets division process.

6.2.2 Microfluidic Assembly of Complex Vesicle Networks as Artificial Cells

Multicompartmentalisation is a significant feature of cells, allowing separation and protection of biological compounds within the membrane walls. These systems have recently been developed for use as cell mimicry. (259, 260) In each confined compartment, different independent enzymatic reactions take place simultaneously, imitating accurately (high spatiotemporal control) the biochemical reactions occur in eukaryotic cells. (261) By designing and preparation of these complex systems, we can have simplified biomimetic models serve as a tool for better understanding of complex cellular mechanism. A hierarchical capillary microfluidic device could tackle the issue of fabrication of highly monodisperse well-defined multicompartment systems, Figure 6.2. Briefly, the entrapped single vesicle is formed by microfluidically prepared double emulsion templated and then are reinjected into microfluidic device as the inner phase to construct lager vesicle-loaded double emulsion droplets. Further, the capillary microfluidic device offers considerable flexibility in encapsulation of distinct droplets in the host droplets, (262) which enables the creation of complex inner vesicle networks in the matrix cell model.

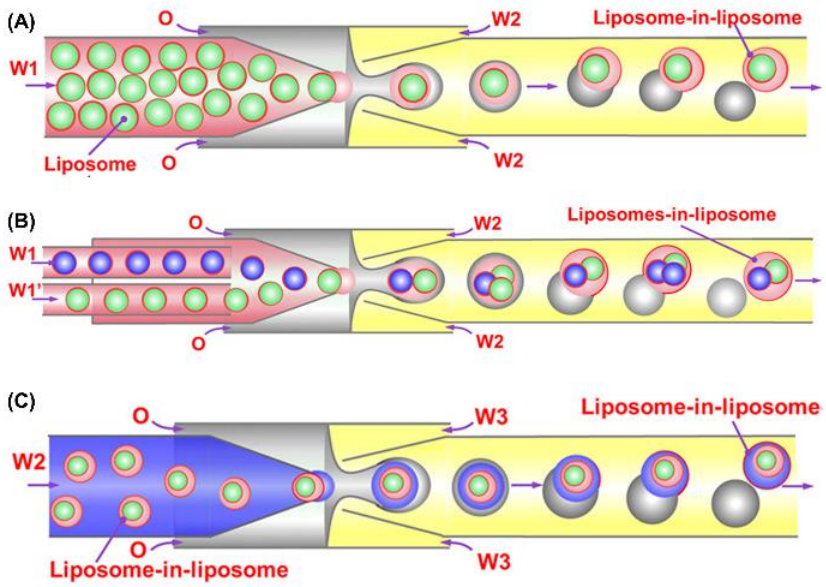

Figure 6.2 Schematics illustration of multistep microfluidic devices for the hierarchical assembly of complex vesicle networks (multicompartment systems) as new structured artificial cell models. Image modified from (263).

6.2.3 Highly Oriented Transmembrane Proteins Induced by Asymmetric Lipid Bilayer

In natural cell membranes, the transmembrane proteins have a well-defined orientation leads to specific biological function. (264, 265) However, the integral membrane proteins are randomly inserted without a preferred direction losing the information about the orientation as long as they are incorporated into the artificial symmetric model membranes. In Chapter 5, we also demonstrated a microfluidic route to the production of monodisperse asymmetric lipid vesicles with tailored bilayer composition at high-throughput. This asymmetric character of lipid bilayers plays a crucial role for many membrane-related processes like insertion and orientation of transmembrane proteins. (266)

In conclusion, our new microfluidic techniques can produce bilayers with high degree of asymmetry would offer particularly interesting approach to control over the orientation of integral membrane proteins in the membranes.

Bibliography

1. "Synthetic Biology: Applying Engineering to Biology," *Report of a NEST High-Level Expert Group* (EUROPEAN COMMISSION, 2005).

2. S. Peirú, H. G. Menzella, E. Rodríguez, J. Carney, H. Gramajo, Production of the potent antibacterial polyketide erythromycin C in Escherichia coli. *Applied and environmental microbiology* **71**, 2539-2547 (2005).

3. Y. Yong, Y. Yu, C. Li, J. Zhong, H. Song, Bioelectricity enhancement via overexpression of quorum sensing system in Pseudomonas aeruginosa-inoculated microbial fuel cells. *Biosensors and Bioelectronics* **30**, 87-92 (2011).

4. J. Hu, X. Liu, P. X. Ma, Induction of osteoblast differentiation phenotype on poly (L-lactic acid) nanofibrous matrix. *Biomaterials* **29**, 3815-3821 (2008).

5. S. A. Benner, A. M. Sismour, Synthetic biology. *Nature reviews. Genetics* **6**, 533 (2005).

6. S. Mukherji, A. Van Oudenaarden, Synthetic biology: understanding biological design from synthetic circuits. *Nature reviews. Genetics* **10**, 859 (2009).

7. A. C. Forster, G. M. Church, Synthetic biology projects in vitro. *Genome research* **17**, 1-6 (2007).

8. P. E. Purnick, R. Weiss, The second wave of synthetic biology: from modules to systems. *Nature reviews Molecular cell biology* **10**, 410-422 (2009).

9. D. E. Cameron, C. J. Bashor, J. J. Collins, A brief history of synthetic biology. *Nature Reviews Microbiology* **12**, 381-390 (2014).

10. D. Endy, Foundations for engineering biology. *Nature* **438**, 449 (2005).

11. Biobricks Foundation Homepage (2012). https://biobricks.org/

12. Max Planck Gesellschaft (2014). https://www.mpg.de/8219292/synthetic_biology

13. P. L. Luisi, Toward the engineering of minimal living cells. *The Anatomical Record* **268**, 208-214 (2002).

14. D. G. Gibson, J. I. Glass, C. Lartigue, V. N. Noskov, R.-Y. Chuang, M. A. Algire, G. A. Benders, M. G. Montague, L. Ma, M. M. Moodie, Creation of a bacterial cell controlled by a chemically synthesized genome. *science* **329**, 52-56 (2010).

15. C. A. Hutchison, R.-Y. Chuang, V. N. Noskov, N. Assad-Garcia, T. J. Deerinck, M. H. Ellisman, J. Gill, K. Kannan, B. J. Karas, L. Ma, Design and synthesis of a minimal bacterial genome. *Science* **351**, 1-11 (2016).

16. V. Noireaux, A. Libchaber, A vesicle bioreactor as a step toward an artificial cell assembly. *Proceedings of the national academy of sciences of the United States of America* **101**, 17669-17674 (2004).

17. P. Schwille, Bottom-up synthetic biology: engineering in a tinkerer's world. *Science* **333**, 1252-1254 (2011).

18. Y. Elani, Construction of membrane-bound artificial cells using microfluidics: a new frontier in bottom-up synthetic biology. *Biochemical Society Transactions* **44**, 723-730 (2016).

19. C. Xu, S. Hu, X. Chen, Artificial cells: from basic science to applications. *Materials Today* **19**, 516-532 (2016).

20. Y.-H. M. Chan, S. G. Boxer, Model membrane systems and their applications. *Current opinion in chemical biology* **11**, 581-587 (2007).

21. T. Osaki, S. Takeuchi, Artificial Cell Membrane Systems for Biosensing Applications. *Analytical chemistry* **89**, 216-231 (2016).

22. H. Bayley, Sequencing single molecules of DNA. *Current opinion in chemical biology* **10**, 628-637 (2006).

23. H.-H. Shen, T. Lithgow, L. Martin, Reconstitution of membrane proteins into model membranes: seeking better ways to retain protein activities. *International journal of molecular sciences* **14**, 1589-1607 (2013).

24. M. L. Wagner, L. K. Tamm, Tethered polymer-supported planar lipid bilayers for reconstitution of integral membrane proteins: silane-polyethyleneglycol-lipid as a cushion and covalent linker. *Biophysical Journal* **79**, 1400-1414 (2000).

25. J. Salafsky, J. T. Groves, S. G. Boxer, Architecture and function of membrane proteins in planar supported bilayers: a study with photosynthetic reaction centers. *Biochemistry* **35**, 14773-14781 (1996).

26. L. Tsofina, E. Liberman, A. Babakov, Production of bimolecular protein-lipid membranes in aqueous solution. *Nature* **212**, 681-683 (1966).

27. H. Bayley, B. Cronin, A. Heron, M. A. Holden, W. L. Hwang, R. Syeda, J. Thompson, M. Wallace, Droplet interface bilayers. *Molecular BioSystems* **4**, 1191-1208 (2008).

28. K. Funakoshi, H. Suzuki, S. Takeuchi, Lipid bilayer formation by contacting monolayers in a microfluidic device for membrane protein analysis. *Analytical chemistry* **78**, 8169-8174 (2006).

29. M. Booth, V. R. Schild, F. Downs, H. Bayley, Functional aqueous droplet networks. *Molecular BioSystems*, (2017).

30. W. L. Hwang, M. Chen, B. Cronin, M. A. Holden, H. Bayley, Asymmetric droplet interface bilayers. *Journal of the American Chemical Society* **130**, 5878-5879 (2008).

31. G. Maglia, A. J. Heron, W. L. Hwang, M. A. Holden, E. Mikhailova, Q. Li, S. Cheley, H. Bayley, Droplet networks with incorporated protein diodes show collective properties. *Nature nanotechnology* **4**, 437-440 (2009).

32. P. Stano, P. L. Luisi, Theory and construction of semi-synthetic minimal cells. *Synthetic biology handbook*, 209-258 (2016).

33. D. A. Hammer, N. P. Kamat, Towards an artificial cell. *FEBS letters* **586**, 2882-2890 (2012).

34. A. D. Bangham, R. Horne, Negative staining of phospholipids and their structural modification by surface-active agents as observed in the electron microscope. *Journal of molecular biology* **8**, 660-668 (1964).

35. M. I. Angelova, D. S. Dimitrov, Liposome electroformation. *Faraday discussions of the Chemical Society* **81**, 303-311 (1986).

36. S. F. Fenz, K. Sengupta, Giant vesicles as cell models. *Integrative Biology* **4**, 982-995 (2012).

37. P. Walde, K. Cosentino, H. Engel, P. Stano, Giant vesicles: preparations and applications. *ChemBioChem* **11**, 848-865 (2010).

38. K. Kamiya, S. Takeuchi, Giant liposome formation toward the synthesis of well-defined artificial cells. *Journal of Materials Chemistry B*, (2017).

39. H. C. Shum, D. Lee, I. Yoon, T. Kodger, D. A. Weitz, Double emulsion templated monodisperse phospholipid vesicles. *Langmuir* **24**, 7651-7653 (2008).

40. L. Lu, J. W. Schertzer, P. R. Chiarot, Continuous microfluidic fabrication of synthetic asymmetric vesicles. *Lab on a chip* **15**, 3591-3599 (2015).

41. C. Martino, Droplet-based microfluidics for artificial cell generation: a brief review. *Interface focus* **6**, 20160011 (2016).

42. A. C. Siegel, S. K. Tang, C. A. Nijhuis, M. Hashimoto, S. T. Phillips, M. D. Dickey, G. M. Whitesides, Cofabrication: a strategy for building multicomponent microsystems. *Accounts of chemical research* **43**, 518-528 (2010).

43. G. M. Whitesides, The origins and the future of microfluidics. *Nature* **442**, 368-373 (2006).

44. P. Abgrall, A. Gue, Lab-on-chip technologies: making a microfluidic network and coupling it into a complete microsystem—a review. *Journal of Micromechanics and Microengineering* **17**, R15 (2007).

45. T. M. Pearce, J. C. Williams, Microtechnology: meet neurobiology. *Lab on a chip* **7**, 30-40 (2007).

46. A. C. Rowat, J. C. Bird, J. J. Agresti, O. J. Rando, D. A. Weitz, Tracking lineages of single cells in lines using a microfluidic device. *Proceedings of the National Academy of Sciences* **106**, 18149-18154 (2009).

47. L.-H. Hung, A. P. Lee, Microfluidic devices for the synthesis of nanoparticles and biomaterials. *Journal of Medical and Biological Engineering* **27**, 1 (2007).

48. Y. Huang, B. Agrawal, D. Sun, J. S. Kuo, J. C. Williams, Microfluidics-based devices: New tools for studying cancer and cancer stem cell migration. *Biomicrofluidics* **5**, 013412 (2011).

49. S.-Y. Teh, R. Lin, L.-H. Hung, A. P. Lee, Droplet microfluidics. *Lab on a chip* **8**, 198-220 (2008).

50. H. A. Stone, A. D. Stroock, A. Ajdari, Engineering flows in small devices: microfluidics toward a lab-on-a-chip. *Annu. Rev. Fluid Mech.* **36**, 381-411 (2004).

51. C. N. Baroud, F. Gallaire, R. Dangla, Dynamics of microfluidic droplets. *Lab on a chip* **10**, 2032-2045 (2010).

52. A. Utada, E. Lorenceau, D. Link, P. Kaplan, H. Stone, D. Weitz, Monodisperse double emulsions generated from a microcapillary device. *Science* **308**, 537-541 (2005).

53. T. M. Squires, S. R. Quake, Microfluidics: Fluid physics at the nanoliter scale. *Reviews of modern physics* **77**, 977 (2005).

54. S. Matosevic, Synthesizing artificial cells from giant unilamellar vesicles: State - of - the art in the development of microfluidic technology. *Bioessays* **34**, 992-1001 (2012).

55. K. Ren, J. Zhou, H. Wu, Materials for microfluidic chip fabrication. *Accounts of chemical research* **46**, 2396-2406 (2013).

56. X. Hou, Y. S. Zhang, G. T.-D. Santiago, M. M. Alvarez, J. Ribas, S. J. Jonas, P. S. Weiss, A. M. Andrews, J. Aizenberg, A. Khademhosseini, Interplay between materials and microfluidics. *Nature Reviews Materials* **2**, 17016 (2017).

57. D. C. Duffy, J. C. McDonald, O. J. Schueller, G. M. Whitesides, Rapid prototyping of microfluidic systems in poly (dimethylsiloxane). *Analytical chemistry* **70**, 4974-4984 (1998).

58. Y. Ma, J. Thiele, L. Abdelmohsen, J. Xu, W. T. Huck, Biocompatible macro-initiators controlling radical retention in microfluidic on-chip photo-polymerization of water-in-oil emulsions. *Chemical Communications* **50**, 112-114 (2014).

59. R. K. Shah, J.-W. Kim, J. J. Agresti, D. A. Weitz, L.-Y. Chu, Fabrication of monodisperse thermosensitive microgels and gel capsules in microfluidic devices. *Soft Matter* **4**, 2303-2309 (2008).

60. S. H. Kim, J. W. Kim, J. C. Cho, D. A. Weitz, Double-emulsion drops with ultra-thin shells for capsule templates. *Lab on a chip* **11**, 3162-3166 (2011).

61. P. Zhu, L. Wang, Passive and active droplet generation with microfluidics: a review. *Lab on a chip* **17**, 34-75 (2017).

62. L. Shang, Y. Cheng, Y. Zhao, Emerging Droplet Microfluidics. *Chemical Reviews*, (2017).

63. C. Cramer, P. Fischer, E. J. Windhab, Drop formation in a co-flowing ambient fluid. *Chemical Engineering Science* **59**, 3045-3058 (2004).

64. R. Hooke, 1665 Micrographia. *London: Martyn and Allestry*, (2003).

65. G. Weber, Uses of fluorescence in biophysics: some recent developments. *Annual review of biophysics and bioengineering* **1**, 553-570 (1972).

66. W. T. Mason, *Fluorescent and luminescent probes for biological activity: a practical guide to technology for quantitative real-time analysis*. (Academic Press, 1999).

67. E. Sezgin, P. Schwille, Fluorescence techniques to study lipid dynamics. *Cold Spring Harbor perspectives in biology* **3**, a009803 (2011).

68. A. Kyrychenko, Using fluorescence for studies of biological membranes: a review. *Methods and Applications in Fluorescence* **3**, 042003 (2015).

69. J. F. W. Herschel, No. I. On a Case of Superficial Colour Presented by a Homogeneous Liquid Internally Colourless. *Philosophical Transactions of the Royal Society of London*, 143-145 (1845).

70. J. R. Lakowicz, in *Principles of fluorescence spectroscopy*. (Springer, 1999), pp. 1-23.

71. J. W. Lichtman, J.-A. Conchello, Fluorescence microscopy. *Nature methods* **2**, 910-919 (2005).

72. Microscopy Resource Center (2012). http://www.olympusmicro.com

73. LibreTexts https://chem.libretexts.org/

74. G. G. Stokes, On the change of refrangibility of light. *Philosophical Transactions of the Royal Society of London* **142**, 463-562 (1852).

75. M. Y. Berezin, S. Achilefu, Fluorescence lifetime measurements and biological imaging. *Chemical reviews* **110**, 2641-2684 (2010).

76. W. Baschong, L. Landmann, in *Cell Biology: A Laboratory Handbook*. (2006), pp. 5-17.

77. C. A. Combs, Fluorescence microscopy: a concise guide to current imaging methods. *Current Protocols in Neuroscience*, 2.1. 1-2.1. 14 (2010).

78. M. Minsky, Memoir on inventing the confocal scanning microscope. *Scanning* **10**, 128-138 (1988).

79. S. W. Paddock, Principles and practices of laser scanning confocal microscopy. *Molecular biotechnology* **16**, 127-149 (2000).

80. J. Korlach, P. Schwille, W. W. Webb, G. W. Feigenson, Characterization of lipid bilayer phases by confocal microscopy and fluorescence correlation spectroscopy. *Proceedings of the National Academy of Sciences* **96**, 8461-8466 (1999).

81. S. Pautot, B. J. Frisken, D. Weitz, Engineering asymmetric vesicles. *Proceedings of the National Academy of Sciences* **100**, 10718-10721 (2003).

82. S. Matosevic, B. M. Paegel, Layer-by-layer cell membrane assembly. *Nature chemistry* **5**, 958-963 (2013).

83. B. D. Venetta, Microscope phase fluorometer for determining the fluorescence lifetimes of fluorochromes. *Review of Scientific Instruments* **30**, 450-457 (1959).

84. X. F. Wang, T. Uchida, S. Minami, A fluorescence lifetime distribution measurement system based on phase-resolved detection using an image dissector tube. *Applied Spectroscopy* **43**, 840-845 (1989).

85. W. Becker, A. Bergmann, C. Biskup, Multispectral fluorescence lifetime imaging by TCSPC. *Microscopy research and technique* **70**, 403-409 (2007).

86. E. B. van Munster, T. W. Gadella, in *Microscopy techniques*. (Springer, 2005), pp. 143-175.

87. W. Becker, *The bh TCSPC handbook*. (Becker & Hickl, 2014).

88. W. Becker, A. Bergmann, M. Hink, K. König, K. Benndorf, C. Biskup, Fluorescence lifetime imaging by time - correlated single - photon counting. *Microscopy research and technique* **63**, 58-66 (2004).

89. D. V. O'Connor, D. Phillips, Time-correlated single photon counting. *Applied Optics* **25**, 460-463 (1986).

90. J. Yguerabide, Nanosecond fluorescence spectroscopy of macromolecules. *Methods in enzymology* **26**, 498-578 (1972).

91. G. K. Batchelor, *An introduction to fluid dynamics*. (Cambridge university press, 2000).

92. D. B. Weibel, G. M. Whitesides, Applications of microfluidics in chemical biology. *Current opinion in chemical biology* **10**, 584-591 (2006).

93. A. E. Kamholz, B. H. Weigl, B. A. Finlayson, P. Yager, Quantitative analysis of molecular interaction in a microfluidic channel: the T-sensor. *Analytical chemistry* **71**, 5340-5347 (1999).

94. J. P. Brody, P. Yager, R. E. Goldstein, R. H. Austin, Biotechnology at low Reynolds numbers. *Biophysical journal* **71**, 3430-3441 (1996).

95. J. P. Brody, P. Yager, Diffusion-based extraction in a microfabricated device. *Sensors and Actuators A: Physical* **58**, 13-18 (1997).

96. P. Becher, Emulsions: theory and practice. (1965).

97. F. Leal-Calderon, V. Schmitt, J. Bibette, *Emulsion science: basic principles*. (Springer Science & Business Media, 2007).

98. L. L. Schramm, *Emulsions, foams, and suspensions: fundamentals and applications*. (John Wiley & Sons, 2006).

99. L. Rayleigh, in *Proc. R. Soc. London*. (1879), vol. 29, pp. 71-97.

100. J. Atencia, D. J. Beebe, Controlled microfluidic interfaces. *Nature* **437**, 648-655 (2005).

101. R. K. Shah, H. C. Shum, A. C. Rowat, D. Lee, J. J. Agresti, A. S. Utada, L.-Y. Chu, J.-W. Kim, A. Fernandez-Nieves, C. J. Martinez, Designer emulsions using microfluidics. *Materials Today* **11**, 18-27 (2008).

102. N.-N. Deng, C.-L. Mou, W. Wang, X.-J. Ju, R. Xie, L.-Y. Chu, Multiple emulsion formation from controllable drop pairs in microfluidics. *Microfluidics and nanofluidics* **17**, 967-972 (2014).

103. T. Thorsen, R. W. Roberts, F. H. Arnold, S. R. Quake, Dynamic pattern formation in a vesicle-generating microfluidic device. *Physical review letters* **86**, 4163 (2001).

104. H. A. Stone, Dynamics of drop deformation and breakup in viscous fluids. *Annual Review of Fluid Mechanics* **26**, 65-102 (1994).

105. G. F. Christopher, S. L. Anna, Microfluidic methods for generating continuous droplet streams. *Journal of Physics D: Applied Physics* **40**, R319 (2007).

106. S. L. Anna, H. C. Mayer, Microscale tipstreaming in a microfluidic flow focusing device. *Physics of Fluids* **18**, 121512 (2006).

107. P. Garstecki, H. A. Stone, G. M. Whitesides, Mechanism for flow-rate controlled breakup in confined geometries: a route to monodisperse emulsions. *Physical Review Letters* **94**, 164501 (2005).

108. T. Young, An essay on the cohesion of fluids. *Philosophical Transactions of the Royal Society of London* **95**, 65-87 (1805).

109. R. C. Hayward, A. S. Utada, N. Dan, D. A. Weitz, Dewetting instability during the formation of polymersomes from block-copolymer-stabilized double emulsions. *Langmuir* **22**, 4457-4461 (2006).

110. H. C. Shum, J.-W. Kim, D. A. Weitz, Microfluidic fabrication of monodisperse biocompatible and biodegradable polymersomes with controlled permeability. *Journal of the American Chemical Society* **130**, 9543-9549 (2008).

111. H. C. Shum, E. Santanach-Carreras, J.-W. Kim, A. Ehrlicher, J. Bibette, D. A. Weitz, Dewetting-induced membrane formation by adhesion of amphiphile-laden interfaces. *Journal of the American Chemical Society* **133**, 4420-4426 (2011).

112. C. Martino, S. H. Kim, L. Horsfall, A. Abbaspourrad, S. J. Rosser, J. Cooper, D. A. Weitz, Protein expression, aggregation, and triggered release from polymersomes as artificial cell - like structures. *Angewandte Chemie International Edition* **51**, 6416-6420 (2012).

113. R. R. New, *Liposomes: a practical approach*. (Oxford University Press, USA, 1990), vol. 58.

114. M. M. Hanczyc, J. W. Szostak, Replicating vesicles as models of primitive cell growth and division. *Current opinion in chemical biology* **8**, 660-664 (2004).

115. V. Noireaux, R. Bar-Ziv, J. Godefroy, H. Salman, A. Libchaber, Toward an artificial cell based on gene expression in vesicles. *Physical biology* **2**, P1 (2005).

116. A. Jahn, W. N. Vreeland, M. Gaitan, L. E. Locascio, Controlled vesicle self-assembly in microfluidic channels with hydrodynamic focusing. *Journal of the American Chemical Society* **126**, 2674-2675 (2004).

117. A. Jahn, W. N. Vreeland, D. L. DeVoe, L. E. Locascio, M. Gaitan, Microfluidic directed formation of liposomes of controlled size. *Langmuir* **23**, 6289-6293 (2007).

118. A. Jesorka, O. Orwar, Liposomes: technologies and analytical applications. *Annu. Rev. Anal. Chem.* **1**, 801-832 (2008).

119. P. Stano, P. Carrara, Y. Kuruma, T. P. de Souza, P. L. Luisi, Compartmentalized reactions as a case of soft-matter biotechnology: synthesis of proteins and nucleic acids inside lipid vesicles. *Journal of Materials Chemistry* **21**, 18887-18902 (2011).

120. P. Carrara, P. Stano, P. L. Luisi, Giant vesicles "colonies": a model for primitive cell communities. *ChemBioChem* **13**, 1497-1502 (2012).

121. R. Dimova, R. Lipowsky, Lipid membranes in contact with aqueous phases of polymer solutions. *Soft Matter* **8**, 6409-6415 (2012).

122. M. S. Long, C. D. Jones, M. R. Helfrich, L. K. Mangeney-Slavin, C. D. Keating, Dynamic microcompartmentation in synthetic cells. *Proceedings of the National Academy of Sciences* **102**, 5920-5925 (2005).

123. K. Simons, W. L. Vaz, Model systems, lipid rafts, and cell membranes 1. *Annu. Rev. Biophys. Biomol. Struct.* **33**, 269-295 (2004).

124. P. Girard, J. Pécréaux, G. Lenoir, P. Falson, J.-L. Rigaud, P. Bassereau, A new method for the reconstitution of membrane proteins into giant unilamellar vesicles. *Biophysical journal* **87**, 419-429 (2004).

125. N. Kahya, E.-I. Pécheur, W. P. de Boeij, D. A. Wiersma, D. Hoekstra, Reconstitution of membrane proteins into giant unilamellar vesicles via peptide-induced fusion. *Biophysical Journal* **81**, 1464-1474 (2001).

126. M. Dezi, A. Di Cicco, P. Bassereau, D. Lévy, Detergent-mediated incorporation of transmembrane proteins in giant unilamellar vesicles with controlled physiological contents. *Proceedings of the National Academy of Sciences* **110**, 7276-7281 (2013).

127. I. L. Jørgensen, G. C. Kemmer, T. G. Pomorski, Membrane protein reconstitution into giant unilamellar vesicles: a review on current techniques. *European Biophysics Journal*, 1-17 (2016).

128. B. M. Discher, Y.-Y. Won, D. S. Ege, J. C. Lee, F. S. Bates, D. E. Discher, D. A. Hammer, Polymersomes: tough vesicles made from diblock copolymers. *Science* **284**, 1143-1146 (1999).

129. B. M. Discher, H. Bermudez, D. A. Hammer, D. E. Discher, Y.-Y. Won, F. S. Bates, Cross-linked polymersome membranes: vesicles with broadly adjustable properties. *The Journal of Physical Chemistry B* **106**, 2848-2854 (2002).

130. S. Belegrinou, J. Dorn, M. Kreiter, K. Kita-Tokarczyk, E.-K. Sinner, W. Meier, Biomimetic supported membranes from amphiphilic block copolymers. *Soft Matter* **6**, 179-186 (2010).

131. D. E. Discher, F. Ahmed, Polymersomes. *Annu. Rev. Biomed. Eng.* **8**, 323-341 (2006).

132. L. Zhang, A. Eisenberg, Multiple morphologies of" crew-cut" aggregates of polystyrene-b-poly (acrylic acid) block copolymers. *Science* **268**, 1728 (1995).

133. K. P. Davis, T. P. Lodge, F. S. Bates, Vesicle membrane thickness in aqueous dispersions of block copolymer blends. *Macromolecules* **41**, 8289-8291 (2008).

134. O. Onaca, R. Enea, D. W. Hughes, W. Meier, Stimuli - Responsive Polymersomes as Nanocarriers for Drug and Gene Delivery. *Macromolecular bioscience* **9**, 129-139 (2009).

135. N. P. Kamat, J. S. Katz, D. A. Hammer, Engineering polymersome protocells. *The journal of physical chemistry letters* **2**, 1612 (2011).

136. H. Bermudez, A. K. Brannan, D. A. Hammer, F. S. Bates, D. E. Discher, Molecular weight dependence of polymersome membrane elasticity and stability. *arXiv preprint cond-mat/0110088*, (2001).

137. M. Delcea, A. Yashchenok, K. Videnova, O. Kreft, H. Möhwald, A. G. Skirtach, Multicompartmental Micro - and Nanocapsules: Hierarchy and Applications in Biosciences. *Macromolecular bioscience* **10**, 465-474 (2010).

138. D. E. Discher, V. Ortiz, G. Srinivas, M. L. Klein, Y. Kim, D. Christian, S. Cai, P. Photos, F. Ahmed, Emerging applications of polymersomes in delivery: from molecular dynamics to shrinkage of tumors. *Progress in polymer science* **32**, 838-857 (2007).

139. D. van Swaay, Microfluidic methods for forming liposomes. *Lab on a chip* **13**, 752-767 (2013).

140. H. C. Shum, J. Thiele, S.-H. Kim, Microfluidic fabrication of vesicles. *Advances in transport phenomena 2011*, 1-28 (2014).

141. S. Matosevic, B. M. Paegel, Stepwise synthesis of giant unilamellar vesicles on a microfluidic assembly line. *Journal of the American Chemical Society* **133**, 2798-2800 (2011).

142. P. C. Hu, S. Li, N. Malmstadt, Microfluidic fabrication of asymmetric giant lipid vesicles. *ACS applied materials & interfaces* **3**, 1434-1440 (2011).

143. N.-N. Deng, W. Wang, X.-J. Ju, R. Xie, L.-Y. Chu, Spontaneous transfer of droplets across microfluidic laminar interfaces. *Lab on a chip* **16**, 4326-4332 (2016).

144. Y.-C. Tan, K. Hettiarachchi, M. Siu, Y.-R. Pan, A. P. Lee, Controlled microfluidic encapsulation of cells, proteins, and microbeads in lipid vesicles. *Journal of the American Chemical Society* **128**, 5656-5658 (2006).

145. F. Kong, X. Zhang, M. Hai, Microfluidics fabrication of monodisperse biocompatible phospholipid vesicles for encapsulation and delivery of hydrophilic drug or active compound. *Langmuir* **30**, 3905-3912 (2014).

146. E. Lorenceau, A. S. Utada, D. R. Link, G. Cristobal, M. Joanicot, D. A. Weitz, Generation of polymerosomes from double-emulsions. *Langmuir* **21**, 9183-9186 (2005).

147. L. R. Arriaga, S. S. Datta, S. H. Kim, E. Amstad, T. E. Kodger, F. Monroy, D. A. Weitz, Ultrathin shell double emulsion templated giant unilamellar lipid vesicles with controlled microdomain formation. *Small* **10**, 950-956 (2014).

148. S. Deshpande, Y. Caspi, A. E. Meijering, C. Dekker, Octanol-assisted liposome assembly on chip. *Nature communications* **7**, (2016).

149. F. H. Crick, in *Symp Soc Exp Biol.* (1958), vol. 12, pp. 8.

150. F. Crick, Central dogma of molecular biology. *Nature* **227**, 561-563 (1970).

151. N.-N. Deng, M. Yelleswarapu, W. T. Huck, Monodisperse Uni-and Multicompartment Liposomes. *Journal of the American Chemical Society* **138**, 7584-7591 (2016).

152. H. Saito, Y. Kato, M. Le Berre, A. Yamada, T. Inoue, K. Yosikawa, D. Baigl, Time - Resolved Tracking of a Minimum Gene Expression System Reconstituted in Giant Liposomes. *ChemBioChem* **10**, 1640-1643 (2009).

153. K. Nishimura, T. Matsuura, K. Nishimura, T. Sunami, H. Suzuki, T. Yomo, Cell-free protein synthesis inside giant unilamellar vesicles analyzed by flow cytometry. *Langmuir* **28**, 8426-8432 (2012).

154. Y. Shimizu, A. Inoue, Y. Tomari, T. Suzuki, T. Yokogawa, K. Nishikawa, T. Ueda, Cell-free translation reconstituted with purified components. *Nature biotechnology* **19**, 751-755 (2001).

155. Y. Lu, Cell-free synthetic biology: Engineering in an open world. *Synthetic and Systems Biotechnology*, (2017).

156. M. W. Nirenberg, J. H. Matthaei, The dependence of cell-free protein synthesis in E. coli upon naturally occurring or synthetic polyribonucleotides. *Proceedings of the National Academy of Sciences* **47**, 1588-1602 (1961).

157. W. Yu, K. Sato, M. Wakabayashi, T. Nakaishi, E. P. Ko-Mitamura, Y. Shima, I. Urabe, T. Yomo, Synthesis of functional protein in liposome. *Journal of bioscience and bioengineering* **92**, 590-593 (2001).

158. Y. Elani, R. V. Law, O. Ces, Protein synthesis in artificial cells: using compartmentalisation for spatial organisation in vesicle bioreactors. *Physical Chemistry Chemical Physics* **17**, 15534-15537 (2015).

159. N.-N. Deng, M. Yelleswarapu, L. Zheng, W. T. Huck, Microfluidic Assembly of Monodisperse Vesosomes as Artificial Cell Models. *Journal of the American Chemical Society*, (2016).

160. T.-Y. D. Tang, D. van Swaay, J. R. Anderson, S. Mann, In vitro gene expression within membrane-free coacervate protocells. *Chemical Communications* **51**, 11429-11432 (2015).

161. S.-Y. Teh, R. Khnouf, H. Fan, A. P. Lee, Stable, biocompatible lipid vesicle generation by solvent extraction-based droplet microfluidics. *Biomicrofluidics* **5**, 044113 (2011).

162. S. Ota, S. Yoshizawa, S. Takeuchi, Microfluidic formation of monodisperse, cell - sized, and unilamellar vesicles. *Angewandte Chemie International Edition* **48**, 6533-6537 (2009).

163. D. Saeki, S. Sugiura, T. Kanamori, S. Sato, S. Ichikawa, Microcompartmentalized cell-free protein synthesis in semipermeable microcapsules composed of polyethylenimine-coated alginate. *Journal of bioscience and bioengineering* **118**, 199-204 (2014).

164. M. Chanasakulniyom, C. Martino, D. Paterson, L. Horsfall, S. Rosser, J. M. Cooper, Expression of membrane-associated proteins within single emulsion cell facsimiles. *Analyst* **137**, 2939-2943 (2012).

165. C. Martino, L. Horsfall, Y. Chen, M. Chanasakulniyom, D. Paterson, A. Brunet, S. Rosser, Y. J. Yuan, J. M. Cooper, Cytoskeletal protein expression and its association within the hydrophobic membrane of artificial cell models. *ChemBioChem* **13**, 792-795 (2012).

166. L. Liguori, B. Marques, J. L. Lenormand, A Bacterial Cell - Free Expression System to Produce Membrane Proteins and Proteoliposomes: From cDNA to Functional Assay. *Current Protocols in Protein Science*, 5.22. 21-25.22. 30 (2008).

167. R. Kalmbach, I. Chizhov, M. C. Schumacher, T. Friedrich, E. Bamberg, M. Engelhard, Functional cell-free synthesis of a seven helix membrane protein: in situ insertion of bacteriorhodopsin into liposomes. *Journal of molecular biology* **371**, 639-648 (2007).

168. H. Matsubayashi, Y. Kuruma, T. Ueda, In vitro synthesis of the E. coli Sec translocon from DNA. *Angewandte Chemie International Edition* **53**, 7535-7538 (2014).

169. S.-H. Kim, J. W. Kim, J.-C. Cho, D. A. Weitz, Double-emulsion drops with ultra-thin shells for capsule templates. *Lab on a chip* **11**, 3162-3166 (2011).

170. T. S. Shim, S. H. Kim, S. M. Yang, Elaborate design strategies toward novel microcarriers for controlled encapsulation and release. *Particle & Particle Systems Characterization* **30**, 9-45 (2013).

171. C. Nardin, M. Winterhalter, W. Meier, Giant free-standing ABA triblock copolymer membranes. *Langmuir* **16**, 7708-7712 (2000).

172. C. Nardin, T. Hirt, J. Leukel, W. Meier, Polymerized ABA triblock copolymer vesicles. *Langmuir* **16**, 1035-1041 (2000).

173. M. Lomora, F. Itel, I. A. Dinu, C. G. Palivan, Selective ion-permeable membranes by insertion of biopores into polymersomes. *Physical Chemistry Chemical Physics* **17**, 15538-15546 (2015).

174. F. Itel, M. Chami, A. Najer, S. Lörcher, D. Wu, I. A. Dinu, W. Meier, Molecular organization and dynamics in polymersome membranes: A lateral diffusion study. *Macromolecules* **47**, 7588-7596 (2014).

175. L. Song, M. R. Hobaugh, C. Shustak, S. Cheley, H. Bayley, J. E. Gouaux, Structure of staphylococcal α-hemolysin, a heptameric transmembrane pore. *Science* **274**, 1859-1865 (1996).

176. C. G. Palivan, R. Goers, A. Najer, X. Zhang, A. Car, W. Meier, Bioinspired polymer vesicles and membranes for biological and medical applications. *Chemical Society Reviews* **45**, 377-411 (2016).

177. J. Pietzsch, Mind the membrane. Horizon Symposia: Living Frontier, (2004).

178. R. B. Gennis, *Biomembranes: molecular structure and function*. (Springer Science & Business Media, 2013).

179. W. K. Subczynski, A. Wisniewska, Physical properties of lipid bilayer membranes: relevance to membrane biological functions. *Acta Biochimica Polonica-English Edition* **47**, 613-626 (2000).

180. J. J. García, L. López - Pingarrón, P. Almeida - Souza, A. Tres, P. Escudero, F. A. García - Gil, D. X. Tan, R. J. Reiter, J. M. Ramírez, M. Bernal - Pérez, Protective effects of melatonin in reducing oxidative stress and in preserving the fluidity of biological membranes: a review. *Journal of Pineal Research* **56**, 225-237 (2014).

181. K. Tsuda, I. Nishio, Membrane fluidity and hypertension. *American Journal of Hypertension* **16**, 259-261 (2003).

182. M. Shinitzky, Membrane fluidity and cellular functions. *Physiology of membrane fluidity* **1**, 1-51 (1984).

183. G. Lenaz, G. P. Castelli, Membrane fluidity: molecular basis and physiological significance. *Structure and properties of cell membranes* **1**, 93-136 (1985).

184. G. Deliconstantinos, V. Villiotou, J. C. Stavrides, Modulation of particulate nitric oxide synthase activity and peroxynitrite synthesis in cholesterol enriched endothelial cell membranes. *Biochemical pharmacology* **49**, 1589-1600 (1995).

185. J. Klaver, E. Greve, H. Goslinga, H. Geijssen, J. Heuvelmans, Blood and plasma viscosity measurements in patients with glaucoma. *British journal of ophthalmology* **69**, 765-770 (1985).

186. O. Nadiv, M. Shinitzky, H. Manu, D. Hecht, C. Roberts, D. LeROITH, Y. Zick, Elevated protein tyrosine phosphatase activity and increased membrane viscosity are associated with impaired activation of the insulin receptor kinase in old rats. *Biochemical Journal* **298**, 443-450 (1994).

187. R. Rosencranz, S. A. Bogen, Clinical laboratory measurement of serum, plasma, and blood viscosity. *Pathology Patterns Reviews* **125**, S78-S86 (2006).

188. S. J. Singer, G. L. Nicolson, The fluid mosaic model of the structure of cell membranes. *Science* **175**, 720-731 (1972).

189. G. S. Zubenko, U. Kopp, T. Seto, L. L. Firestone, Platelet membrane fluidity individuals at risk for Alzheimer's disease: a comparison of results from fluorescence spectroscopy and electron spin resonance spectroscopy. *Psychopharmacology* **145**, 175-180 (1999).

190. G. Lenaz, Lipid fluidity and membrane protein dynamics. *Bioscience reports* **7**, 823-837 (1987).

191. G. Buech, W. Herrmann, H.-H. Borchert, Measurement of Microviscosity in Vesicular Membranes by Electron Spin Resonance. *Applied Magnetic Resonance* **33**, 269-283 (2008).

192. L. Coderch, J. Fonollosa, M. De Pera, J. Estelrich, A. De La Maza, J. Parra, Influence of cholesterol on liposome fluidity by EPR: relationship with percutaneous absorption. *Journal of Controlled Release* **68**, 85-95 (2000).

193. B. A. van den Bergh, P. W. Wertz, H. E. Junginger, J. A. Bouwstra, Elasticity of vesicles assessed by electron spin resonance, electron microscopy and extrusion measurements. *International journal of pharmaceutics* **217**, 13-24 (2001).

194. A. Ferretti, A. Knijn, E. Iorio, S. Pulciani, M. Giambenedetti, A. Molinari, S. Meschini, A. Stringaro, A. Calcabrini, I. Freitas, Biophysical and structural characterization of 1 H-NMR-detectable mobile lipid domains in NIH-3T3 fibroblasts. *Biochimica et Biophysica Acta (BBA)-Molecular and Cell Biology of Lipids* **1438**, 329-348 (1999).

195. M. Bouchard, N. Boudreau, M. Auger, Membrane fluidity response to odorants as seen by 2H-NMR and infrared spectroscopy. *Biochimica et Biophysica Acta (BBA)-Biomembranes* **1282**, 233-239 (1996).

196. M. F. Brown, S. Lope-Piedrafita, G. V. Martinez, H. I. Petrache, in *Modern Magnetic Resonance*. (Springer, 2008), pp. 249-260.

197. A. S. Klymchenko, R. Kreder, Fluorescent probes for lipid rafts: from model membranes to living cells. *Chemistry & biology* **21**, 97-113 (2014).

198. M. A. Haidekker, T. Ling, M. Anglo, H. Y. Stevens, J. A. Frangos, E. A. Theodorakis, New fluorescent probes for the measurement of cell membrane viscosity. *Chemistry & biology* **8**, 123-131 (2001).

199. C. Klein, T. Pillot, J. Chambaz, B. Drouet, Determination of plasma membrane fluidity with a fluorescent analogue of sphingomyelin by FRAP measurement using a standard confocal microscope. *Brain research protocols* **11**, 46-51 (2003).

200. M. J. Dayel, E. F. Hom, A. Verkman, Diffusion of green fluorescent protein in the aqueous-phase lumen of endoplasmic reticulum. *Biophysical journal* **76**, 2843-2851 (1999).

201. D. Marguet, P. F. Lenne, H. Rigneault, H. T. He, Dynamics in the plasma membrane: how to combine fluidity and order. *The EMBO journal* **25**, 3446-3457 (2006).

202. Y. Chen, B. C. Lagerholm, B. Yang, K. Jacobson, Methods to measure the lateral diffusion of membrane lipids and proteins. *Methods* **39**, 147-153 (2006).

203. A. J. García-Sáez, D. C. Carrer, P. Schwille, Fluorescence correlation spectroscopy for the study of membrane dynamics and organization in giant unilamellar vesicles. *Liposomes: Methods and Protocols, Volume 2: Biological Membrane Models*, 493-508 (2010).

204. K. Bacia, S. A. Kim, P. Schwille, Fluorescence cross-correlation spectroscopy in living cells. *Nature methods* **3**, 83 (2006).

205. S. Chiantia, J. Ries, P. Schwille, Fluorescence correlation spectroscopy in membrane structure elucidation. *Biochimica et Biophysica Acta (BBA)-Biomembranes* **1788**, 225-233 (2009).

206. A. Benda, M. Beneš, V. Marecek, A. Lhotský, W. T. Hermens, M. Hof, How to determine diffusion coefficients in planar phospholipid systems by confocal fluorescence correlation spectroscopy. *Langmuir* **19**, 4120-4126 (2003).

207. V. Mueller, A. Honigmann, C. Ringemann, R. Medda, G. Schwarzmann, C. Eggeling, FCS in STED microscopy: studying the nanoscale of lipid membrane dynamics. *SY Tetin Fluorescence Fluctuation Spectroscopy* **519**, 1-38 (2013).

208. R. P. Feynman, There's plenty of room at the bottom. *Engineering and science* **23**, 22-36 (1960).

209. M. K. Kuimova, G. Yahioglu, J. A. Levitt, K. Suhling, Molecular rotor measures viscosity of live cells via fluorescence lifetime imaging. *Journal of the American Chemical Society* **130**, 6672-6673 (2008).

210. Y. Wu, M. Štefl, A. Olzyńska, M. Hof, G. Yahioglu, P. Yip, D. R. Casey, O. Ces, J. Humpolíčková, M. K. Kuimova, Molecular rheometry: direct determination of viscosity in L_o and L_d lipid phases via fluorescence lifetime imaging. *Physical Chemistry Chemical Physics* **15**, 14986-14993 (2013).

211. M. R. Dent, I. López-Duarte, C. J. Dickson, P. Chairatana, H. L. Anderson, I. R. Gould, D. Wylie, A. Vyšniauskas, N. J. Brooks, M. K. Kuimova, Imaging plasma membrane phase behaviour in live cells using a thiophene-based molecular rotor. *Chemical Communications* **52**, 13269-13272 (2016).

212. M. K. Kuimova, Mapping viscosity in cells using molecular rotors. *Physical Chemistry Chemical Physics* **14**, 12671-12686 (2012).

213. M. A. Haidekker, E. A. Theodorakis, Molecular rotors—fluorescent biosensors for viscosity and flow. *Organic & Biomolecular Chemistry* **5**, 1669-1678 (2007).

214. T. Förster, G. Hoffmann, Die viskositätsabhängigkeit der fluoreszenzquantenausbeuten einiger farbstoffsysteme [Effect of viscosity

on the fluorescence quantum yield of some dye system]. *Journal of physical chemistry* **75**, 63-76 (1971).

215. A. K. Singh, J. Das, Liposome encapsulated vitamin A compounds exhibit greater stability and diminished toxicity. *Biophysical chemistry* **73**, 155-162 (1998).

216. R. K. Benninger, O. Hofmann, B. Önfelt, I. Munro, C. Dunsby, D. M. Davis, M. A. Neil, P. M. French, A. J. de Mello, Fluorescence - Lifetime Imaging of DNA – Dye Interactions within Continuous - Flow Microfluidic Systems. *Angewandte Chemie International Edition* **46**, 2228-2231 (2007).

217. D. M. Owen, P. M. Lanigan, C. Dunsby, I. Munro, D. Grant, M. A. Neil, P. M. French, A. I. Magee, Fluorescence lifetime imaging provides enhanced contrast when imaging the phase-sensitive dye di-4-ANEPPDHQ in model membranes and live cells. *Biophysical journal* **90**, L80-L82 (2006).

218. M. K. Kuimova, Molecular rotors image intracellular viscosity. *CHIMIA International Journal for Chemistry* **66**, 159-165 (2012).

219. I. López-Duarte, T. T. Vu, M. A. Izquierdo, J. A. Bull, M. K. Kuimova, A molecular rotor for measuring viscosity in plasma membranes of live cells. *Chemical Communications* **50**, 5282-5284 (2014).

220. J. A. Levitt, M. K. Kuimova, G. Yahioglu, P.-H. Chung, K. Suhling, D. Phillips, Membrane-bound molecular rotors measure viscosity in live cells via fluorescence lifetime imaging. *The Journal of Physical Chemistry C* **113**, 11634-11642 (2009).

221. D. Paterson, J. Reboud, R. Wilson, M. Tassieri, J. Cooper, Integrating microfluidic generation, handling and analysis of biomimetic giant unilamellar vesicles. *Lab on a chip* **14**, 1806-1810 (2014).

222. N. Boens, W. Qin, N. Basarić, J. Hofkens, M. Ameloot, J. Pouget, J.-P. Lefèvre, B. Valeur, E. Gratton, M. VandeVen, Fluorescence lifetime standards for time and frequency domain fluorescence spectroscopy. *Analytical chemistry* **79**, 2137-2149 (2007).

223. M. R. Dent, I. López-Duarte, C. J. Dickson, N. D. Geoghegan, J. M. Cooper, I. R. Gould, R. Krams, J. A. Bull, N. J. Brooks, M. K. Kuimova, Imaging phase separation in model lipid membranes through the use of BODIPY based molecular rotors. *Physical Chemistry Chemical Physics* **17**, 18393-18402 (2015).

224. M. S. Bretscher, Asymmetrical lipid bilayer structure for biological membranes. *Nature* **236**, 11-12 (1972).

225. J. E. Rothman, J. Lenard, Membrane asymmetry. *Science* **195**, 743-753 (1977).

226. A. Verkleij, R. Zwaal, B. Roelofsen, P. Comfurius, D. Kastelijn, L. Van Deenen, The asymmetric distribution of phospholipids in the human red cell membrane. A combined study using phospholipases and freeze-etch electron microscopy. *Biochimica et Biophysica Acta (BBA)-Biomembranes* **323**, 178-193 (1973).

227. H. Nikaido, Molecular basis of bacterial outer membrane permeability revisited. *Microbiology and molecular biology reviews* **67**, 593-656 (2003).

228. J. S. Slusky, R. L. Dunbrack, Charge asymmetry in the proteins of the outer membrane. *Bioinformatics* **29**, 2122-2128 (2013).

229. J. W. Schertzer, M. Whiteley, A bilayer-couple model of bacterial outer membrane vesicle biogenesis. *MBio* **3**, e00297-00211 (2012).

230. H.-T. Cheng, E. London, Preparation and properties of asymmetric vesicles that mimic cell membranes effect upon lipid raft formation and transmembrane helix orientation. *Journal of Biological Chemistry* **284**, 6079-6092 (2009).

231. R. Zwaal, P. Comfurius, E. Bevers, Surface exposure of phosphatidylserine in pathological cells. *Cellular and molecular life sciences* **62**, 971-988 (2005).

232. B. Fadeel, D. Xue, The ins and outs of phospholipid asymmetry in the plasma membrane: roles in health and disease. *Critical reviews in biochemistry and molecular biology* **44**, 264-277 (2009).

233. D. Marquardt, B. Geier, G. Pabst, Asymmetric lipid membranes: towards more realistic model systems. *Membranes* **5**, 180-196 (2015).

234. M. S. Bretscher, Phosphatidyl-ethanolamine: differential labelling in intact cells and cell ghosts of human erythrocytes by a membrane-impermeable reagent. *Journal of molecular biology* **71**, 523IN1527-1526IN3528 (1972).

235. J. Sancez-Yagüe, J. Cabezas, M. Llanillo, Estimation of the asymmetrical arrangement of plasma membrane aminophospholipids. An experimental assay for students of biochemistry and molecular biology. *Biochemical Education* **15**, 213-215 (1987).

236. G. MEER, B. J. POORTHUIS, K. W. WIRTZ, J. A. KAMP, L. L. DEENEN, Transbilayer distribution and mobility of phosphatidylcholine in intact erythrocyte membranes. *European Journal of Biochemistry* **103**, 283-288 (1980).

237. J. Krebs, H. Hauser, E. Carafoli, Asymmetric distribution of phospholipids in the inner membrane of beef heart mitochondria. *J Biol Chem* **254**, 5308-5316 (1979).

238. J. F. Tait, D. Gibson, Measurement of membrane phospholipid asymmetry in normal and sickle-cell erythrocytes by means of annexin V binding. *The Journal of laboratory and clinical medicine* **123**, 741-748 (1994).

239. G. Koopman, C. Reutelingsperger, G. Kuijten, R. Keehnen, S. Pals, M. Van Oers, Annexin V for flow cytometric detection of phosphatidylserine expression on B cells undergoing apoptosis. *Blood* **84**, 1415-1420 (1994).

240. A. Bangham, R. Horne, Action of saponin on biological cell membranes. *Nature* **196**, 953-955 (1962).

241. A. D. Bangham, R. Horne, Negative staining of phospholipids and their structural modification by surface-active agents as observed in the electron microscope. *Journal of molecular biology* **8**, 660IN662-668IN610 (1964).

242. K. Kurihara, M. Tamura, K. Shohda, T. Toyota, K. Suzuki, T. Sugawara, Self-reproduction of supramolecular giant vesicles combined with the amplification of encapsulated DNA. *Nature chemistry* **3**, 775-781 (2011).

243. L. R. Arriaga, S. S. Datta, S. H. Kim, E. Amstad, T. E. Kodger, F. Monroy, D. A. Weitz, Ultrathin shell double emulsion templated giant unilamellar lipid vesicles with controlled microdomain formation. *Small* **10**, 950-956 (2014).

244. C. Martino, S. H. Kim, L. Horsfall, A. Abbaspourrad, S. J. Rosser, J. Cooper, D. A. Weitz, Protein expression, aggregation, and triggered release from polymersomes as artificial cell-like structures. *Angewandte Chemie* **51**, 6416-6420 (2012).

245. N.-N. Deng, M. Yelleswarapu, W. T. Huck, Monodisperse uni-and multi-compartment liposomes. *Journal of the American Chemical Society*, (2016).

246. K. Karamdad, R. Law, J. Seddon, N. Brooks, O. Ces, Studying the effects of asymmetry on the bending rigidity of lipid membranes formed by microfluidics. *Chemical Communications* **52**, 5277-5280 (2016).

247. J. N. Lee, C. Park, G. M. Whitesides, Solvent compatibility of poly (dimethylsiloxane)-based microfluidic devices. *Analytical chemistry* **75**, 6544-6554 (2003).

248. B. Lohse, P.-Y. Bolinger, D. Stamou, Encapsulation efficiency measured on single small unilamellar vesicles. *Journal of the American Chemical Society* **130**, 14372-14373 (2008).

249. P. Stano, T. P. de Souza, P. Carrara, E. Altamura, E. D'Aguanno, M. Caputo, P. L. Luisi, F. Mavelli, Recent biophysical issues about the preparation of solute-filled lipid vesicles. *Mechanics of Advanced Materials and Structures* **22**, 748-759 (2015).

250. A. Seth, G. Béalle, E. Santanach - Carreras, A. Abou - Hassan, C. Ménager, Design of vesicles using capillary microfluidic devices: from magnetic to multifunctional vesicles. *Advanced Materials* **24**, 3544-3548 (2012).

251. H. C. Shum, E. Santanach-Carreras, J. W. Kim, A. Ehrlicher, J. Bibette, D. A. Weitz, Dewetting-induced membrane formation by adhesion of amphiphile-laden interfaces. *Journal of the American Chemical Society* **133**, 4420-4426 (2011).

252. P. Umbanhowar, V. Prasad, D. Weitz, Monodisperse emulsion generation via drop break off in a coflowing stream. *Langmuir* **16**, 347-351 (2000).

253. J. C. McIntyre, R. G. Sleight, Fluorescence assay for phospholipid membrane asymmetry. *Biochemistry* **30**, 11819-11827 (1991).

254. M. Schulz, S. Werner, K. Bacia, W. H. Binder, Controlling molecular recognition with lipid/polymer domains in vesicle membranes. *Angewandte Chemie International Edition* **52**, 1829-1833 (2013).

255. M. Schulz, A. Olubummo, K. Bacia, W. H. Binder, Lateral surface engineering of hybrid lipid–BCP vesicles and selective nanoparticle embedding. *Soft Matter* **10**, 831-839 (2014).

256. 2017 Future Symposium on BUILDING A SYNTHETIC CELL (2017). http://www.syntheticcell.eu/

257. I. A. Chen, P. Walde, From self-assembled vesicles to protocells. *Cold Spring Harbor perspectives in biology* **2**, a002170 (2010).

258. Y. Chen, W. Gao, C. Zhang, Y. Zhao, Three-dimensional splitting microfluidics. *Lab on a chip* **16**, 1332-1339 (2016).

259. M. Marguet, C. Bonduelle, S. Lecommandoux, Multicompartmentalized polymeric systems: towards biomimetic cellular structure and function. *Chemical Society Reviews* **42**, 512-529 (2013).

260. C. Schmitt, A. H. Lippert, N. Bonakdar, V. Sandoghdar, L. M. Voll, Compartmentalization and transport in synthetic vesicles. *Frontiers in bioengineering and biotechnology* **4**, (2016).

261. S. Mann, Systems of creation: the emergence of life from nonliving matter. *Accounts of chemical research* **45**, 2131-2141 (2012).

262. W. Wang, R. Xie, X.-J. Ju, T. Luo, L. Liu, D. A. Weitz, L.-Y. Chu, Controllable microfluidic production of multicomponent multiple emulsions. *Lab on a chip* **11**, 1587-1592 (2011).

263. N.-N. Deng, M. Yelleswarapu, L. Zheng, W. T. Huck, Microfluidic assembly of monodisperse vesosomes as artificial cell models. *Journal of the American Chemical Society* **139**, 587-590 (2016).

264. A. W. Scotto, D. Goodwyn, D. Zakim, Reconstitution of membrane proteins: sequential incorporation of integral membrane proteins into preformed lipid bilayers. *Biochemistry* **26**, 833-839 (1987).

265. E. Altamura, F. Milano, R. R. Tangorra, M. Trotta, O. H. Omar, P. Stano, F. Mavelli, Highly oriented photosynthetic reaction centers generate a proton gradient in synthetic protocells. *Proceedings of the National Academy of Sciences* **114**, 3837-3842 (2017).

266. Q. Lin, E. London, The influence of natural lipid asymmetry upon the conformation of a membrane-inserted protein (Perfringolysin O). *Journal of Biological Chemistry* **289**, 5467-5478 (2014).